UNIVERSIDADE TÉCNICA DE LISBOA

INSTITUTO SUPERIOR TÉCNICO

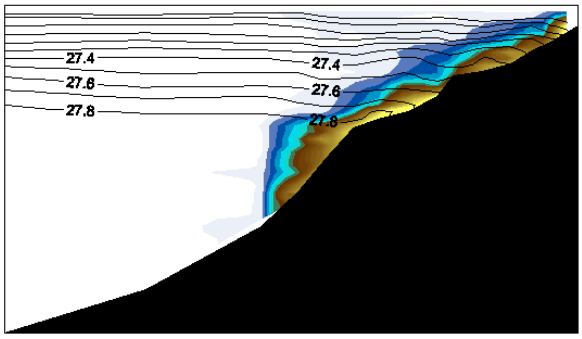

FINE SEDIMENTS RESUSPENSION PROCESSES AND TRANSPORT IN NAZARÉ SUBMARINE CANYON

Ana Carla Martins Garcia

(Mestre)

Dissertação para obtenção do Grau de Doutor em Engenharia do Ambiente

Orientador:	Doutor Ramiro Joaquim de Jesus Neves
Co – Orientador:	Doutor Henrique Manuel da Mota dos Santos Coelho

Jurí

Presidente:	Reitor da Universidade Técnica de Lisboa
Vogais:	Doutor Rui Pires Matos Taborda
	Doutor Tjeerd Cornelis Elco van Weering
	Doutor Aires José Pinto dos Santos
	Doutor José Manuel de Saldanha Gonçalves Matos
	Doutor Ramiro Joaquim de Jesus Neves
	Doutor Henrique Manuel da Mota dos Santos Coelho

Outubro de 2008

[…] I thought I would sail about a little and see the watery part of the world. It is a way I have of driving off the spleen, and regulating the circulation. Whenever I find myself growing grim about the mouth; whenever it is a damp, drizzly November in my soul; whenever I find myself involuntarily pausing before coffin warehouses, and bringing up the rear of every funeral I meet; and especially whenever my hypos get such an upper hand of me, that it requires a strong moral principle to prevent me from deliberately stepping into the street, and methodically knocking people's hats off – then, I account it high time to get to sea as soon as I can. […]

Herman Melville
(Moby Dick)

Acknowledgments

This thesis is the final stop of a long history which had its start in 1997.

I change my PhD theme three times. I moved from the Algarve to Lisbon. I changed university and thesis coordinator, but even with all these changes I never gave up and I do have to thank so many persons who supported me along this journey.

First, I would like to thank to Prof. Ramiro Neves, my thesis coordinator, for accepting me in his group (Maretec), a simple field marine geologist with null knowledge in modelling. Thank you for all the trust and support throughout these long 5 years.

My very special thanks go to Prof. Henrique Coelho, my co-coordinator and my friend, for introducing me to hardest part of the physical oceanography, for helping me out during all this period and especially for the encouragement each time I was feeling down.

To Manuela Juliano I would like to thank for her friendship, for reviewing my thesis for the comments, for the discussions that resulted in some improvements and for her fabulous "programmes" without with I would have never redone all the figures in time (and never so pretty).

I also want to thank my colleagues at Maretec - Ângela Canas, Fank Braunschweig (now at Action Modulers), Luis Fernandes, Madalena Santos, Paulo Chambel Leitão (now at Hidromod), Pedro Pina (now at Bentley), Rodrigo Fernandes, for all the help with the MOHID (the model, the pre and post processors, e.g.), and data bases. Without their help I would have never manage to put the model running and be able to do some of the draws within this thesis. To Susana Nunes for the support in my other Maretec tasks, especially in the final phase of this thesis.

To the rest of the group thank you for supporting me during my bad humour crises.

Field data exploited in this thesis was collected between 2002 and 2006, on board the Netherlands Research Vessel from the NIOZ – PELAGIA. A huge thanks to Henko de Stigter, that year after year kept inviting me for his canyons cruises, for all the good conversations and discussions, which much contributed to this work.

I cannot forget all the crew members, technicians and scientists, who made my time in that ship, so easy to go. My special thanks are also going to Henko, Bob, Willem, Pedro

Mendes, Joana, Joana Beja, José, Roel, Klass, Ron and John (the cook from the 2005 cruise – delightful).

But our work, our knowledge doesn't start with the beginning of a thesis, and in my case I have a long background and many are those who contributed to this work in one way or another.

I would like to thank to Prof Alveirinho Dias that initiated me in the Marine Geology field and with whom I worked for 9 years. The first 4 years I spent in IH (Instituto Hidrográfico), my initiation in Marine Geology and in the hard life of working on board of a ship. Although these four years don't have a direct influence in this work, they made part of my journey; I also want to thank Anabela Oliveira, Luis Rosa, João Duarte, Aurora Rodrigues, Manuela Matos, Aida Seabra, Jorge da Silva and Ana Isabel. The other 5 years I lived in Algarve, "those were the best days of my life…..".

For many reasons, scientific, personal, etc…. I cannot forget my colleagues at the CIACOMAR (Srº Cunha, Ana Matias, Ana Vila, Isabel Mendes, Patricia Silva, Miguel Castro, Brad Moris, Óscar Ferreira), at the University (Joaquim Luís, Delminda Moura, Paulo Relvas, Tomasz Boski, Paulo Pedro, Paulo Santana, ….) at Montinho dos Pardais (Cristina, Henrique, Ana and Mariano) neither my big friends - Ricardo, Dinora, Tita, Patricia, Vincent, Clarinda…..

And the most special thanks to Cristina Veiga-Pires…..

And the last, but not the least to those that are the most important people in my life, my parents (Luis e Céu) my sister Cátia, my brother in law Fernando and the joy of my eyes - my two small nephews Tiago e Diogo and also to Jorge.

This work was supported by a Doctoral Grant, reference SFRH/BD/1346/2000, from the "Fundação para a Ciência e Tecnologia".

To the Memory of
Willem Polman

Abstract

The results obtained during the oceanographic cruises PE204 (November 2002), PE218 (October/November 2003) and PE236 (April/May 2005) in Nazaré Canyon reveal the presence of high concentrations of suspended material in the canyon axis between the 1600 and the 300 m depth and also reveal that near bottom concentration oscillate with the semi-diurnal tide frequency, with the higher values and thickness during ebb tide. In order to confirm that these oscillations were related with internal tide, simulations using the numerical model MOHID were performed, forcing the model only with tide. The model reproduced all the main patterns observed in the data.

To evaluate how the geometry relates with the formation of these turbid layers it was taken in consideration the "Internal Wave Linear Theory", which relates the angle of propagation of the internal waves (s) and the slope of the topography (α). Results show that the upper canyon is near critical in almost all of his extent, with critical ($s/\alpha = 1$) areas around the 1500 m, 1000 m and the 300-400 m depth, which match with the turbidity maximums found at the canyon axis. Internal tides are then the major process for resuspension of fine particles in the upper Nazaré Canyon

Simulations were also performed using lagrangian tracers as bottom sediments, to observe the effect of tide and tide and SW and NW wind on the transport of fine particles. On the shelf the transport and sediment suspension of fine particles depends on the wind direction. Deeper, below the 200 m depth, the transport depends mainly on the currents direction, on the tidal effect and on the density of the nepheloid layers.

Key-Words: Nazaré Canyon; Suspended Material; Internal Waves; Transport patterns; Numerical model MOHID.

Resumo

Resultados obtidos durante as campanhas oceanográficas PE204 (Novembro 2002), PE218 (Outubro/Novembro 2003), PE236 (Abril/Maio 2005), no canhão da Nazaré revelaram a presença de elevadas concentrações de matéria em suspensão no eixo do canhão, entre os 1600 e os 300 m de profundidade. Verificou-se ainda, que a concentração junto ao fundo era variável com o período da maré semi-diurna, com os maiores valores e espessuras na baixa-mar, parecendo relacionados com a presença de ondas internas. De forma a confirmar estas observações, realizaram-se simulações para o período das campanhas utilizando o modelo MOHID, forçando só com maré. O modelo reproduziu as observações de campo.

Para avaliar como a geometria do canhão estaria relacionada com a formação destes níveis nefeloides, aplicou-se a "teoria linear das ondas internas", que relaciona o ângulo de propagação das ondas internas (s) e o declive da topografia (α). Os resultados indicam que a parte superior da canhão é quase crítica em toda a sua extensão, com zonas críticas (s/α =1) por volta dos 1500, 1000 e 300-400 m de profundidade, coincidindo estas com os máximos observados na turbidez, donde se conclui que as ondas internas são o principal processo na resuspensão de partículas finas na parte superior do canhão.

Experimentalmente, simularam-se os sedimentos finos utilizando traçadores lagrangianos, e observou-se qual o efeito da maré e desta combinada com ventos de NW e SW, no transporte destas partículas. Na plataforma o transporte e a velocidade (tempo) a que os sedimentos são suspensos dependem da direcção do vento. Abaixo dos 200 m o transporte e o tempo de residência das partículas no interior do canhão é função da direcção das correntes, do efeito da maré e da densidade dos níveis nefeloides.

Palavras-Chave: Canhão da Nazaré; Matéria em Suspensão; Ondas Internas; Transporte; Modelo Numérico MOHID.

Acronyms List

ADI – Alternate Direction Input
BOBO – Bottom Boundary Benthic Lander
BNL – Bottom Nepheloid Layer
CA – Critical Angle
CSD – Critical Shear Deposition
CSE – Critical Shear Erosion
CTD – Conductivity, Temperature, Depth
DOP – Departamento de Oceanografia e Pescas
E - East
ECOMARGE - ECOsystèmes de MARGE continentale
EUROSTRATAFORM – European Margin Strata Formation
EUROMARGINS - Slope Stability on Europe's Passive Continental Margins
FTU – Formaline Turbid Units
GOTM – General Ocean Turbulence Model
HERMES - Hotspot Ecosystems Research on the Margins of European Seas
INL – Intermidiate Nepheloid Layer
InterMARGINS – Continental Margins Research
MW – Mediterranean Water
MOHID – Water Modelling System
N - North
NACW – North Atlantic Central Water
NADW – North Atlantic Deep Water
NE - Northeast
NIOZ – Netherland Institute for Sea Research
NIW – Non-linear Internal Waves
NNE – North- Northeast
NW - Northwest
OBS – Optical Backscatter
OMARC - Ocean margin deep-water research consortium
OMEX – Ocean Margin EXchange
PSU – Practical Salinity Unit
POM – Princeton Ocean Model
PPE – Perturbation Potential Energy
RMSE – Root Mean Square Error
S - South
SE - Southeast

SEEP - Shelf Edge Exchange Processes
SEPLAT – Sedimentos da Plataforma
SNL – Surface Nepheloid Layer
SML – Surface Mixed Layer
SPM – Suspended Particulate Matter
STRATAFORM – Strata Formation
SST – Sea Surface Temperature
SSW – South-Southwest
SW - Southwest
TKE – Turbulent Kinetic Energy
TVD – Total Variation Diminishing
W- West
WNW – West-Northwest
Ws – Settling Velocity

INDEX

List of Figures

List of Tables

Chapter 1

INTRODUCTION

Continental margins, in the broad sense, include the area situated between the shoreline and the deep ocean. They consist on the continental shelf, the shelf edge, the continental slope and rise; represent about 20% of the total world ocean (Figure 1). The shelf break constitutes a pronounced topographic discontinuity separating the continental shelf, characterized by a gentle slope (typically 0.1^{o}) from the continental slope having an average slope of about 4^{o}. It occurs typically at a depth of approximately 130 m, except in the Polar Regions were it is often below 350 m, this is due to the isostatic pressure of ice in the continent. The bathymetric discontinuity plays a major role in the ocean dynamical process, controlling vertical and horizontal mixture at the shelf edge (Wollast, 2002).

Continental margins are very different worldwide; they show different topographic, biological and geological features.

Wide continental shelves and extensive continental margins are typical of passive margins (such as those that we can find surrounding the western Atlantic and the western Indian Ocean), they are located in areas of low seismic activity. On the other end narrow shelves and steep slopes are characteristic of seismically active areas, none as active margins (most of the Pacific Ocean). Both passive and active margins are found in all major ocean basins.

We can observe profound differences within the sedimentation systems which occur in tectonically passive continental margins and those on active margins were the active plate subduction is. Passive continental margins have undergone thermal subsidence following the original separation of continents by creating space for the accumulation of sediments for more than 100 million years. Active margins suffer strong tectonic deformation, and sediments that escape the margin to be deposited in the adjacent trench may be subsequently tectonically plastered into the continental margin.

Margin Morphology and more specifically the shelf wide is a very important characteristic from the point of view of the relative ability of the shelf to retain

allochtonous and autochtonus particulate material by deposition and accumulation on the continental shelf (Wollast, 2002).

Continental shelves are places of transition between the continents and the deep oceanic basins. The distribution of the sediments on a shelf is rarely regular, and their occurrence is influenced by many environmental factors ranging from the characteristics of the sediment supply (e.g. riverine discharges, coastal erosion and accumulation of biogenic material) to the physical mechanisms (wave climate, tides, currents and vertical movements) that act as distributional processes. The geological history of a shelf is normally of high complexity, this history is documented in sedimentary sequences, faults, folding and erosional horizons that result from the rifting and spreading events, sea-level fluctuations, subsidence and the effects of climate changes. In addition to sediment supply, environmental conditions and a region's geological history are major influences which prevail in the sedimentary processes and environment over a shelf, through the determination of coastal and shelf morphology and their differential subsidence (Dias *et al*., 2002).

The actual shape of the shelves must be seen as a product of low-sea level processes. In the past 1 million years sea-level has only been as high as at present for less than 5% of the time, and it has been high only for the past 7000 years. During this period the maximum lowering at peak glacial times was 120 – 130 m below the present level, which uncovers, effectively, all the continental shelves at the present depth of the shelf-break (130 – 150 m), corresponding to the depth of significant wave attack on an outer shelf at low sea level stand. Thus, for most of the later Quaternary period shelves were partially uncovered and were the locus of fluvial and Aeolian sediment deposition and dispersal. At low sea-level, sediments were discharged directly into the ocean basins with reduced trapping in coastal plains. Consequently, for the Quaternary as a whole, the lowering of the sea-level is by far the most efficient mechanism of sediment transport to the ocean basins. (McCave, 2002)

The scientific advances of the last decades have revealed the extreme importance of ocean margins in all areas of human activities: political (Exclusive Economic Zones), industrial (oil, gas and inerts exploitation; communications), ecological (fisheries, environmental assessments), military (potential or actual theatres of operation), etc.

The relevance of the continental margins is now recognized. In the last few years several projects (e.g. ECOMARGE, SEEP I, SEEP II, OMEX I, OMEX I-II, OMEX II, STATAFORM, EUROSTRATAFORM, EUROMARGINS, HERMES) have been financed and networks (e.g. InterMARGINS, OMARC) have been created focusing on the continental margin systems. These projects and their studies are fundamental for sustainable seabed exploitation, for environmental impacts as well as for studies on climatic changes.

One area of interest is to follow the fate of sediment particles from their origin in rivers to the deep sea and understand how they form the strata on ocean margins.

McCave (2002) concluded that "we don't know how much material is presently supplied to the sea, but is probably less than we think […], we don't know how much of that escapes to the open ocean (maybe 10-20%), and we don't know its size distribution […]."

It is recognised that continental margins constitute the most significant interface on Earth for sediment distribution. About 90% of the sediment generated by erosion on land is deposited on the continental margins, where it is (sometimes temporarily) stored in major deltaic deposits, as shelf deposits and on the continental slope. Associated with development of these depositional systems are the transport, settling and burial of riverine, deltaic and shelf-derived particles and of organic carbon, and other associated anthropogenic, allochtonous particles. After their initial transport into the marine system by rivers, particles are dispersed on the shelf and at the shelf edge under the combined influence of local hydrodynamic conditions (currents, waves, etc), and meteorology. Subsequently they may become transported, resuspended and further transported and distributed over the continental shelf and slope. (McCave, 2002; Palanques *et al.*, 2006).

Another mean of transport of particles from the shelf over the slope and into the deep sea is through channels and submarine canyons, bringing the sediment far out into the abyssal plains.

The work on this thesis was undertaken in the scope of the EUROSTRATAFORM European Project (http://www.noc.soton.ac.uk /gg/ EUROSTRATAFORM / index.html), which aimed to identify and model the sedimentary processes and their forcing conditions operating on the European continental margin, that lead to the

development, evolution and architecture of the sedimentary sequences forming the continental margin.

Figure 1 is a schematic cartoon showing different sediment transport pathways across a continental margin.

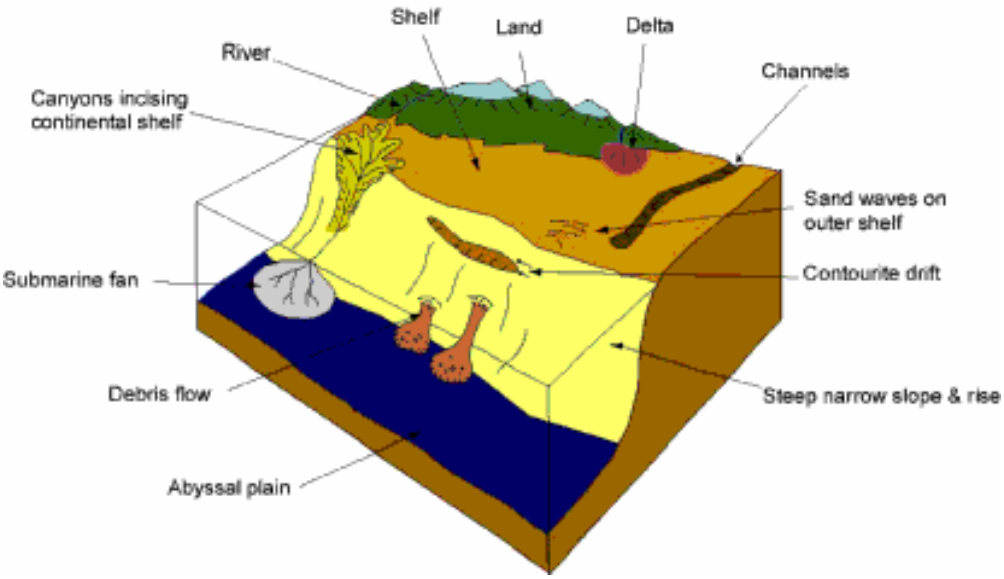

Figure 1 - Schematic cartoon showing different sediment transport pathways across a continental margin (http://www.noc.soton.ac.uk/gg/EUROSTRATAFORM/index.html).

Under the EUROSTRATAFORM project four representative areas of study were chosen (two located in the Mediterranean Sea and two along the NE Atlantic continental margin of Europe, Figure 2), which cover a complete range of physiographical and environmental settings, and also have key characteristics that can be compared with, extrapolated to and modelled for other margin systems.

The Mediterranean sites (Adriatic Sea and Gulf of Lions) reflect the impact of large river outflow systems on sedimentation across the shelf, continental slope and deep basin. The NE Atlantic sites (off western Iberia and Northern Norway) allow the study of shelf-canyon-slope sedimentary systems both with direct connection to, and distinct separation from, river input.

The content of this thesis is integrated in the Western Iberian Margin area, where several submarine canyons cut the continental shelf almost to the coastline, as it is the case of the Nazaré Canyon were our study is focused (Figure 3).

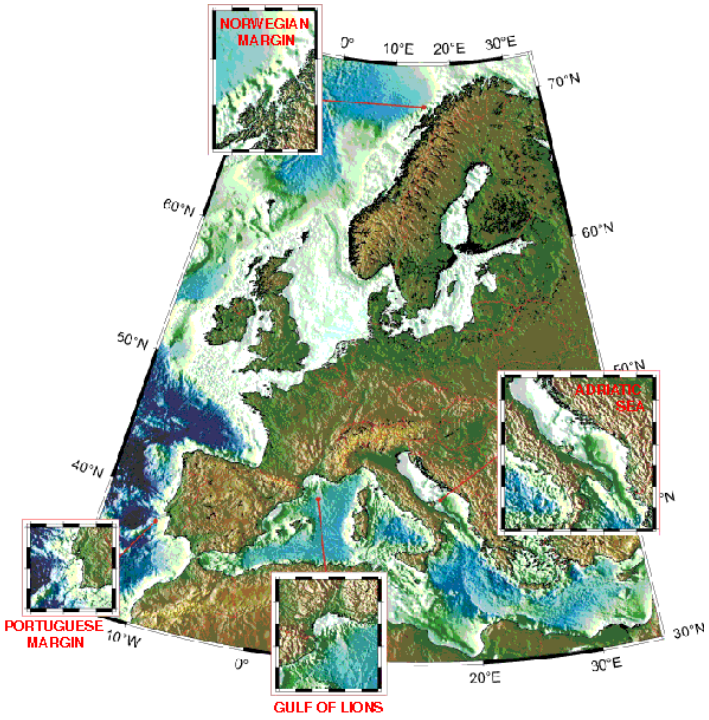

Figure 2 - Map to show the study areas under investigation in the EUROSTRATAFORM project (http://www.noc.soton.ac.uk/gg/EUROSTRATAFORM/index.html).

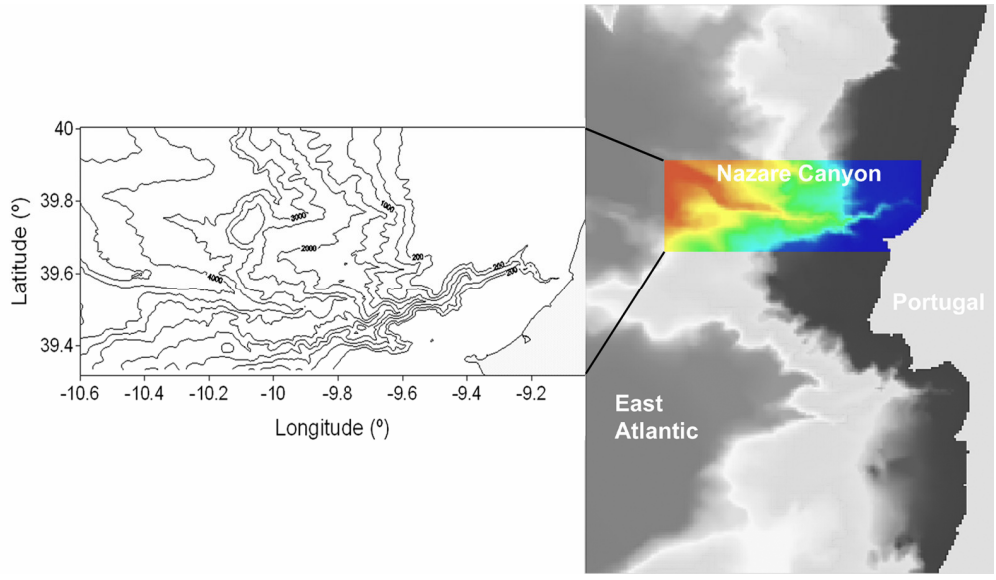

Figure 3 – General Settings of the study area.

The study of canyon systems under the EUROSTRATAFORM project aimed to achieve the following objectives (Eurostrataform, 2006b):

(i) Definition, measurements and modelling of the forcing conditions governing sediment and organic particle transport from the shelf via canyons to the deep sea at contrasting sectors of the European continental margin.

(ii) Definition, measurement and modelling of the particle transport pathways from the shelf via canyons to the deep sea at contrasting sectors of the European continental margin.

(iii) Definition and modelling of particle transport, fluxes, accumulation and mixing processes, and of the time scales involved, from the shelf via canyons to the deep sea at contrasting sectors of the European continental margin.

(iv) Establishment of temporal and spatial variability of the governing sediment transport processes, pathways and fluxes and their role and contribution towards construction of the margin and the sedimentary record.

The work done on this thesis is focused on the Nazaré Canyon system (Figure 3) and it aimed to contribute for objectives (i) to (iii).

Nephelometry observations, performed during several cruises in the Nazaré Canyon area revealed high concentrations of fine sediment forming persistent and important nepheloid layers at a considerable distance from the coast and at deep levels along the canyon axis indicating high canyon resuspension activity, but these were insufficient for understanding the processes involved. For this reason a numerical model – MOHID - was used. Numerical models are a powerful tool because they allow us to integrate processes in space and time giving an overview, while the observations are restricted in time and space. The results on the model have shown that the atmospheric forcing and the waves have an important role in resuspension and transport in the canyon head area, especially during storm events. Resuspension promoted by turbidity currents (currents usually triggered by earthquakes or slumping, where, high-speed sediment-laden water, flows down the slope under the clear water, causing a great deal of erosion and subsequent sedimentation in features classified as turbidites) is responsible for increasing turbidity observed at depths bigger than 3000 m.

The results obtained show that internal tides play a major role in the sediment resuspension in the Nazaré Canyon.

The major goal of this study was to verify if **internal tide by itself can be responsible for a large portion of the observed suspended sediment distribution patterns within and around the Nazaré Canyon**. To achieve this goal we performed a set of numerical modelling experiments where the only forcing considered was tide. The model results were compared with nephelometry field data and were used to identify resuspension areas. Further goals of this study are to gain insight into **how canyon geometry affects propagation and dissipation of internal waves**. We also aimed to **understand the role of this phenomenon in the resuspension and transport of fine sediments within the canyon** by using the model with the real bathymetry and also by comparing results with field data.

The thesis is structured into 7 chapters, including this Introduction, Conclusions and Recommendations for future work, with the following contents:

Chapter 2 – Oceanographic and Sedimentological features of the West Iberian Margin, inserting the Nazaré canyon in its regional context. In this chapter the state of the art for the West Iberian margin is described in what concerns geomorphology, sedimentary cover, wind forcing and wave conditions, currents and sediment transport processes.

Chapter 3 – Submarine Canyons. This chapter presents an overview and the actual knowledge of the processes that might influence sediment transport in submarine canyons. As an introduction to the Nazaré canyon regional and local settings and the state of the art in what concerns currents, sediment cover, sediment fluxes between other aspects will also be described.

Chapter 4 – Suspended Particle Material in Nazaré Canyon. In this chapter, CTD and Nephelometry profiles from 5 years cruises (2002 to 2006) will be analysed in what concerns Temperature, Salinity, Density and Suspended Particulate Matter (SPM), in order to formulate hypotheses for the processes involved in sediment resuspension within this canyon and to verify if internal tide can be a major process for sediment resuspension in Nazaré canyon.

Chapter 5 – Modelling Internal Tide in Nazaré Canyon. In this chapter it is shown how the internal tide is a major process for sediment resuspension within this canyon by comparing MOHID results and field data.

Chapter 6 – Transport and Residence Time Resuspended Particles. Lagrangian tracers permit us to know the origin and fate of a particle. Lagrangian fine particle simulations were performed to observe resuspension, transport and deposition in the canyon and adjacent shelf, identifying the origin of the particles that are deposited in each region.

Chapter 7 – Conclusion, Synthesis and Future Work.

Chapter 2

OCEANOGRAPHIC AND SEDIMENTOLOGICAL FEATURES OF THE WEST IBERIAN MARGIN

2.1 MORPHOLOGY

The West Iberian margin is extended almost for 800 km, being characterized by a narrow shelf varying from less than 5 km (in front of Espichel Cape) and a little bit over 60 Km at the Estremadura Plateau (Figure 4). The depth of the shelf edge is not always constant, varying between 120 m depth (e.g. near Raso Cape) and over 400 m depth at the Estremadura Plateau once again. The slow shelf gradients, south of Sines, take some authors (e.g. Dias, 1987) to consider the shelf edge around the 1000 m depth. The continental slope is cut by several valleys, ravines and submarine canyons which make the transition to the deep sea. Although the Iberian continental shelf may be considered morphologically regular and gentle four major accidents abruptly interrupt this relief: the submarine canyons of Nazaré, Lisbon, Setúbal and São Vicente.

2.2 TIDES

The Portuguese continental shelf is integrated in the North Atlantic amphidromic system, located in an area of transition from meso-tides to macro-tides. The barotropic tides along the western Portuguese margin propagate from south to north and are dominated by the semidiurnal principal lunar (*M2*), with a mean average amplitude of 1 m reaching typical maximum sea level amplitudes of almost 2m along the coast during spring tides (Eurostraform, 2006a).

In Coastal areas, estuaries and lagoons, tidal currents are a major cause for particles supply and distribution, mainly during spring tide periods.

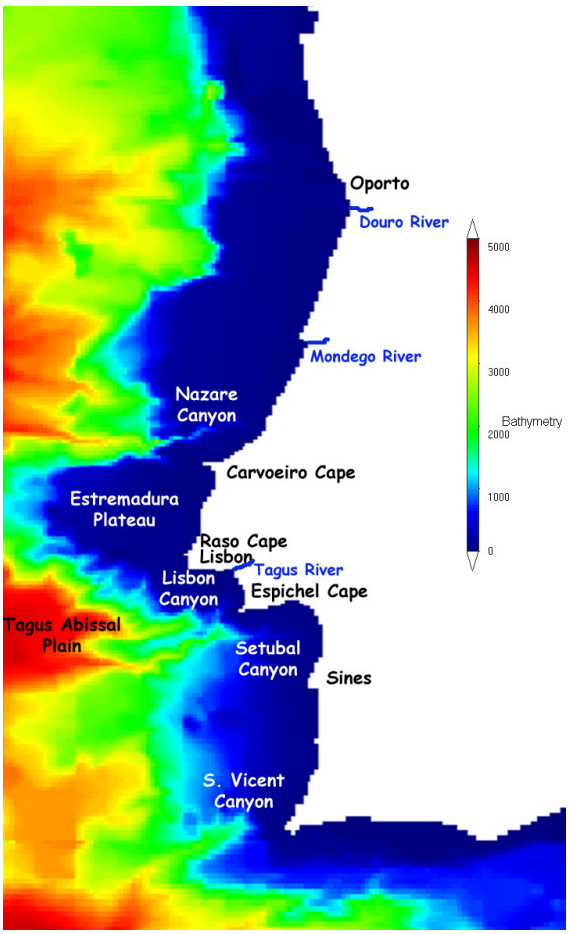

Figure 4 – Bathymetric map with the most relevant locations.

The *M2* tidal currents reach velocities of about 5 cm s^{-1} with the maximum values occurring at the Estremadura Plateau, on the south of the Nazaré Canyon. Diurnal period constituents are weak except over this plateau, where the barotropic principal declination (*K1*) tidal currents reach magnitudes comparable with the *M2* tidal currents (Eurostrataform, 2006a).

Oceanic barotropic tides interact with the continental slope topography. Depending on the characteristics of the topography and water column stratification, they can leak their energy into baroclinic (internal) tidal motions which propagate towards deeper levels. This process is expected to be particularly important in the canyons. (Eurostrataform, 2006a).

2.3 WIND AND WAVE CONDITIONS

According to Fiúza *et al*. (1982), Portugal is climatologically affected by the Azores anticyclone and in less extent by the Iceland depression.

Typically from March to August the Azores anticyclone moves along the 38ºW meridian from 27ºN until 33ºN. From November to February it moves eastward, reaching 23ºN around January. This is a consequence of the winter atmospheric high pressures located in Europe and in Africa. This situation gives origin to weak west winds during the winter and relatively strong North and Northwest winds during the summer.

The local waves depend mostly on the wind intensity and direction. The frequency of the waves from North and Northwest increases from 32% in February until 53% in August, the waves from South and Southwest vary from 16% in February to 6% in August (Magalhães, 1999).

According to Carvalho & Barceló (1966), the wave conditions in the west coast has an average period between 6 and 18 seconds, being more frequent the ones between 9 and 11 seconds. On the open ocean the most frequent (around 100 days/year) wave direction is from W10ºN and W20ºN, while waves with directions between W and S only occur around 75 days/year. Waves from N and NW are frequent all year around (80%), while waves from other directions occur mainly during the winter period and are almost absent during the summer months from June to September. Wave heights above 1 m are observed during 95% of the year and above 4 m occur 5% of the year. These wave conditions generate an almost permanent alongshore southward current.

Pires and Pessanha (1986) observed that in the Northern Portuguese Coast the wave direction W20ºN is related to waves, with a period of 8 seconds and 2 m height. In the southern West coast the most frequent wave direction is from NW with a period of 7 seconds and 1.6 m height.

Vitorino *et al*. (2002a) based on almost three years of observations (July 1996 to June 1999) in the northern West Portuguese coast observed that, in winter conditions, there are significant wave heights and periods exceeding 3 m and 8 s respectively, and high standard deviations were found mainly between November and January. During the summer the wave regime was characterized by low energy conditions. From June to September significant wave heights, mean periods and peak periods were consistently

less than 3 m, 8 s and 12 s respectively, with the lowest values between June and August.

2.3.1 Storms

The storms and other highly energetic events are observed in the western Iberian coast mainly during the winter and transition periods.

The storms (especially the ones from SW) that reach the west Portuguese coast may have catastrophic results when coincident with high spring tides. The storms from January 1937 (Pereira, 1937) and from February/March 1978 (Daveau *et al*., 1978) caused severe damages in several areas of the coast. As an example, during the 1937 storm the groyne of Sines Port break in several places over a distance of 650 m under waves that reach 8.5 m of significant height (Feio & Almeida, 1978).

The study of storms and their main characterization has become an object of study in the last few decades with increasing incidences in the last 40 years. The first results are those from Carvalho & Barceló (1966), who observed waves reaching 11 m of significant height. According to these authors the violence of the storms decreases southward.

Costa (1992/3/4) based on the observation of data, taken over 20 years of wave buoys instruments, concluded that in the west coast storms are more violent and frequent northward. The majority are from NW and WNW with significant heights below 6 m but in extreme cases may reach more than 8 m height.

Vitorino *et al*. (2002a) reported that there are two types of storms which affect the western Iberian margin. The first one corresponds to exceptionally strong NW or SW swells that affect the area for one or two days, these events are very frequent and are the most common types of storm that occur during the winter and transition periods off the western Iberian coast. These storms can generate wave conditions in the coast with significant wave heights of up to 7.5 m and peak periods of about 16.5 s, as during the storms of November 1997 and April 1998. The second type of storm, known as "westerly storms", involves a succession of highly energetic storms that affect the western Iberian margin for one or two weeks, and maintained a sustained environment of highly energetic conditions. During the period of observations Vitorino *et al*. (2002a) identified only two times this kind of storm, in November 1997 and December 1998.

During the latter storm the waves had significant wave heights of ~8.7 m and peak periods of 20 s.

2.3.2 Upwelling and Downwelling

The zonal gradient of atmospheric pressure established between the Azores anticyclone and the Iberian Peninsula during the summer is reinforced by the development of an atmospheric depression over central Iberia, and drives a regime of sustained northerly, upwelling favourable winds. The summer upwelling regime lasts from July to September (Fiúza *et al*., 1982). It is characterized by the development of equatorward jets and energetic upwelling filaments, which extends offshore through hundreds of kilometres (Haynes *et al*., 1993; Alvarez *et al*., 2005). Spatial and temporal variability in the extent and intensity of upwelling off the Iberian Peninsula is well documented by satellite imagery of sea-surface temperature and pigment concentrations (Haynes *et al*., 1993; Alvarez *et al*., 2005).

As stated before in winter, the Azores anticyclone is displaced to its most southern position and the Iceland depression is reinforced. Wind forcing conditions are characterized by perturbed westerly winds, which frequently have a southerly component and establish a downwelling regime all over the shelf (Fiúza *et al*., 1982).

Although this is the most common feature of the Iberian Margin, some years due to unusual weather conditions upwelling can develop for considerable periods during winter time (Vitorino *et al*., 2002a).

The upwelling phenomenon is responsible for the rising of the deep cold waters which are rich in nutrients from depths around 60 and 120 m deep (Fiúza *et al*., 1982). The pulsed input of new nutrients in such a system influences the composition and temporal variability of the pelagic food web and thus affects the quality and quantity of export fluxes (Peinert *et al*., 1989 in Joint & Wassman, 2001).

Upwelled water with its maturating pelagic communities is transported offshore far beyond the continental margin in filaments associated with the major capes along the coast. Bypassing the shelf and slope, final sedimentation of organic matter from this upwelled water may thus take place over the abyssal plain — far away from the source of upwelling (Joint & Wassman, 2001).

2.4 OCEAN CIRCULATION SYSTEM

The general ocean circulation pattern in the West Iberian Margin is highly influenced by the atmospheric circulation having a strong seasonal regime (e.g. Haynes *et al*., 1993; Vitorino *et al*., 2000; Coelho *et al*., 2002; Eurostrataform, 2004; Peliz *et al*., 2005; Eurostrataform, 2006a) that can influence the water column (in the shelf and at the slope). It is characterized by strong coastal upwelling in summertime, together with the generation of associated upwelling filaments which occur in response to the strong north/northwesterly winds. As a result of this regime the general circulation pattern is dominated by an equatorward flow on the continental shelf and slope (from the surface down to 500 m depth). During the summer, the area is also protected from the influence of atmospheric synoptic low pressure systems, showing a low energy wave regime (significant wave heights of about 2 m).

During the winter, the northerly component of the wind weakens, or even reverses, reversing the surface flow and this way originating a relatively narrow, warmer ($T=18^{o}$-$19^{o}C$, over 1-$3^{o}C$ higher than the surrounding waters) and saltier (S=36 at 50m deep and over 0.2 PSU higher than the surrounding waters), poleward current flowing along the edge and slope of the west Portuguese continental margin, N and NW Spain and SW France, that can be identified in satellite images (Haynes & Barton, 1990; Frouin *et al*., 1990; Mazé *et al*., 1997; Vitorino *et al*., 2000). These conditions are downwelling favorable and are responsible for a highly energetic wave regime with significant wave heights exceeding 5 m during storms. Below this surface regime a poleward subsurface flow persists all year round extending from 200-300 m down to 1500 m (below the Mediterranean Water).

Modeling results for circulation in the Western Iberian Margin (Coelho *et al*, 2002) reproduced the major circulation patterns for this area and suggested a close relation between the topography and the decrease in water transport further north. These results also showed that, if the meridional component of windstress is not strong enough to reverse the flow, a permanent poleward flow will occur even during summer, if not on the shelf at least over the slope. A later study performed by Peliz *et al*. (2005) based on field data and satellite images supports the idea of a permanent poleward flow as stated by Coelho *et al*. (2002). According to these authors, the density-

driven component of this poleward current together with the wind also plays an important role in the seasonality of this poleward current.

Below the slope current (1500 m) a permanent low velocity southward current is observed.

2.5 SEDIMENTARY COVER

Due to the Portuguese Hydrographic Institute SEPLAT (Cartography of the Surface Sediments of the Portuguese Continental Shelf) program, that consisted in collecting surface sediment samples on each nautical mile along the Portuguese continental shelf there is a good knowledge on the sedimentary cover of the Portuguese shelf. For the Galician shelf this information is more scarce (Rey & Díaz del Rio, 1987; Rey & Medialdea, 1989 and Díaz del Rio *et al*., 1992), the only map available on the sedimentary shelf cover is the one from Dias *et al*., (2002a, 2002b), undertaken in the aim of the European OMEX II-II project.

The characteristics of the surface sediments are influenced by several factors, such as the sources of sediment supply from the continent and the near bottom energetic levels.

A first integrated study on the sediment characteristics of the Portuguese continental shelf was done by Dias (1987) and latter, further developed by Magalhães (1999). According to these authors the non consolidated sedimentary shelf cover is mainly composed by high grain sediment sizes that show high energetic levels near the bottom. The major sedimentary fraction is sand, locally other fractions as gravel, silt and mud, are dominant in the sediments (Figure 5).

The most energetic area of the shelf is considered to be the area between Nazaré and Raso Cape, in which beside the abundance in gravel there is an accentuated lack of silty-clay materials. Contrary to the region between Raso Cape and Setúbal submarine canyon that is protected from the dominant wave direction, show a sedimentary cover in agreement with the lowest energetic levels.

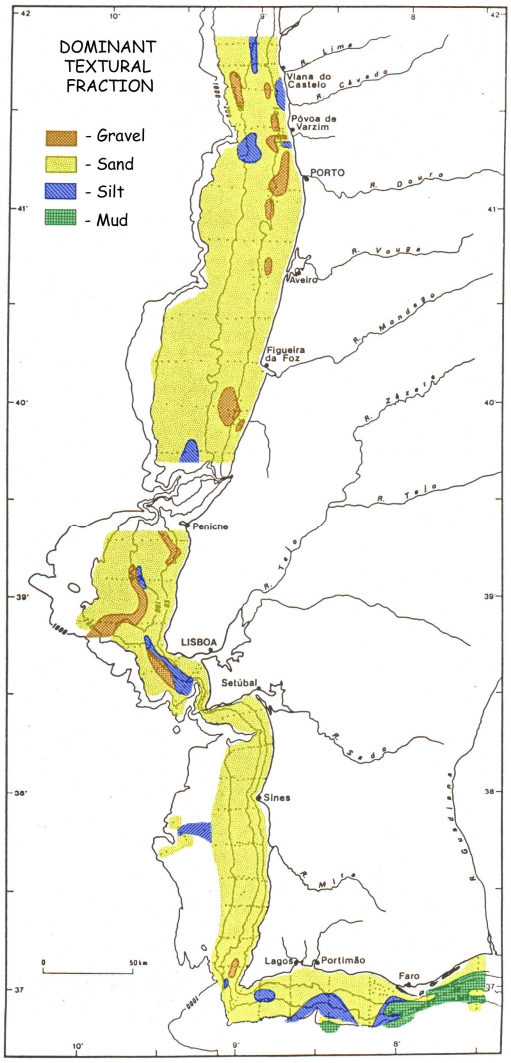

Figure 5 – Distribution of the dominant textural fractions in the Portuguese continental shelf (adapted from Dias, 1987).

As in other shelves world wide the external shelf is finer grained, plus bioclastic and less gravely than the internal shelf, which is also related with the energetic levels and the lower supply of terrigenous particles to the higher depths.

Gravel can only be considered abundant (> 25%) north of Raso cape. This fraction is related with the most important river paleo-mouths and ebb tide deltas, and with paleo-littorals and it can be found in two belts more or less parallel to the coast line. The internal belt, is usually better defined being the gavel of higher dimensions and

terrigenous when compared with the deepest belt. South of Raso cape gravel particles are mainly of biogenic origin.

Sand fraction is more detritic than biogenic. The detritic dominates the internal shelf while the biogenic prevails at depths higher than 80 m.

The silty – mud fraction is deeply related with the exportation by the water bodies and the erosion of bad consolidated cliffs with higher percentage of this kind of material.

2.6 SEDIMENT TRANSPORT AND REMOBILIZATION

Rivers are considered to be the major suppliers of material to the Portuguese continental margin mainly in the northern region. Littoral erosion and in less extent eolian transport and erosion of submerse outcrops, that also contribute with particles to the margin deposits.

These materials will be transported and deposited under the combined effect of processes such as water masses stratification, currents, waves, upwelling and downwelling, etc. A detailed study on this subject was performed by Taborda (1999); he applied a sediment transport model for characterizing the sediment dynamics on the Portuguese continental shelf.

Waves are considered to be the major process for sediment remobilization or resuspension (Dias, 1987; Magalhães, 1993, 1999; Taborda, 1993, 1999; Vitorino *et al.*, 2002a, 2002b). Once overcome the shear erosion velocity, the particles suspended near the bottom will start moving and finally being transported, when over the influence of a current.

Studies performed by Magalhães (1999) on the potential for wave remobilization on the Portuguese shelf considering most frequent wave conditions and storm conditions for the Portuguese coast (see also section 2.3), reveal that particles from the littoral and from fine deposits that exist on the middle-shelf are remobilized under the most frequent wave conditions. Under storm conditions, the majority of the shelf and continental slope particles are remobilized. He also observed that silt, fine and very fine sand are frequently remobilized in deeper waters, but with less frequency. The coarse sand fractions are frequently remobilized in the existent deposits on the internal

and middle shelf; these materials are only remobilized from the external shelf in exceptional conditions.

Chapter 3

SUBMARINE CANYONS

3.1 INTRODUCTION

A **submarine canyon** is a steep-sided valley on the sea floor of the continental slope. While many submarine canyons are found as extensions to large rivers, others don't have such association. Canyons cutting the continental slopes have been found at depths greater than 2000 m below sea level. They are formed by powerful turbidity currents, triggered by volcanic and earthquake activity. Many submarine canyons continue as submarine channels across the continental rise and may extend for hundreds of kilometres.

Submarine canyons are considered to be preferential pathways for shelf-slope exchanges. Suspended sediment concentrations inside submarine canyons are many times higher than concentrations present at comparable locations on the adjacent open-slope areas (Baker, 1976; Schmidt *et al*., 2001; van Weering *et al*., 2002; Puig *et al*., 2003; Stigter *et al*., 2007; Trunchetto *et al*., 2007).

The processes that feed canyon heads and transport sediment along their axis are also of great diversity, depending primarily on the type and amount of sediment that reaches the canyon, and on the oceanographic regime and its impact in the canyon area (Hickey *et al*., 1986; Gardner, 1989; Durrieu de Madron, 1994; Trincardi *et al*., 2007).

The amount of sediment transferred off-shelf can determine the type of transport processes in the submarine canyons. According to Palanques *et al*. (2008), some authors have categorized sediment transport processes in submarine canyons into two types: gravity-driven turbidity currents and flow-driven resuspension and transport events. Nowadays, the most frequent processes monitored in submarine canyons by moored instruments are flow-driven resuspension and transport events. Several mechanisms can produce these flows, such as storms, internal waves, tidal motions and dense shelf water cascading (Gardner, 1989; Mulder & Syvitski, 1995; Okey, 1997; Puig & Palanques, 1998; Puig *et al*., 2004; Palanques *et al*., 2006; Canals *et al*., 2006).

So, the transport of sediment in every canyon is unique due to the specificity of hydrodynamic setting and topographic features. Observational data and numerical simulations are thus needed in order to describe the multiplicity of dynamical processes and shelf-slope exchanges in canyon environments.

3.2 PROCESSES THAT MAY INFLUENCE SEDIMENT TRANSPORT IN A SUBMARINE CANYON

3.2.1 Turbidity Currents

Turbidity current is an influx of rapidly moving, sediment-laden water down a slope into a larger body of water. It is also called a density current because the suspended sediment results in the current. It has a higher density than the clear water into which it flows. Such currents can occur in lakes and oceans, in some cases as by-products of earthquakes or mass movements such as slumps. The sedimentary deposits formed while the current looses energy are named turbidites and can be preserved as Bouma* sequences.

Turbidity currents are characteristic of areas where there is seismic instability and an underwater slope, especially submarine canyons and trench slopes of convergent plate margins and continental slopes and submarine canyons of passive margins.

The mechanism by which a soft sediment slide or debris flow evolves into turbidity current has been inferred mainly from physical and theoretical modelling (Allen, 1971 in Lewis & Barnes, 1999). A collapsing pile of sediment that moves rapidly down slope rapidly increase its volume by two to six times more, after entraining water via regularly spaced tunnels beneath its overhanging head (Lewis & Barnes, 1999).

As the slope of the flow increases, the speed of the current increases. As the speed of the flow increases, turbulence also increases, and the current draws up more sediment.

* The ideal Bouma sequence, result of a turbiditic event, is formed by a sequence of 5 beds, from the top to the bottom: (a) Pelagic and hemipelagic muds; (b) Parallel laminated silts; (c) Cross laminated sands; Ripples; (d) Parallel laminated sands and (e) Massive sands with a gravelly base.

The increase in sediment increases the density of the current, and thus its speed, even further.

According to Heezen & Ewing (1952), some minutes after the 1929 Grand Banks earthquake, off the coast of Newfoundland, transatlantic telephone cables began breaking sequentially, farther and farther downslope, away from the epicenter. Twelve cables were snapped in a total of 28 places. Exact times and locations were recorded for each break. Investigators suggested that a 100 km h^{-1} submarine landslide or turbidity current of water saturated sediments swept 600 km down the continental slope from the earthquake's epicenter, snapping the cables as it passed through them.

The Kaikoura Canyon (New Zeland) is an example of a canyon where turbidity currents are a major process on the transport of sediments to the deep sea (Lewis & Barnes, 1999). Initially, sediments are transported along the shelf by currents and waves to the head of the canyon, earthquakes are the triggering process for the turbidity current to occur.

3.2.2 Surface Waves

In an experiment performed during the winter 2000 (Puig *et al*., 2004) using a bottom-boundary layer tripod deployed at 120 m depth in the northern thalweg of the Eel Canyon (California), it was observed that an increase of the near-bottom suspended-sediment concentrations, that was recorded at the canyon head, was not directly related to the Eel River discharge, but was clearly linked to the occurrence of storms. Bottom-boundary layer measurements revealed that during intensifications of the orbital wave velocity, sediment transport at the head of the canyon occurred as the sediment gravity flowed directed down-canyon. The origin of such flows is not related to the formation of fluid mud on the shelf or to intense wave-current sediment resuspension around the canyon head region. Rather, liquefaction of sediment deposited at the head of the canyon (induced by wave-load excess pore water pressures during storms) combined with elevated slopes around the canyon head appear to be the mechanisms initiating sediment transport. The resulting fluidized-sediment layer can easily be eroded, entrained into the water column, and transported down-canyon as a sediment gravity flow. These storm-induced sediment gravity flows are not only typical of the Eel Canyon but have also been identified in other canyon

such as the Kao-Ping Canyon (Lui *et al*., 2002) and Cap the Creus Canyon (Palanques *et al*., 2006, 2008).

3.2.3 Low frequency currents

Durrieu de Madron (1994) analysed the big variability in shape of the hydrographic structures and the SPM distribution as well as the flow patterns in Grand-Rhône canyon in the Gulf of Lion (Mediterranean). Some of the observed hydrographic patterns suggested a meandering southwestward along-slope current (Liguro - Provençal current) in the lower canyon and an anticyclonic flow in the head of the canyon. These patters were interpreted as resulting from the along-slope circulation response to the canyon topography. SPM results indicate the influence of the along-slope circulation as a major driving force of shelf-slope exchanges. Puig *et al*. (2000) studding another canyon in the NW Mediterranean area, the Foix submarine canyon, reach the same conclusion, considering that near bottom slope currents were the most important process for sediment transport in this canyon.

3.2.4 Barotropic Tide

The barotropic tide is basically a large-scale wave with a wavelength of about 6000 km that sloshes around the ocean basins, while is being forced by the gravitational forces of the moon and sun.

The tidal rise and fall of the sea surface and the associated horizontal currents have been recognized and studied for hundreds of years (Cartwright, 1999). They are important for navigation, generating turbulent mixing near the seafloor, and interacting with other oceanic flows and processes. The vertical movement of the ocean surface, typically of the order of a meter, is mainly associated with barotropic tidal currents. These currents are uniform in what concerns depth, apart from a reduction near the seafloor by bottom friction, as much as for water of constant density. There is, however, a small component of the surface displacement associated with motions of tidal origin in the density-stratified interior of the ocean. These baroclinic, or internal, tides have horizontal currents that are typically identical in strength to the barotropic tidal currents, of order 0.1 m s^{-1} in the deep ocean and 1 m s^{-1} in shallow seas, but have a rich vertical structure.

3.2.5 Internal Tide

Internal tides are internal gravity waves generated in stratified waters by the interaction of surface (barotropic) tidal currents with variable bottom topography. The coupling mechanism remains poorly understood; however, the internal tides are generally most strongly excited at a distinct bathymetric feature such as a seamount or at the continental shelf-break. The main consequence of this interaction is the oscillation of the thermocline with the tidal period, playing an important role dissipating tidal energy and leading to a mixture in the deep ocean (Garrett & Kunze, 2007).

Internal tides induce dramatic vertical displacements of density surfaces in the interior of the ocean, often several tens of meters and even hundreds of meters in some locations. These displacements and the associated currents, perturb the average state of the ocean, and also have major effects in sediment transport (Cacchione *et al*., 2002; McPhee-Shaw, 2006). The most important oceanographic effect of internal tides is that the vertical shear of the horizontal currents associated with them, or with other internal waves into which they transfer their energy, it can be strong enough to lead to instability and turbulence. The associated mixing affects the ocean structure and circulation and drives vertical fluxes of nutrients (Garrett & Kunze, 2007).

Integrated studies using moored current meters, transmissometers, sediment traps revealed internal tides as a major process for sediment resuspension and transport in several canyons, such as the Baltimore Canyon (Gardner, 1989), Monterey Canyon (Rosenfeld *et al*., 1999), and Hudson Canyon (Hotchkiss & Wunsch, 1981).

3.2.6 Cascading

Dense shelf water cascading is a climate-driven oceanographic phenomenon common on high latitude continental margins but also on mid latitude and tropical margins (Ivanov *et al*., 2004).

Physically, this seasonal process of cascading is a specific type of gravity current, sometimes called shelf convection: dense water formed by cooling, evaporation or surface-layer freezing over the continental shelf descends down the continental slope to a greater depth (Cooper & Vaux, 1949; Lane-Serff, 2001 all in Ivanov *et al*., 2004).

According to Shapiro *et al*. (2003 in Ivanov *et al*., 2004), the life cycle of the cascades is subdivided into different phases. The *pre-conditioning stage* is the stage when dense water is accumulated on the shelf and a density front is formed. The *short active stage* corresponds to the period when the leading edge of the dense water accelerates down-slope. The *main stage* relates to a quasi-steady flow with noticeable down-slope component. The *final stage* is when the descended water spreads isopycnical off the slope, but traces of the cascade may still be detected by inclined isopycnical over the slope.

The Gulf of Lions is one of the regions in the Mediterranean where this phenomenon occurs almost every year. Winter heat losses and evaporation induced by persistent, cold and dry northerly winds cause densification and mixture of coastal waters. Despite the buoyancy gain induced by freshwater inputs, once denser than surrounding waters, surface waters over the shelf sink, overflow the shelf edge and cascade downslope until they reach their equilibrium depth. The preferential cyclonic circulation of the coastal current and the narrowing of the shelf at the southwestern end of the Gulf cause most of the off-shelf sediment transport during dense shelf water cascading events to occur through the Cap de Creus Canyon (Palanques *et al*., 2006, 2008; Ogston *et al*., 2008). Dense shelf water cascading in the Gulf of Lions submarine canyons can reach high current speeds and transport coarse particles which are able to generate meter thick sandy deposits in canyon head environments (Ogston *et al*., 2008).

3.3 THE NAZARÉ CANYON

3.3.1 Introduction

The Western Iberian Margin is characterized by a narrow shelf ranging from 25 to 50 km, with several canyons cutting the slope. The most noticeable of these structures is the narrow deep canyon of Nazaré, one of the largest canyons in Europe (Figure 3). A 227 km long *gouf* like structure (Vanney & Mougenot, 1990) that cuts the continental shelf in a west-east direction almost all the way to the coast line (approximately 0.3 km apart). The canyon floor decreases from a depth of 100 m at the head down to a depth

of 5000 m. The average slope of the canyon axis is 2.2% and the maximum is 8.2% (Gomes, 2001-2002).

Canyons that incise the shelf, as the Nazaré canyon, are of particular importance because their presence drastically alters the regional bathymetry by reducing the distance between terrestrial sediment sources and the shelf break, introducing steep slopes closer to the shore line and intersecting the along-shelf sediment transport system.

In the case of the Nazaré canyon the littoral along-shore sediment transport from the northern shelf (estimated in $1x10^6$ m^3 y^{-1} (Oliveira *et al*., 1982; Taborda, 1993)), has been recognized as the major factor for the active and marked thalweg erosion and canyon head retreat (Duarte & Taborda, 2003).

Nazaré canyon is considered to have a strong structural origin (Vanney & Mougenot, 1990; Gomes, 2001-2002). The inexistence of a major river aligned with the head of the canyon helps to support this idea.

A detailed bathymetry of the Nazaré canyon head is presented in Duarte *et al*. (2000) and Duarte & Taborda (2003). The canyon head morphology shows a meandering thalweg limited laterally by almost vertical walls, around 25 m high, dominated by a gullied relief, showing an excess of active slope retreat (Duarte *et al*., 2000; Duarte & Taborda, 2003).

Studies performed under the Eurostrataform project permitted to divide the Nazaré canyon in 3 major areas (Figure 6) (Eurostrataform, 2006a). The upper part of the Nazaré Canyon is a sharp V-shaped valley; it is deeply incised into the shelf and steep upper slope, descending from the shore to 2700 m depth over a length of 70 km measured along the canyon axis. The middle part of the canyon is a broad meandering valley with terraced slopes and a narrow V-shaped axial channel, incised into the middle slope. It descends from 2700 to 4000 m depth over 50 km length. The lower canyon, located on the lower continental slope, is a flat-floored valley with one or two incised axial channels. The lower canyon valley descends very gently from 4000 to 5000 m depth over a length of 100 km; its flat floor gradually increases in width from about 3 km to over 15 km at the mouth of the canyon (de Stigter *et al*., 2007).

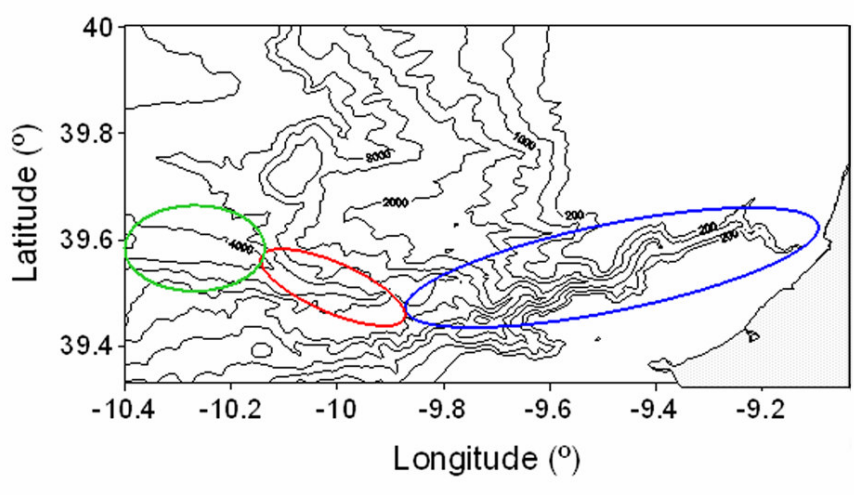

Figure 6– Ellipses correspond to the canyon divisions. Blue is Upper Canyon, Red the Middle Canyon and Green the Lower Canyon.

3.3.2 Canyon Dynamics

During the EUROSTATAFORM project the team from the NIOZ (Netherlands institute for sea research) made several deployments (Figure 7) using a BOBO (Bottom Boundary) benthic lander, developed by the NIOZ. Records of near-bed current dynamics demonstrate the presence of moderate strong tidal currents in the upper and middle canyon, directed predominantly along the canyon axis and typically alternating in up-canyon and down-canyon direction with a semi-diurnal frequency (de Stigter *at al*., 2007). Maximum current speeds observed during a short 2-day deployment at 343 m were 30–35 cm s^{-1}. When the current speed exceeded a threshold of about 25 cm s^{-1}, sharp increases in SPM concentration were noticed, which rapidly dropped off upon waning of the current.

During a 9-day deployment at 1126 m, current speed remained most of the time below 15 cm s^{-1} and only rarely exceeded the 20 cm s^{-1}.

During a deployment of 8 months at 3010 m depth in the middle canyon, current speed showed a very regular semi-diurnal variation, as well as a distinct spring–neap tidal cycle on the longer term. Spring-tide current speed maxima reached 25–35 cm s^{-1}. Sharp increases in SPM concentration occurred regularly when speeds exceeded 15–20 cm s^{-1}. Weaker currents were measured in the lower canyon. During a 6-month

deployment at 4298 m, current speed showed semi-diurnal maxima of 10–15 cm s^{-1}. Most of this period, SPM concentration was very low, showing no appreciable variation related to current speed.
In the canyon mouth at 4975 m depth, a 12-month deployment recorded current speeds never exceeding 5 cm s^{-1}.

Currentmeter moorings deployed at 1600 m and 3200 m depth in the canyon axis by the Portuguese Hydrographic Institute revealed that the low frequency circulation in Nazaré Canyon is rather complex, reflecting several of the key characteristics of this canyon. The Nazaré Canyon is under the influence of different forcing mechanisms, which act at the surface (wind forcing, interactions with shelf circulation) or at intermediate and deep levels (interactions with intermediate slope currents at the canyon mouth). The canyon topographic meandering is also expected to impose important dynamical constraints to the canyon ocean circulation (Eurostrataform, 2006a).
The current measurements collected from the upper canyon revealed that low frequency currents at levels above the canyon rim (160 m depth) were predominantly aligned in the along-shelf direction and correlated with the local winds. Below the canyon rim, the low frequency currents are strongly polarized in the along-axis direction.
These observations suggest that the canyon response, directly forced by the local winds and by interactions with the shelf circulation, occupies the layers from the depth of the canyon rim to about 500 m depth. This response is complex, including an along-axis flow in the upper levels (150 m) and a compensatory flow in the deeper levels (400 m).
At the Mediterranean Water (MW) depths (800-1200 m), the low frequency flow in the upper canyon is no longer correlated with the wind forcing fluctuations, and instead it shows tendency for up-canyon flow. Below the MW levels to near-bottom levels, the current measurements at the upper canyon revealed a persistent down-canyon low frequency flow. This deep circulation found in the outer parts of the upper Nazaré canyon must play an important role in the exportation of particulate matter (Eurostrataform, 2006a).

3.3.3 Particle Fluxes and Recent Sedimentation

Along the EUROSTRATAFORM project mass flux rates were determined (de Stigter *et al*., 2007) in the axis of the Nazaré canyon (Figure 7).

At the upper canyon, the BOBO lander deployed at 343m depth register an average horizontal SPM flux of 12.4×10^3 gm^{-2} d^{-1} in the down-canyon direction and 6.8×10^3 gm^{-2} d^{-1} in the up-canyon direction, implying a net down-canyon SPM transport of 5.6×10^3 gm^{-2} d^{-1}. Sediment deposition rate measured in the sediment trap was 64.5 gm^{-2} d^{-1}. At 1126 m, it was recorded an average flux of 141.5 gm^{-2} d^{-1}.

At the middle canyon during the deployment at 3010 m, average horizontal SPM fluxes of 1.9×10^3 gm^{-2} d^{-1} down-canyon and 0.7×10^3 gm^{-2} d^{-1} up-canyon imply a net down-canyon SPM transport of 1.2×10^3 gm^{-2} d^{-1}. Sediment deposition rate measured in the sediment trap recorded an average flux of 9.2 gm^{-2} d^{-1}.

In the lower canyon during the BOBO deployment at 4298 m, SPM concentration was very low, showing no appreciable variation related to the speed of the current. Horizontal SPM fluxes in the order of 0.1×10^3 gm^{-2} d^{-1} both in a down-canyon and up-canyon direction imply negligible net SPM transport. Sediment deposition rate measured in the sediment trap recorded an average flux of 0.9 gm^{-2} d^{-1}. In the canyon mouth at 4975 m depth, the deposition flux, on an average of 30- day intervals, was between 0.1 and 0.2 gm^{-2} d^{-1}.

During these deployments in several occasions occasional picks of turbidity and mass flux occurred, some related with the increasing of the current speed, where mass fluxes recorded in the sediment traps increased 5 to 50 times the average of the values measured.

Sediment accumulation rates calculated from 210Pb profiles (de Stigter *et al*., 2007) were highly variable for the upper canyon, ranging between 2 and 76 gm^{-2} d^{-1}. Irregular profiles observed in cores from about 1000 m depth are indicative of a more complex sedimentation history. Conspicuously high accumulation rates of 8–33 gm^{-2} d^{-1} were also found in the middle canyon around 3000 m depth. For the lower canyon cores, relatively low accumulation rates of 0.6 to 0.9 gm^{-2} d^{-1} were calculated.

Concerning the sedimentological characteristics of the SPM according to de Stigter *et al*. (2007), particulate matter in sediment traps in the upper and middle canyon is fine-grained with a distinct unimodal distribution around 10–20 µm. It consists of 12–15% carbonate and 5–6% organic matter. The temporal variation in particle size and composition was low, even during the longer deployments. Particulate matter collected in sediment traps in the lower canyon differed from that of the upper and middle canyon by its smaller particle size and high carbonate content. At 4298 m, the material deposited under conditions of low deposition flux has a unimodal particle size distribution around 5–10 µm and carbonate content of 25–32%. The deepest trap at 4975 m collected material with carbonate content of 32–41% and the organic matter ranged from 6 to 10%.

Cores and video surveys (de Stigter *et al*., 2007) showed the presence of a terrigenous mud drape covering the bottom and lower walls over the entire length of the canyon. Particle size and composition of the surficial mud are strikingly uniform at least down to around 3000 m. The surface sediment of the canyon down to 3000 m had a distinct unimodal particle size distribution around 10–20 µm, and it is composed of about 9–13% carbonate, 4–8% organic matter and 81–87% of inorganic, non-carbonate material. From 3000 m downward to the lower canyon a divergence of particle size with modes both finer and coarser than 10–20 µm becomes apparent, whereas composition becomes more variable too. In a number of cores from the canyon axis the surficial mud layer was only between 5 and 20 cm thick, with underneath massive turbidite sand. Similar results were obtained by Arzola *et al*. (2008) for the lower canyon. According to these latest authors, there are two main types of turbidity current that occur in the canyon: type 1 are small-volume, high-frequency, carbonaceous-and mica-rich turbidity currents that deposit mainly on the shallower intra-canyon terraces from suspended load fallout, and type 2 are large-volume, low-frequency, canyon-flushing turbidity currents that bypass the upper section and deposit mainly in the deeper parts of the canyon and the abyssal plains. Also according to these authors, turbidity currents are the dominant process of sediment transport, erosion and deposition in the lower Nazaré Canyon, evidenced by the dominance of gravity flow deposits and erosive scours throughout the canyon, which have led to the deep incision into the continental shelf and slope.

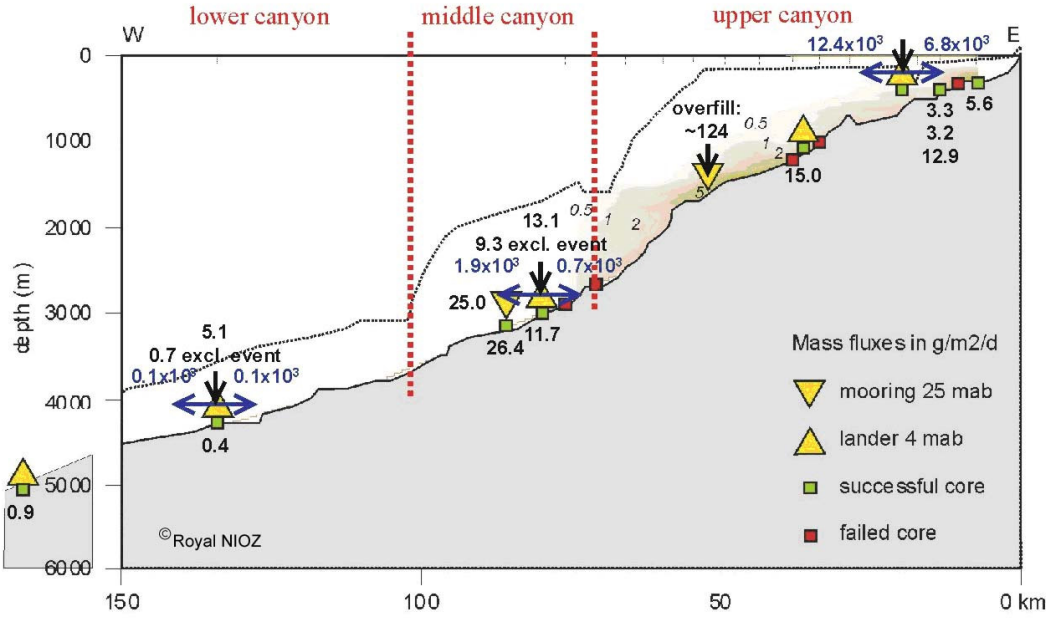

Figure 7 – Axial section of the Nazaré Canyon, showing concentrations of particulate matter in the water (small font), and average mass fluxes of horizontal suspended particulate matter transport up- and down-canyon (blue font), depositional flux in sediment traps (bold black font) and accumulation rate in sediment cores (bold black font). A section of the adjacent shelf and slope N of the canyon is indicated by the dashed line. Sediment trap moorings of CSIC-ICM and IH are indicated by downward pointing yellow triangle (EuroStrataform, 2006a). Figure kindly supplied by Henko de Stigter (Royal NOIZ, NL).

3.3.4 Sediment Sources

Terrigenous sediment supply to the margin is relatively limited, especially because the major rivers Tejo, Douro and Minho debouching on the Portuguese margin have been extensively dammed over the last decades (Dias *et al.*, 2002b). This supply by rivers is done mainly during occasional winter floods.

The erosion of beaches and cliffs mainly in the north of the canyon, are the major suppliers of sediments to the canyon head, which traps the sand transported true littoral drift, which is predominantly directed southwards and, mainly promoted during the winter by the dominantly north-westerly wave regime.

The reworking of shelf deposits (Figure 8) constitutes additional sources of sediment, next to biogenic production. Recent sediment depocenters are found on the inner shelf in the vicinity of river mouths and in mid-shelf mud patches (Jouanneau *et al.*, 1998;

Dias *et al*., 2002; Jouanneau *et al*., 2002), as well as in the upper reaches of the submarine canyons (van Weering *et al*., 2002).

The predominant supply of sediment from the coastal zone is confirmed by the prevalence of terrigenous components in the bulk composition of recent canyon sediments. Mineralogical analysis by Oliveira *et al*. (2007) suggests that the sediments in the upper canyon have origin in the shelf areas, north and south of the canyon, as well as from erosion of the coastal cliffs. Erosion within the canyon is probably a potential additional source of sediment.

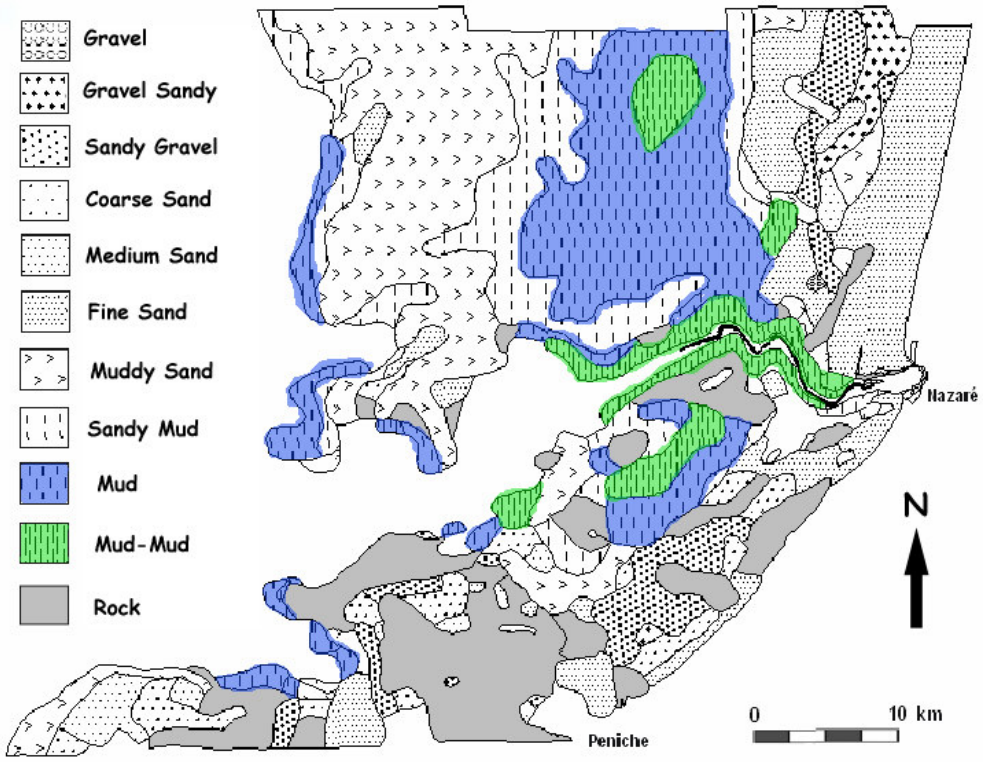

Figure 8 – Spatial sediment distribution of the textural types on the shelf adjacent to Nazaré Canyon on an extension of about 25 Km north and south of the canyon. Blue and Green patches mark the muddy deposits (Adapted form Duarte, 2002).

Chapter 4

FINE SEDIMENT RESUSPENSION PROCESSES IN NAZARÉ CANYON

4.1 INTRODUCTION

In this study numerical modelling tools with information gathered in cruises carried out during the EUROSTRATAFROM and HERMES projects, were combined. Field observations are very important since they permit us to characterize and monitor sea conditions in real time. Nevertheless, they are punctual and sparse in space and time. Numerical models allow us to overcome this limitation, since we can have continuous observations in space and time, being in the present study an essential tool for process studies. In the following sections we describe the nature of the data acquisition and we will present field data results. In the next Chapter we will describe configuration of the numerical experiments, the model results and we will merge model results with field data observations.

4.2 METHODS

4.2.1 Field Methods

Data was collected during five cruises performed on board of the NIOZ Research Vessel PELAGIA: The PE204 (de Stigter & Shipboard Scientific Party, 2003), from 11 to 30 November 2002, the PE218 (de Stigter & Shipboard Scientific Party, 2004) from 11 October to 02 November 2003, the PE225 (de Stigter & Shipboard Scientific Party, 2007a), between 29 April and 24 Mai 2004, the PE236 (de Stigter & Shipboard Scientific Party, 2007b) from 20 April to 18 May 2005 and the PE252 (de Stigter & Shipboard Scientific Party, 2007c) between 30 August and 21 September 2006.

The work performed on board the ship was multidisciplinary; samples were collected for sedimentological, biological, oceanographic and hydrographic purposes.

For the hydrographical characterization of the water column and the study of resuspension processes in the Nazaré canyon in these five cruises CTD (Conductivity, Temperature, Depth) profiles in the water column were preformed in several stations from the surface until 1 meter above the bottom. The sampling stations in the five cruises can be seen in Figure 9.

During the 2002 and 2005 cruises most of the CTD work, in the Nazaré canyon area, consisted in cross canyon sections. In 2003 an along canyon axis section was performed. In 2004 a few stations were occupied around the 2000 m depth and finally in 2006 the work was centred not in the canyon itself but in the margin surrounding the canyon.

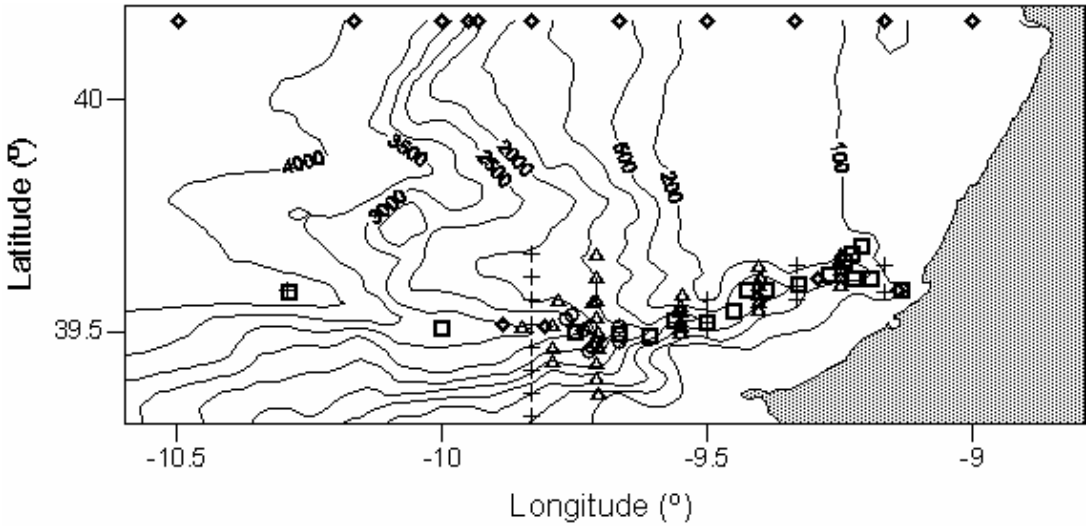

Figure 9 – Location of the CTD stations performed during the five cruises, 64PE204 (✚ - 2002), 64PE218 (□ - 2003), 64PE225 (○ - 2004), 64PE236 (△ - 2005) and 64 PE252 (◇ - 2006).

During the five cruises a CTD /Rosette system was employed for temperature, salinity, turbidity and fluorometry profiling in the water column, and also for collection of water samples for analysis of suspended particulate matter. The system used was equipped with a SBE-9 plus underwater unit, SBE-4 conductivity sensor, SBE-3 temperature sensor, SeaTech transmissometer, Chelsea fluorometer, SeaPoint optical backscatter (OBS)/turbidity sensor, Biospherical PAR sensor, a rosette sampler with a NIOZ-made multivalve bottle controller and 22 Noex bottles of 10 L each.

As a quick check on reliability of Rosette water samples, the temperature of the water samples was measured immediately upon retrieval on deck with an infrared

thermometer, and compared with the temperature recorded by the CTD. In addition, small volume subsamples of rosette samples were collected and stored at 4ºC for later analysis of dissolved silica.

Suspended particulate matter (SPM) was collected to determine the concentration and composition of suspended matter at different levels in the water column, and to allow conversion of water column turbidity measurements into SPM weights (Figure 10).

Figure 10 shows the linear correlation between the OBS measurements (turbidity) and SPM measurements for the 2002, 2003, 2004 and 2005 cruises. For all the cruises the determination coefficient (R^2) is near 1, although the slope of the line is variable. This variation normally is correlated with the composition of the particles.

Previous studies performed in this margin (Oliveira, A., 1994; Garcia, A.C. 1997) showed a strong seasonal composition for SPM in the water column, with a terrigenous component (heavier) dominating during autumn and winter, showing a correlation near 1 and a biological component (lighter) prevailing during spring and summer, with a correlation between 0.5 – 0.7. Nevertheless, when analysing these data no seasonality is observed, for example while in October 2003 the correlation between OBS/SPM is around 1/1 in November 2002 is 0.5/1. Due to this difference it was decided to calculate the average for the four slopes, reaching a correlation of 1FTU = 1.56 mg l^{-1}, value to be considered in this work.

Nepheloid layers are highly concentrated zones in the water column found near the surface and bottom, termed the surface nepheloid layer (SNL) and bottom nepheloid layer (BNL), respectively. The surface nepheloid layer normally is dominated by organic matter from primary production, whereas the bottom nepheloid layer consists primarily of inorganic material resuspended from the bed (McCave, 2002). In some cases the resuspension of sediments at changes in slope gradient coupled with eddying motion in the off-slope flow field causes the suspended material to be dispersed offshore in relatively thin turbid layers termed intermediate nepheloid layers (INL) (McCave, 2002).

Bottom Nepheloid Layers (BNLs) and Intermediate Nepheloid Layers (INLs), as well as clear water levels and surface water from 5 m depth were sampled.

From each water sample, two 5-liter subsamples were drawn off without previous homogenization of the Noex bottle. The subsamples were filtered on board through

pre-weighed Poretics 0.4 µm polycarbonate filters, applying under pressure with a vacuum pump. After filtration, salt water was removed by passing about 10 ml of milli-Q water through the filters, after which the filters were stored in plastic petridishes and dried at ambient temperature for further analysis on land (sediment concentration and properties).

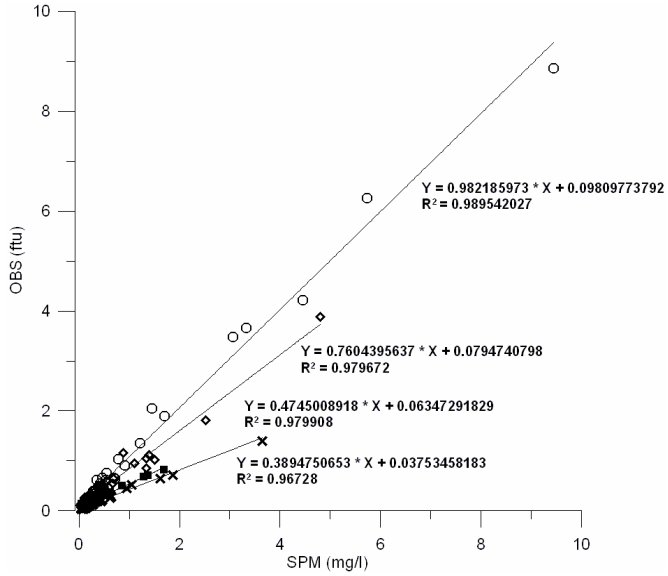

Figure 10 – Linear correlation between optical backscatter (OBS) measurements and suspended particulate matter (SPM) measurements, for four cruises 64PE204 (X – 2002 - November), 64PE218 (O- 2003 - October), 64PE225 (□- 2004 – April/Mai), 64PE236 (◇ - 2005– April/Mai). 1 FTU = 1.56 mg l^{-1}.

In three of the five cruises some stations were repeated (Figure 11) for a tidal cycle to observe the effect of the tide on the water column and also to search for the presence of internal tides and their effect on sediment resuspension. During the 2002 cruise two stations located in the upper canyon axis were chosen, Station 41 and Station 38 (in blue in Figure 11) and repeated, intercalated, for the same tidal cycle. Due to the time taken in transit from one station to the other it was only possible to make 3 surveys in each station.

In 2005 station 11 at 2000 m deep at the canyon axis was repeated every hour during a period of 6 hours.

During the 2006 cruise, four stations in the canyon axis were repeated: station 42, station 41, station 37 and station 38 (in orange Figure 11). Stations 38 and 37 were

sample intercalated along 24 hours. Station 41 and 42 were sampled during 13 hours each with an interval of half an hour between casts.

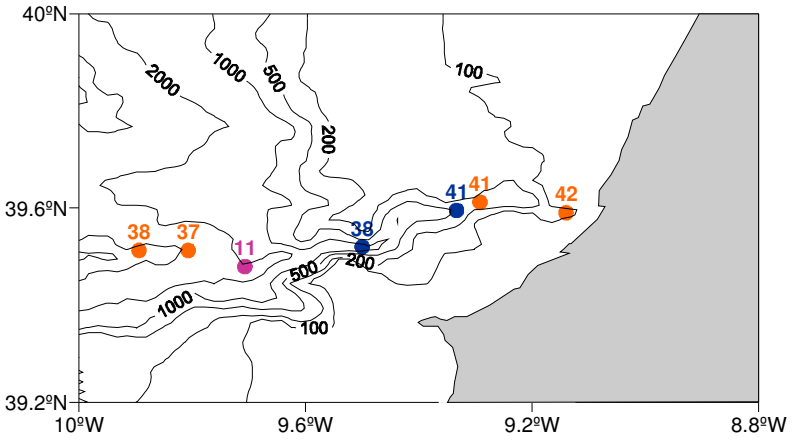

Figure 11 – Location of the repeated stations for the 2002 (blue), 2005 (violet) and 2006 (orange) cruises.

4.3 RESULTS

4.3.1 Atmospheric and wave conditions

In order to have an idea of the atmospheric and wave conditions during the cruises periods a brief analysis of these conditions will be presented. Data are forecasts of the Portuguese Meteorological Institute published in "Diário de Notícias" diary newspaper.

4.3.1.1 PE204 Cruise (2002)

For the 2002 cruise period, between the 11th and the 30th of November (Table 1), the average minimum temperature was around 10ºC and the maximum about 15ºC, for the Nazeré region. The wind was predominantly from the SW quarter with velocities above the 15 km h^{-1} (superior limit of weak winds) reaching sometimes more than 35 km h^{-1} (superior limit of the moderate winds) and in some occasions above 70 km h^{-1}. The sky was dark most of the days with occurrence of precipitation, varying from showers to very intense. Waves were mainly from W with average heights of 4-5 m in most of the days, and reaching 8 m height in the windiest days.

Just as a curiosity the accident with the oil tanker "Prestige", in the Galicia Margin took place on the 13th November.

4.3.1.2 PE218 Cruise (2003)

For the 2003 cruise period, between the 11th and the 31st of October (Table 2), during the fist half of the cruise the weather conditions were quite pleasant. The sky was not very cloudy with few occurring showers once in a wile and very week wind, with average minimum temperatures of 15ºC and maximum surrounding 21ºC. The waves were predominantly from the NW quarter with heights around 1.5 m average.

In the second half of the cruise the wind increased reaching more than 90 Km h^{-1} by the end of the cruise, with variable directions dominating the winds from south. The cloud cover increased and precipitation occurred, all followed by a decrease of the air temperatures with an average minimum of 10ºC and a maximum of 15ºC. The waves became predominantly from SW with heights increasing progressively reaching more than 6 m by the end of the cruise.

4.3.1.3 PE236 Cruise (2005)

For the 2005 cruise period, between the 20th of April and the 18th of May (Table 3), the weather conditions were quite stable. The average minimum air temperature was around 10ºC and the maximum in the order of 23ºC. In the clear days the wind was week (< 15 km h^{-1}) to moderate (15-35 km h^{-1}) and predominantly from NW. The waves, also from NW, had heights around 1.5 m. In the most cloudy and sometimes rainy (showers) days, the wind was predominantly from the SW quarter but still weak to moderate. The waves were also from southwest with a small increase in height reaching 2.5 m.

4.3.1.4 PE252 Cruise (2006)

For the 2006 cruise period, between the 01st and the 21st of September (Table 4), the atmospheric and wave conditions were quite good. The sky was clear becoming progressively cloudier by the end of the cruise. The temperatures were very high in the

beginning of the cruise with an average minimum of around 16ºC and the maximum about 30ºC decreasing in average 4ºC as the clouds started to show up. The wind was moderated most of the time and predominantly from NW (upwelling favourable) as well as wave direction with heights ranging from around 1-1.5 m in the first half of the cruise increasing to around 2.5 m in the second half.

Table 1 – Meteorological data and wave climate for the period of 11th to 30th November 2002. Data are forecasts of the Portuguese Meteorological Institute published in "Diário de Notícias" daily newspaper.

Date	Temperature		Wind		Sky	Waves	
Day	Min (ºC)	Max (ºC)	Intensity (km h-1)	Direction		High (m)	Direction
11	15	18	15-35	W		2-4	W
12	10	16	15-35	SW		2.5–3.5	W
13	11	15	> 35	SW		5	W
14	10	14	> 35	SW		4-5	W
15	10	14	> 35	NW		4-5	W
16	9	14	15-35	SW		4-5	NW
17	10	16	15-35	NW		4-5	W
18	10	17	15-35	SW		4-5	W
19	10	13	15-35	SW		2-3	W
20	7	14	> 35	S		3	W
21	11	14	> 35	W		4-7	W
22	11	14	> 35	SW		5.5–8	W
23	9	13	15-35	SW		5-6	W
24	8	14	15-35	S		3-4	W
25	4	13	<15	W		3-4	W
26	9	13	15-35	S		2.5-3	SW
27	10	16	15-35	SW		3-4.5	SW
28	10	14	<15	W		4-4.5	W
29	10	16	15-35	NW		4-5	W
30	10	16	15-35	NW		3.5-2.5	NW

Table 2 - Meteorological data and wave climate for the period of 11th to the 31st October 2003. Data are forecasts of the Portuguese Meteorological Institute published in "Diário de Notícias" daily newspaper.

Date	Temperature		Wind		Sky	Waves	
Day	Min (°C)	Max (°C)	Intensity (km h^{-1})	Direction		High (m)	Direction
11	16	25	<15	-		1-1.5	NW
12	16	22	<15	-		1-1.5	NW
13	15	22	<15	-		1.5	NW
14	10	23	<15	-		1.5-2	NW
15	15	25	<15	S		1-1.5	W
16	16	24	<15	-		1-1.5	W
17	15	21	<15	-		1-1.5	W
18	10	23	15-35	S		2	W
19	15	18	15-35	S		2-3	SW
20	14	18	<15	W		2	SW
21	14	18	15-35	N		1.5-2	NW
22	9	15	15-35	NW		1.5-2.5	NW
23	8	15	15-35	NW		1.5-2.5	NW
24	5	14	15-355	E		2-3	SW
25	10	12	>35	S		1-2	NW
26	10	15	>35	SW		2-3	SW
27	9	15	15-35	S		2.5-3.5	SW
28	12	20	15-35	S		2-3	SW
29	12	20	15-35	NW		1.5-2.5	SW
30	7	17	>35	W		6-7	SW
31	11	14	>90	W		6-9.5	NW

Table 3 - Meteorological data and wave climate for the period of 20th April to 18th May 2005. Data are forecasts of the Portuguese Meteorological Institute published in "Diário de Notícias" daily newspaper.

Date	Temperature		Wind		Sky	Waves	
Day	Min (ºC)	Max (ºC)	Intensity (km h^{-1})	Direction		High (m)	Direction
20	10	18	<15	W		1.5-2	NW
21	12	19	<15	W		2-3	NW
22	10	17	<15	W		1.5-2.5	NW
23	11	18	<15	W		2-2.5	W
24	7	17	15-35	NW		2.5	W
25	7	19	15-35	NW		1.5-2	NW
26	7	22	<15	W		1.5	NW
27	7	23	15-35	W		1-2	W
28	12	24	15-35	NW		1.5-2	W
29	7	27	15-35	NW		1.5	W
30/04	8	24	<15	S		1-1.5	W
1/05	13	21	15-35	SW		2-3	SW
2	13	22	15-35	SW		2-2.5	SW
3	9	23	15-35	W		3	NW
4	8	23	15-35	NW		2	NW
5	8	23	15-35	N		2-3	NW
6	10	29	15-35	E		2	NW
7	7	27	15-35	NW		1	NW
8	7	27	<15	W		1	NW
9	12	27	<15	W		2	SW
10	7	22	<15	S		1	NW
11	12	22	15-35	S		1-1.5	NW
12	13	20	15-35	W		1-2	SW
13	12	21	15-35	W		1.5-2	SW
14	11	20	15-35	W		2	W
15	9	20	15-35	SW		1-2	W
16	10	18	15-35	W		2.5-3.5	W
17	8	22	>35	NW		2	NW
18	8	23	15-35	NW		1.5-2	W

Table 4 - Meteorological data and wave climate for the period of 1st to 21st September 2006. Data are forecasts of the Portuguese Meteorological Institute published in "Diário de Notícias" daily newspaper.

Date	Temperature		Wind		Sky	Waves	
Day	Min (ºC)	Max (ºC)	Intensity (km h^{-1})	Direction		High (m)	Direction
1	11	31	15-35	NW		1-2	NW
2	16	30	15-35	NW		1-2	NW
3	15	32	15-35	NW		1.5-2	NW
4	16	35	15-35	NW		1.5	NW
5	12	34	15-35	NW		1-1.5	NW
6	15	32	15-35	NW		1.5	NW
7	14	32	<15	NW		1-1.5	NW
8	18	32	15-35	NW		1	NW
9	18	32	15-35	NW		1-1.5	NW
10	15	31	15-35	NW		1	NW
11	15	32	15-35	NW		1-1.5	W
12	16	29	15-35	NW		1	W
13	17	27	15-35	W		1.5-2.5	NW
14	13	26	15-35	NW		3.5	NW
15	12	24	15-35	NW		2-3	NW
16	12	24	15-35	NW		2.5	NW
17	10	28	<15	W		2-2.5	NW
18	12	28	<15	NW		2	W
19	14	28	<15	NW		2-3	NW
20	13	28	15-35	SW		2-3	NW
21	17	23	>35	SW		4.5-6.5	SW

4.3.2 Hydrographic Data and Nephelometry

Temperature (ºC), Salinity (PSU), Density (Kg m $^{-3}$) and Nephelometry (FTU) were analysed for all the 5 cruises performed, during 2002 to 2006, except the 2004 cruise since only a few stations were occupied and all around 2000 m depth (Figure 9).

4.3.2.1 PE204 Cruise (2002)

During the November 2002 cruise CTD casts were performed on a section along the canyon axis and also some cross canyon sections (see Figure 9). Potential temperature and salinity profiles, for all the 2002 stations, revealed a well-defined surface mixed layer (SML) of 100-150 m thick in the most seaward stations. This layer is subjected to high seasonal variability because it depends on the atmospheric conditions and riverine water sources.

Figure 12 represents a Temperature/Salinity diagram for all the stations sampled during the 2002 cruise. We can identify the main water masses present in this region, also referred by several other authors (in Coelho *et al*., 2002) has the structure of the typical water masses for the West Portuguese Margin. The North Atlantic Central Water (NACW) from 100-150 m down to 500 m depth, the Mediterranean Water (MW), from 500-1500 m with a very strong signature (high salinity and temperature values). Below 1500 m, less saline and cold waters indicate the presence of the North Atlantic Deep Water (NADW).

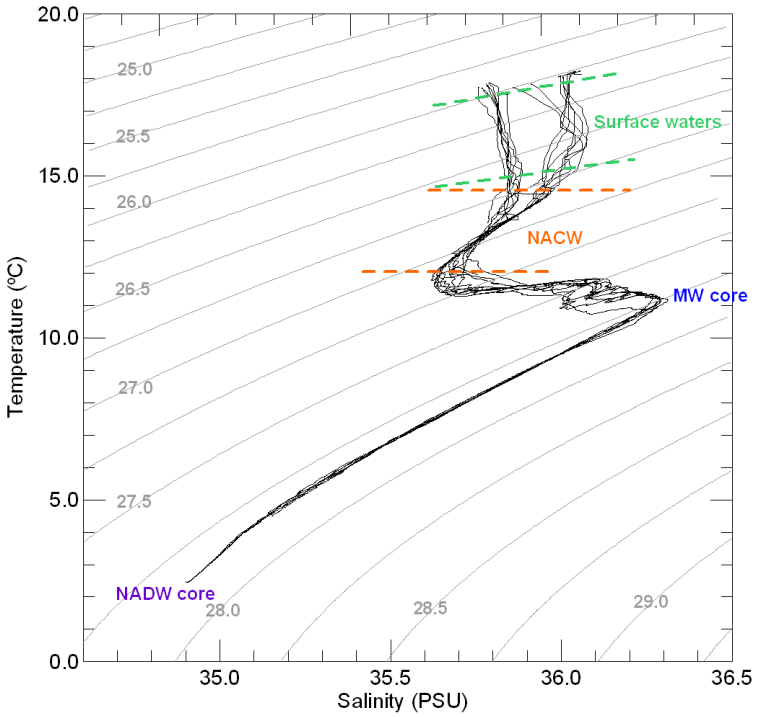

Figure 12 – Temperature/Salinity profiles from CTD stations during the November 2002. It is evident the presence of a surface mixed layer (SML), the north Atlantic central water (NACW), the Mediterranean water (MW) and north Atlantic deep water (NADW), according to van Aken, (2000a,b; 2001).

Figure 13 represents horizontal distribution at surface of CTD temperature, salinity and turbidity measurements for the canyon area during the 2002 cruise. Observations show very homogenous surface water with temperatures ranging between 17º and 18ºC. This homogeneity is confirmed in Figure 14, corresponding to sea surface temperature (SST) AVRHH (left side) and Modis (right side) images. Both images are 7 day average for the period of the cruise when CTD cast were performed.

This homogeneity is also observed in salinity with a variation of only 0.3 PSU, with an E-W gradient from less saline coastal waters to more saline oceanic waters.

The turbidity pattern shows very clear waters (concentrations below 0.1 FTU) in all the canyon area except near the coast over the canyon head, where the Surface Nepheloid Layers (SNL) has concentrations reaching 0.2 FTU.

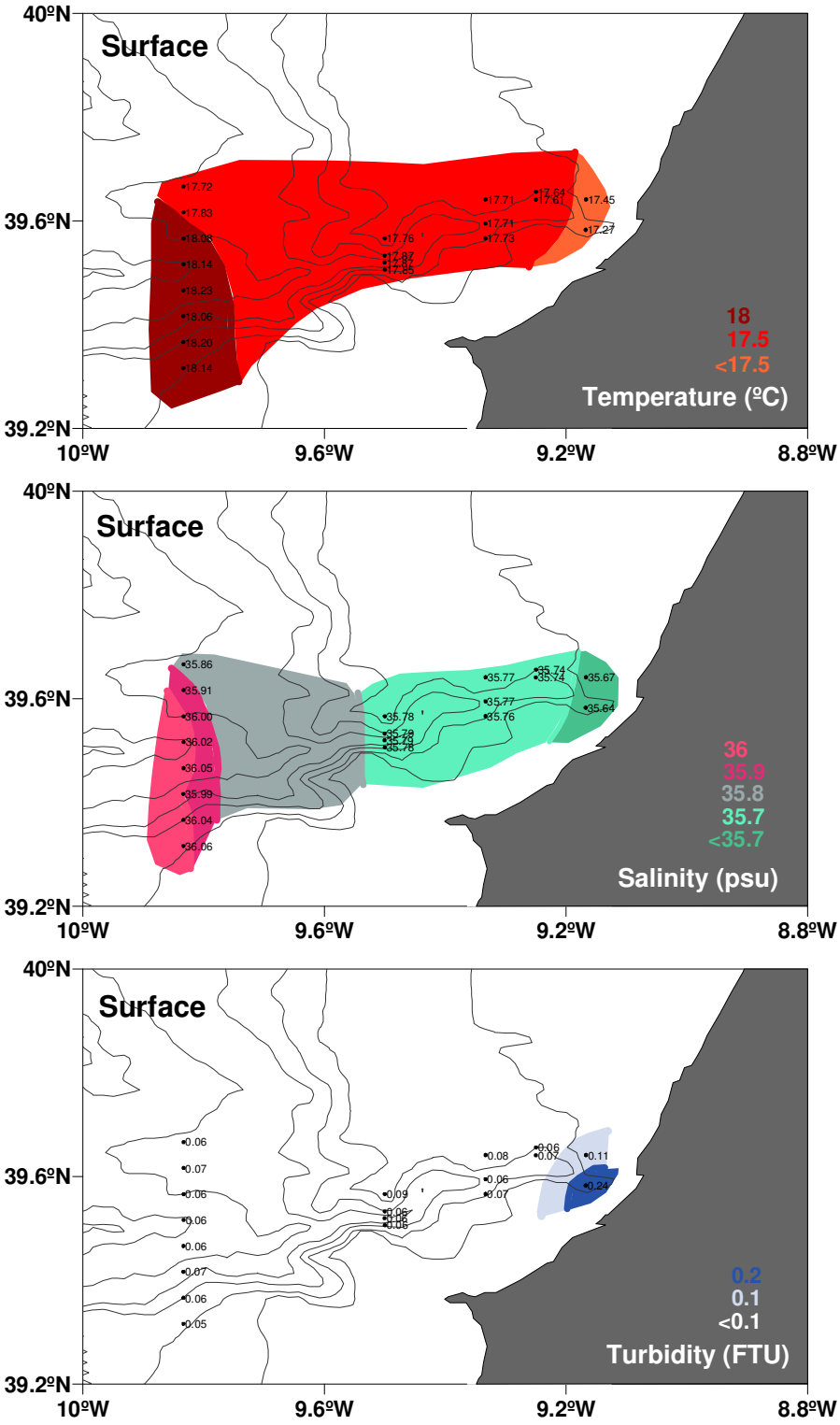

Figure 13 – Horizontal distribution of temperature (ºC), salinity (PSU) and turbidity (FTU) at the surface, obtained from CTD measurements during the 2002 cruise.

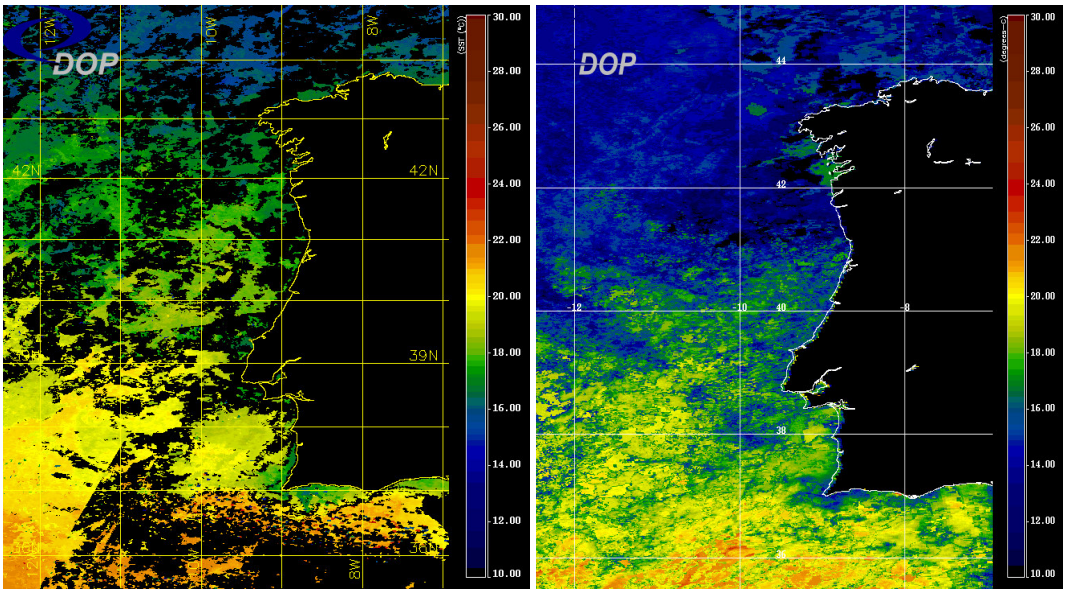

Figure 14 – SST AVHRR (left) and Modis (right) images. 7 day average for the CTD sampling period during the 2002 cruise (09 to 16 November 2002). (http://oceano.horta.uac.pt/detra/) (DOP - Department of Oceanography and Fishery, Azores University).

Figure 15 represents the vertical distribution of the temperature (°C), salinity (PSU), density (Kg m $^{-3}$) and turbidity (FTU) along three cross-canyon sections (A, B and C, from West to East).

The vertical distribution of temperature for the 3 cross sections (Figure 15, 1st column), indicate no significant water temperature differences at surface, as referred, with values ranging between 17° and 18°C in all the covered area. This homogeneous water reaches in depth 50 m, corresponding to well mix water what is confirmed when looking at the density (Figure 15, 3rd column – solid lines) specially in section C (bottom row). The wave height for this period, that was around 4-4.5 m, and the strong permanent winds (Table 1) are responsible for this mixture. At section A (top row) it is visible, between the 1500 m and the 2000 m depth, the fast decrease in temperature, from 11° to 5°C limiting the MW and the NADW, this is confirmed by the salinity (2nd column) where a high gradient can be observe in this area and also by density (solid lines, 3rdcolumn), where the 27.8 kg m^{-3} isopycnal marks the limit between the two water masses.

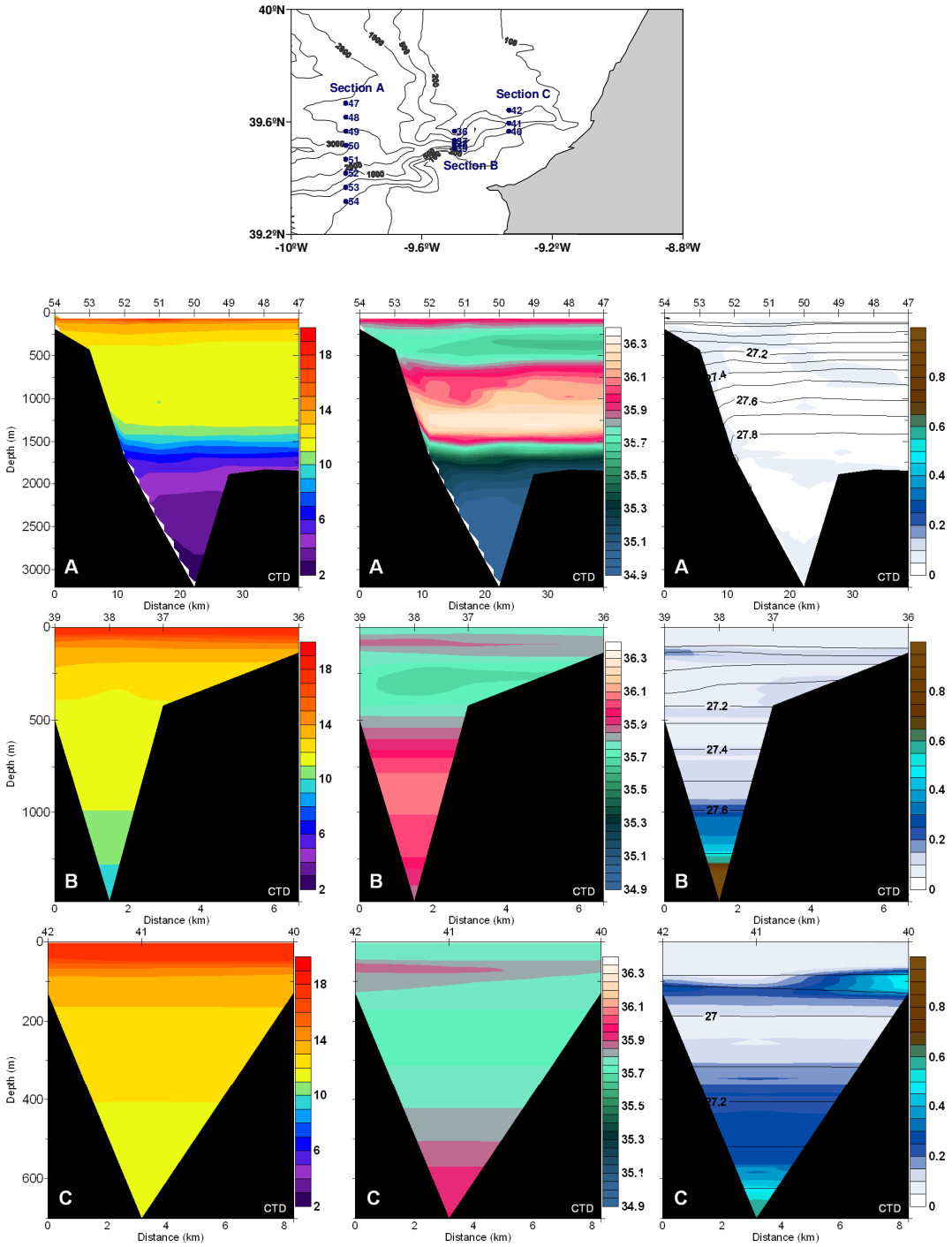

Figure 15 – Vertical distribution, along 3 cross sections A, B and C, obtained during the 2002 cruise, of Temperature (ºC) (1st column), Salinity (PSU) (2nd column), and turbidity (FTU) and density (kg m-3) (3rd column), where contours represent turbidity and solid lines density.

When taking a look at turbidity (contours) in Figure 15 (3rd column) it is observed that the clear surface water reaches the first 100 m depth (limit of the thermocline - SML), where the turbidity values are below 0.1 FTU.

In the deeper and off shore transect (A) the water column is also very clear with values below the 0.1 FTU. Nevertheless, it can still be identified 3 nepheloid layers. A relatively higher turbid bottom nepheloid layer (BNL) at the level of the shelf-break, can be observed in the southern rim of the canyon. Also in the southern wall, at the bottom limit of the MW (~1500 m), an intermediate nepheloid layer (INL) was observed spreading for nearly 15 km across the canyon. This INL extends to the northern wall, where it is centred at 2000 m. It can also be observed in the canyon a BNL occupying the entire canyon axis.

At cross-section B, a mid-canyon transect, it is observed an INL, below the SML around the 150-200 m extending cross canyon. This INL might be an extension over the canyon of a BNL located over the surrounding continental shelf. A BNL at the northern shelf break extending southward is also present between the 300 and the 500 m depth with concentration values around 0.1 FTU. Below the 1000 m depth a progressive increase in turbidity (reaching more than 1.3 FTU) was observed all over the canyon axis. This pattern follows the same distribution as section A (although with a different amplitude – please note the different scales) indicating the presence of a permanent BNL along the axis.

Transect (C) shows an important increase in turbidity generalized through the whole water column. However, a maximum occurred at the shelf break level, on the northern rim. This local maximum (0.5 FTU) was followed by a local minimum (0.1 FTU) and then by a monotonically increase with depth, reaching near the bottom more than 0.6 FTU. Once more the BNL was present in the station at the canyon axis.
In general, for this cruise higher turbidity was found in the narrowest part of the canyon, sections B and C, with the turbidity maximum at mid-canyon where the deepest station reached 1500 m depth. This analysis is corroborated in Figure 16, where

it is represented the near bottom horizontal distribution for CTD temperature (ºC), salinity (PSU) and turbidity (FTU) measurements in Nazaré canyon area during the 2002 cruise. The values correspond to the last CTD measurement, 1 meter above the bottom, for each station. Temperature and salinity represent well the water channelization along the canyon axis, where the warmer and saltier MW (pink) reaches almost the 700 m depth. This mechanism may be responsible for an increase in bottom velocities what may be in the origin of the higher bottom turbidity values found in the narrow part of the canyon axis, with the highest values (above 1 FTU) around the 1500 m depth.

These features are well patent also in Figure 17 and Figure 18, which represent the vertical distribution of the temperature (top) and salinity (bottom) in Figure 17 and turbidity (contours) and density (solid lines) in Figure 18, for the along canyon axis section. Notice that the higher turbidity values are found at the bottom of the MW (pink water mass), where the 27.8 kg m^{-3} isopycnal separates the MW and the NADW. This turbid layer extends along this density interface for more than 20 km long.

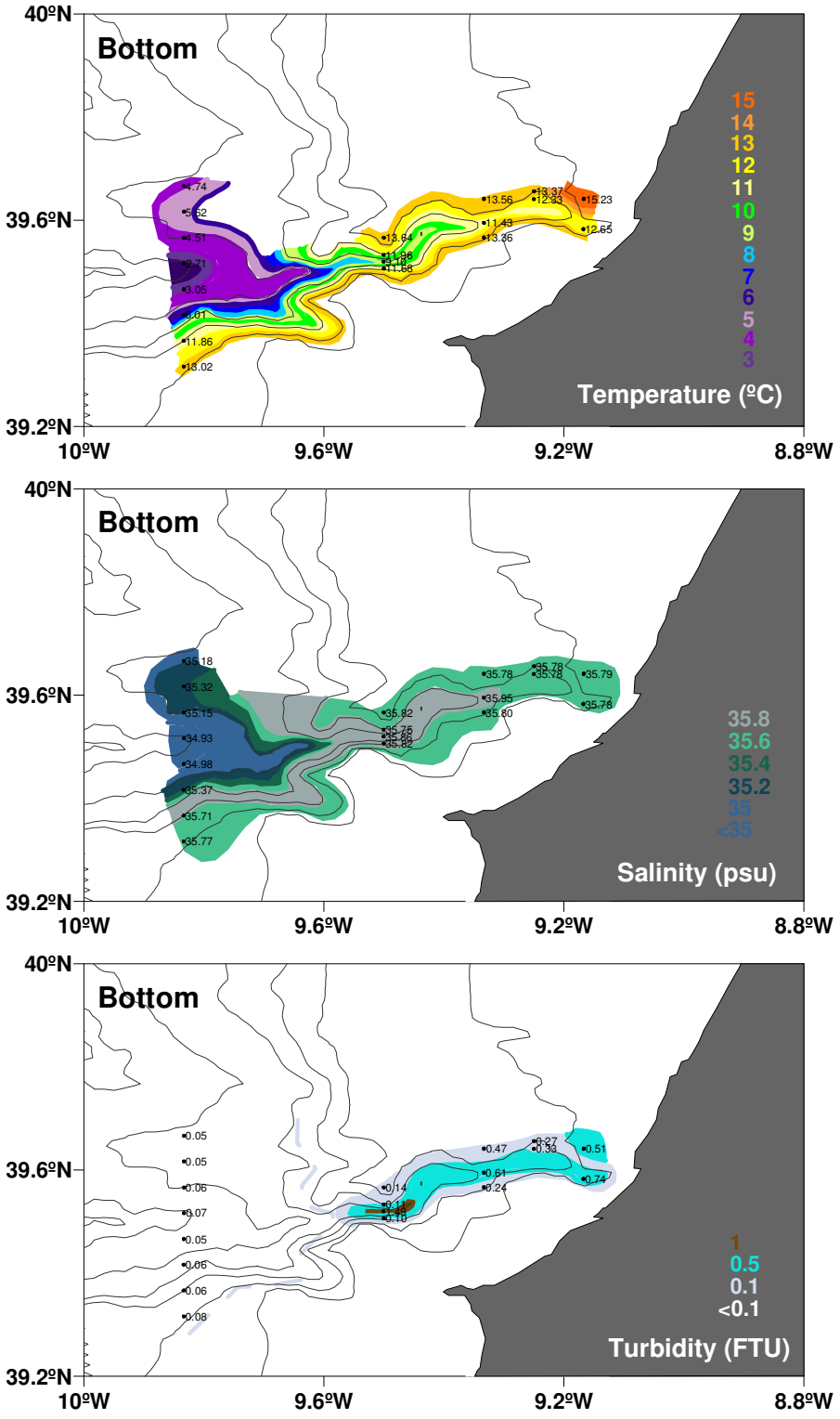

Figure 16 – Horizontal distribution for CTD temperature (ºC), salinity (PSU) and turbidity (FTU) along the bottom layer (1 meter above the bottom for all stations) in the Nazaré canyon during the 2002 cruise.

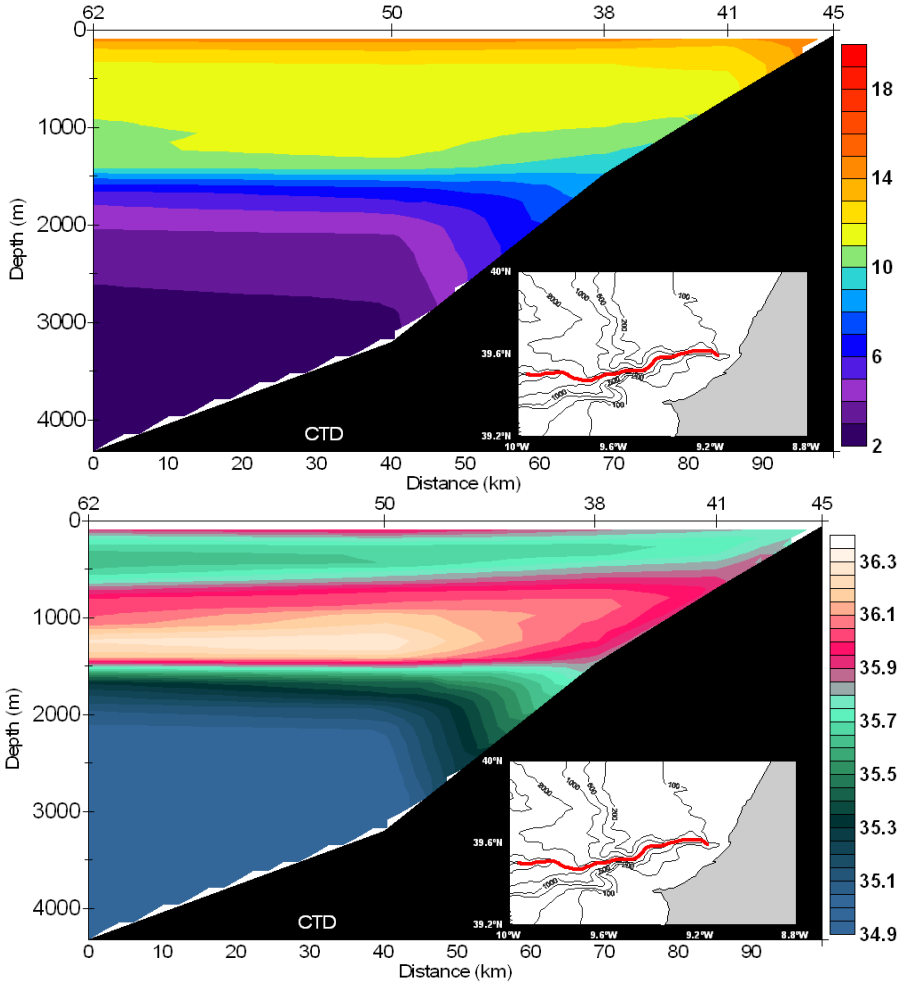

Figure 17 – Vertical distribution of the Salinity (bottom) and Temperature (top), along the canyon axis section, during the 2002 cruise and the respective location.

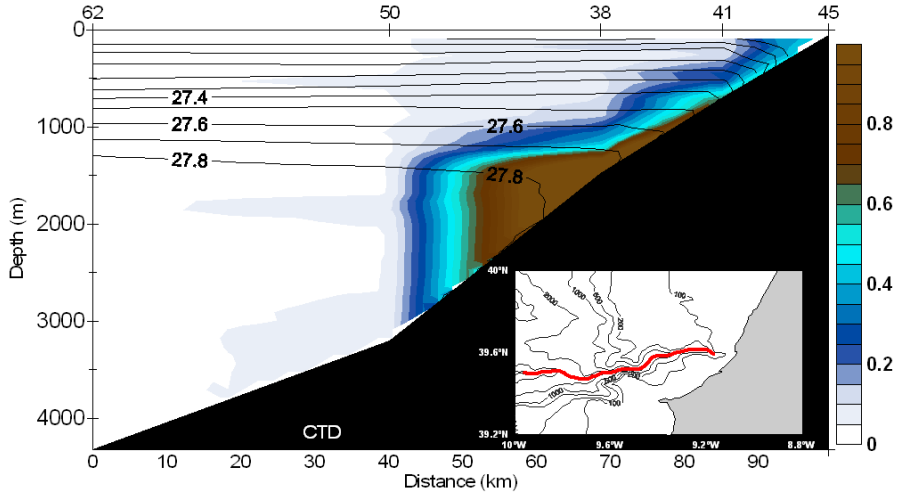

Figure 18 – Vertical distribution of the Density (solid lines) and Turbidity (contours) along the canyon axis section, during the 2002 cruise and the respective location.

To observe the tidal effect on the water column structure, during the 2002 cruise, two stations at the canyon axis (Station 38, at 1600 m and Station 41, at 800 m, Figure 11) were repeated for the same tidal cycle. Figure 19 shows the water column profile for salinity (dashed lines) and turbidity (solid lines) for each cast performed during this tidal cycle, for both stations. By observing the salinity profiles it is possible to notice the vertical displacement of more than 200 m of the maximum salinity at the MW level in the deeper station (station 38). In station 41 this effect can also be observed at the bottom of the SML, but it is less evident.

In station 38 an important BNL is present. Although there is a considerable vertical displacement, the intensity of the nepheloid layer shows little variability. In station 41, on the other hand, the vertical displacement and intensity of the nepheloid layer show a large variability at around 100 m depth.

Since those stations were sampled intercalated for a tidal cycle it was only possible to do 3 surveys in each site. For this reason it is not possible to state that the variability observed in the salinity and turbidity profiles has time scales similar to the semi-diurnal tide, and are a consequence of that process.

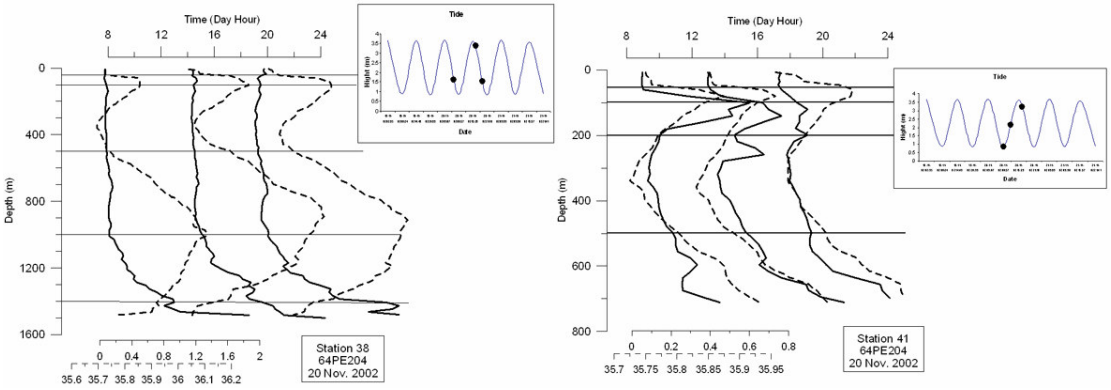

Figure 19 - CTD results for salinity (dashed lines) and turbidity (solid lines) from station 38 and 41 repeated for the same tidal cycle.

4.3.2.2 PE218 Cruise (2003)

As referred previously during the 2003 cruise only a along canyon axis section was performed with the CTD. For that reason no horizontal distributions are presented.

Figure 20, corresponds to SST AVRHH (left side) and Modis (right side) images. Both images are 15 day average of the period of the cruise when CTD casts were performed. In both images it is visible the presence of a coldest (between 16º and 18ºC) coastal front along the Portuguese coast (17º-18ºC) north of Carvoeiro cape and the Galician coast (16º-17ºC) and warmer (around 20ºC in the Nazaré area) oceanic waters.

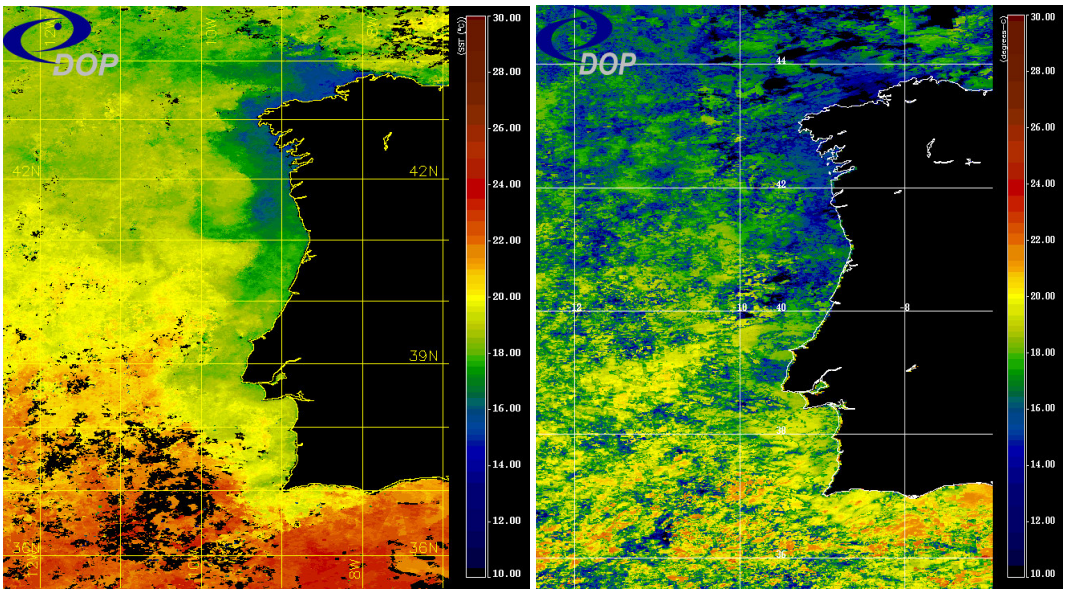

Figure 20 - SST AVHRR (left) and Modis (right) images. 15 day average for the CTD sampling period during the 2003 cruise (13 to 27 October 2003). (http://oceano.horta.uac.pt/detra/) (DOP - Department of Oceanography and Fishery, Azores University).

On Figure 21 it is represented the vertical distribution of the temperature (top) and salinity (bottom) along the canyon axis section. The SML is not horizontally homogeneous, while further off shore the water is more stratified, ranging in depth between 20ºC to 14ºC from the surface to the top of the thermocline (around 150 m depth), in the coastal areas the waters are more mixed with the temperatures ranging between 17ºC at surface and 14ºC at the top of the thermocline (around the 200 m

depth). Is also evident the presence, inside the canyon, of the warmer and saltier MW located between the 1500 m and the 700 m depth (pink water mass).

Figure 22 shows the vertical distribution of the turbidity (contours) and density (solid lines) along the canyon axis section. One of the more evident differences between the 2002 and 2003 observations is the suspended sediments concentrations that, in 2003 reached turbidity values 7 times higher than in 2002. Besides that the SPM pattern is very similar. Maximum turbidity (7 FTU) is again registered at the level of the bottom of the MW, reaching the higher values near the bottom limit of this water mass, the 27.8 kg m^{-3} isopycnal. Once again a continuous turbid layer is found from these depths up to the canyon head with another maximum around the 300-400m depth. The higher concentrations found below the MW until the 3000 m, may be resuspended sediment being transported down-canyon along the BNL, or may be a result of an intensification of the resuspension processes probably connected with the strong spring tide currents. The seaward transport along the isopycnals although present, seems now less important (10 to 15 km). The longer extension of this INL in 2002 may be result of a smaller definition. The number of stations sampled in 2003 is higher than in 2002, this meaning, that the distance between the stations was smaller and the results were more accurate. Although the seaward transport is present, it may be a little bit overestimated in Figure 18.

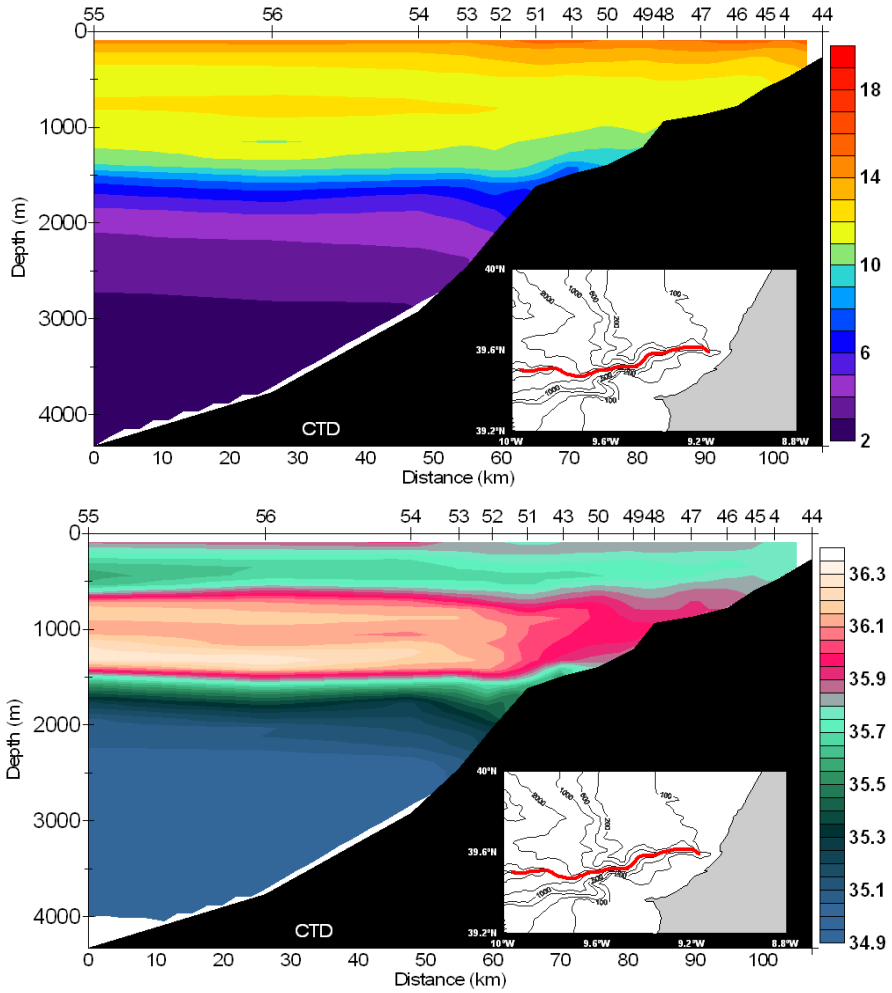

Figure 21- Vertical distribution of the Salinity (bottom) and Temperature (top) along the canyon axis section, during the 2003 cruise and the respective location.

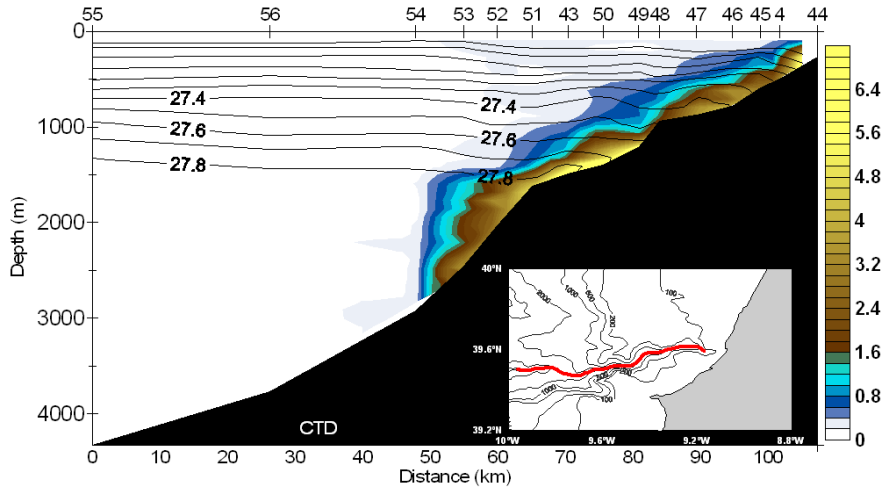

Figure 22 – Vertical distribution of the Density (solid lines) and Turbidity (contours) along the canyon axis section, during the 2003 cruise and the respective location.

4.3.2.3 PE236 Cruise (2005)

Figure 23 represents horizontal distribution at surface of CTD temperature (ºC), salinity (PSU) and turbidity (FTU) measurements for the canyon area during the 2005 cruise. Observations show warmer coastal water with temperatures ranging between 16º and 17ºC, decreasing westward, and deeper oceanic waters with temperatures around 15ºC. This difference is not so clear when we look at Figure 24, corresponding to SST AVRHH (left side) and Modis (right side) images. AVRHH image is a 15 day composite image for the period of 01 to 15 May 2005 (there was no 7 day image available for the second week when the CTD sampling took place) and Modis is a 7 day composite image for the period of 09 to 16 May 2005, that includes the period when CTD cast were performed.

These images (Figure 24) reveal a very homogeneous surface layer with temperatures ranging between 16º and 18ºC in the AVRHH image and between 15º and 17ºC in Modis image. This indicates that instead of a coastal and an oceanic water mass, what are observed in Figure 23 are thin colder or warmer water filaments.

The variability in salinity (0.2 PSU), is more in agreement with the homogenous surface layer observed in the SST images, reinforcing the idea of the thin filaments.

Turbidity concentrations decrease from 0.2 FTU near the coast to below 0.1 FTU off shore. This trend is the same observed in the November 2002 cruise but while the SNL in 2002 was only around 2 km apart from the coast in this case the SNL spreads for more than 30 km away from the coast line. According to Oliveira *et al.* (2002), during the winter (in the northwest Portuguese margin) the SNL is restricted to the inner shelf while in spring or summer it can reach or even cross the shelf break (~ 50 km from the coast). This can be explained by the effect of southerly winds during autumn and winter. They produce shoreward Ekman transport, which restricts the offshore westward extension of this layer. In spring-summer the northerly winds promote offshore transport, and the establishment of a seasonal thermocline allowing the expansion of the SNL to the west.

These were exactly the same conditions observed during the two cruises while in November 2002 we had winds prevailing from SW (Table 1) in April/May 2005 the wind was mainly from NW (Table 3).

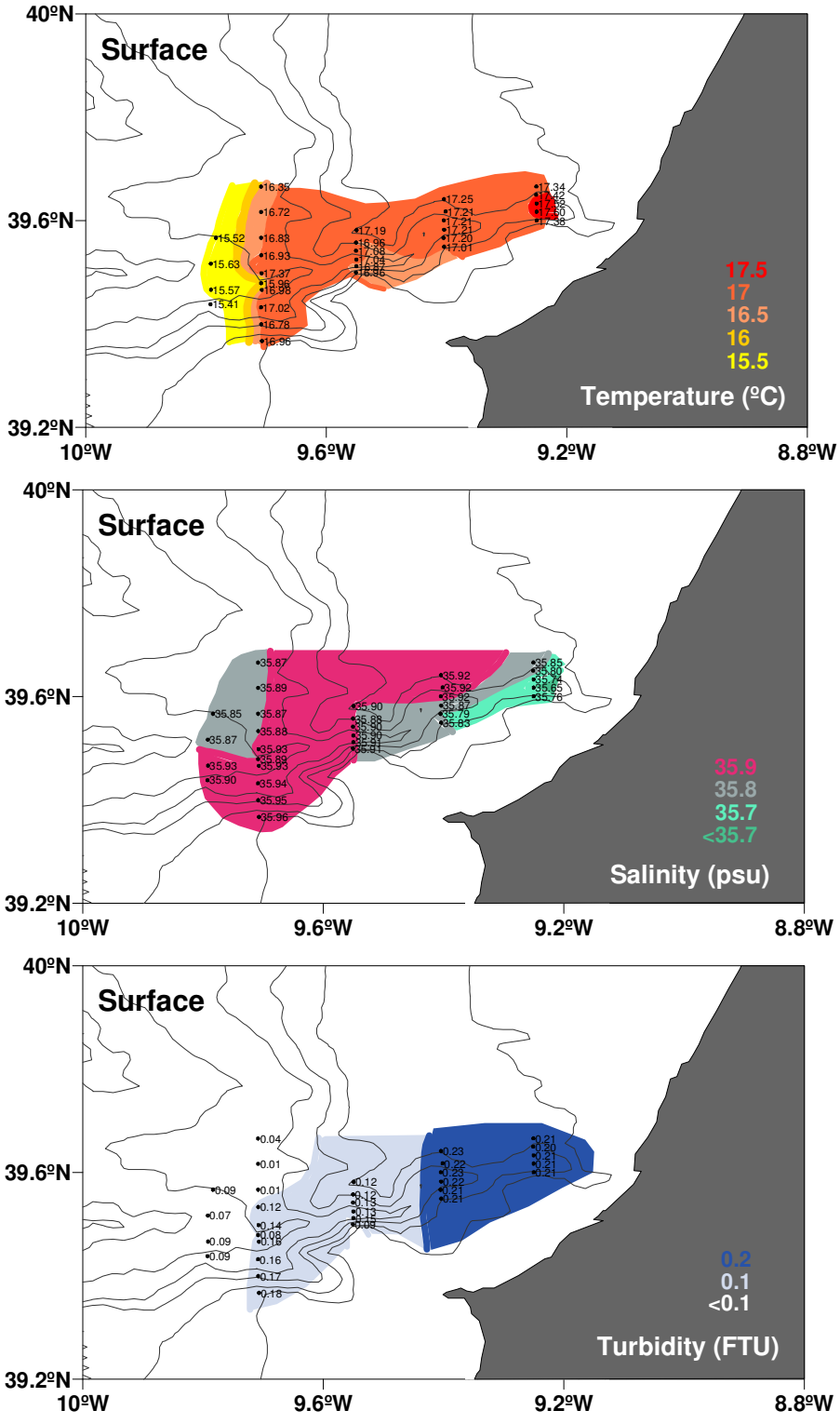

Figure 23 – Horizontal distribution of temperature (ºC), salinity (PSU) and turbidity (FTU) at the surface, obtained from CTD measurements during the 2005 cruise.

Figure 25 represents the vertical distribution of temperature (ºC), salinity (PSU), density (kg m^{-3}) and turbidity (FTU) at four cross-sections taken during the 2005 cruise, identified as D, E, F and G, from West to East.

The vertical distribution of temperature (Figure 25 – 1st column) indicates no significant difference in surface water temperature, with values ranging between 15º (off shore) and 17ºC (near the coast). In this cruise, the SML was thinner with the thermocline around the 50 m depth and well stratified water (wave heights were around 1 m) decreasing in temperature until 14ºC (around 50 m depth).

In section D, below the MW signature (pink water mass), at around 1500 m depth, we again observe a strong gradient in temperature, from 11ºC to 5ºC marking the intermediate layer between the MW and the NADW. This gradient is also present in salinity (2nd column) and in density (3rd column) with the 28.7 kg m^{-3} isopycnic, once more marking the interface between these two water masses.

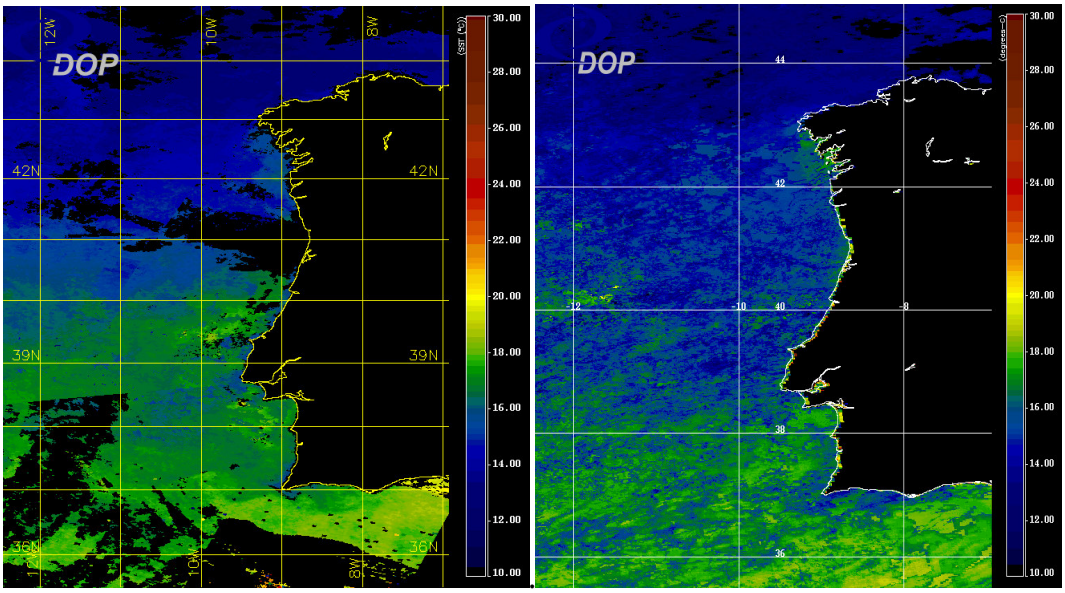

Figure 24 - SST AVHRR (left), 15 day average (01 to 15 May 2005) image and Modis (right) 7 day average (09 to 16 May 2005) image, for the CTD sampling period during the 2005 cruise. (http://oceano.horta.uac.pt/detra/) (DOP - Department of Oceanography and Fishery, Azores University).

Looking at turbidity (contours) in Figure 25 (3rd column) it can be observed that the westward decrease in turbidity values at surface, already analysed in Figure 23, is not only horizontal but also vertical. Near the shore (at cross-section G) the SML shows concentrations of 0.2 FTU up to the top of the thermocline (around the 50 m depth), this layer gets progressively thinner as we go farther offshore, where concentrations reach values below 0.05 FTU (at cross-section D).

Cross-section D, the most seaward section, shows similar results to cross-section A measured during the 2002 cruise, although the concentrations of turbidity found in 2005 are higher than those found on the 2002 cruise. In the southern rim a well developed BNL (0.2 FTU) can be found at the level of the shelf-break. Between 1500 m and 1800 m deep another BNL develops at the northern rim that connects with the southern wall, originating an INL that extends cross canyon, forming a continuous layer around this depth, indicating, again cross canyon transport. Once more the canyon axis station reveals the presence of a BNL (0.2 FTU). Curious is the clear water in the northern area of the profile. This may indicate that this area is out of the canyon influence.

Sections E and F are similar. In section E a BNL is formed at the level of the shelf break in both sides of the canyon rims, but more developed at the southern rim, with concentration values above 0.15 FTU. In section F the pattern is similar to section E although an increase in turbidity is observed in the entire water column. At the canyon axis an important BNL (reaching 0.8 FTU at the bottom) is observed in both sections, extending around 300 m in high in section E and almost 500 m in section F. In both cases turbidity is high in the entire canyon section up to the shelf break.

Section G shows a similar pattern to section B in 2002. Although in 2002 there was a well individualized BNL in the northern rim at the level of the shelf break, in 2005 there was a continuous BNL from the surface until around 500 m depth. Once more a permanent BNL (reaching around 1.2 FTU at the bottom) with almost 200 m thick is present at the canyon axis.

In general, also in this cruise higher turbidity values were found in the narrowest part of the canyon, sections E, F and G, all the way up through the canyon. This analysis is corroborated in Figure 26.

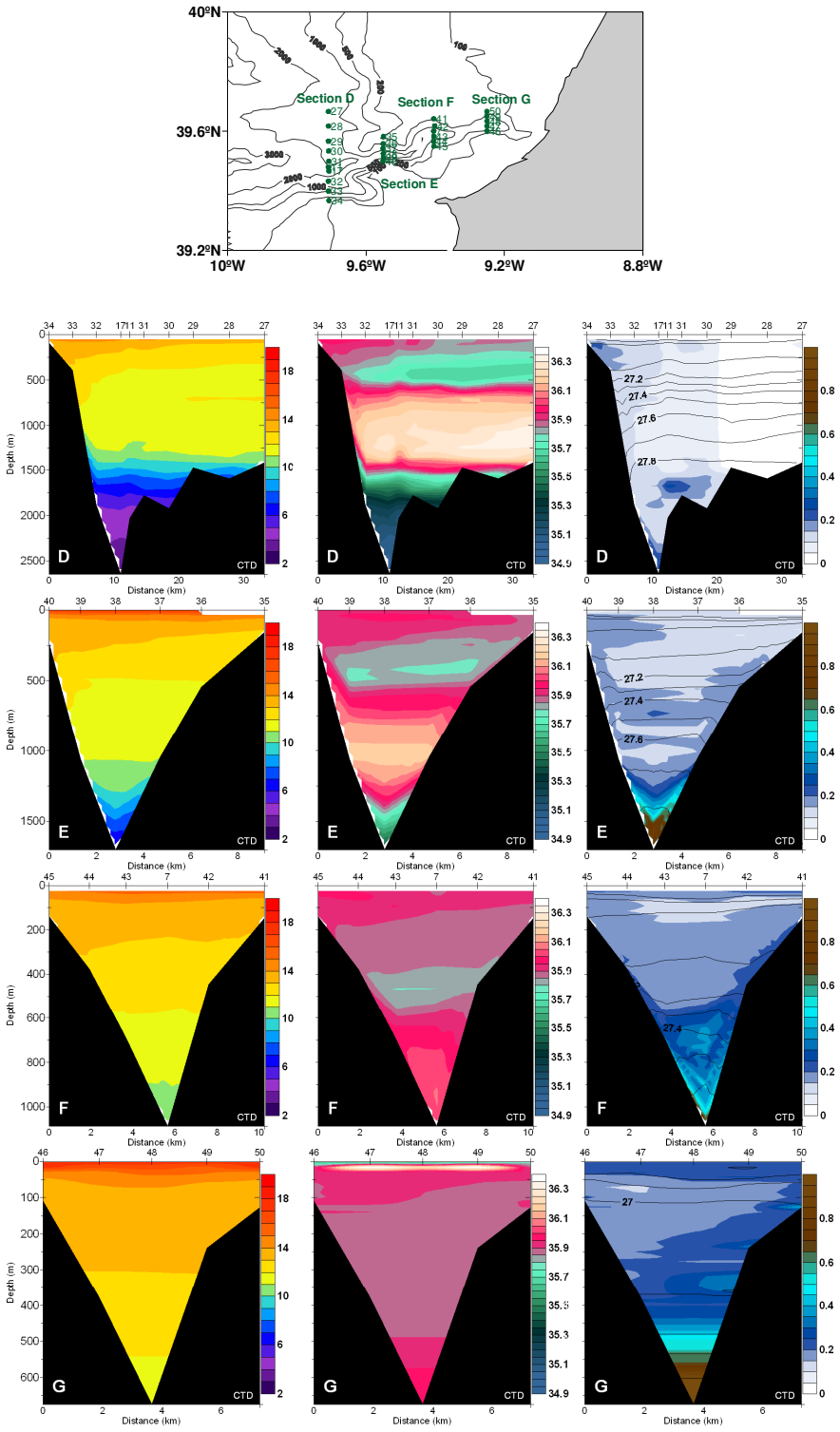

Figure 25 - Vertical distribution, along 4 cross sections D, E, F and G, obtained during the 2005 cruise, of CTD Temperature (ºC) (1st column), Salinity (PSU) (2nd column) and Turbidity (FTU) and Density (Kg m^{-3}) (3rd column), where contours represent turbidity and solid lines density.

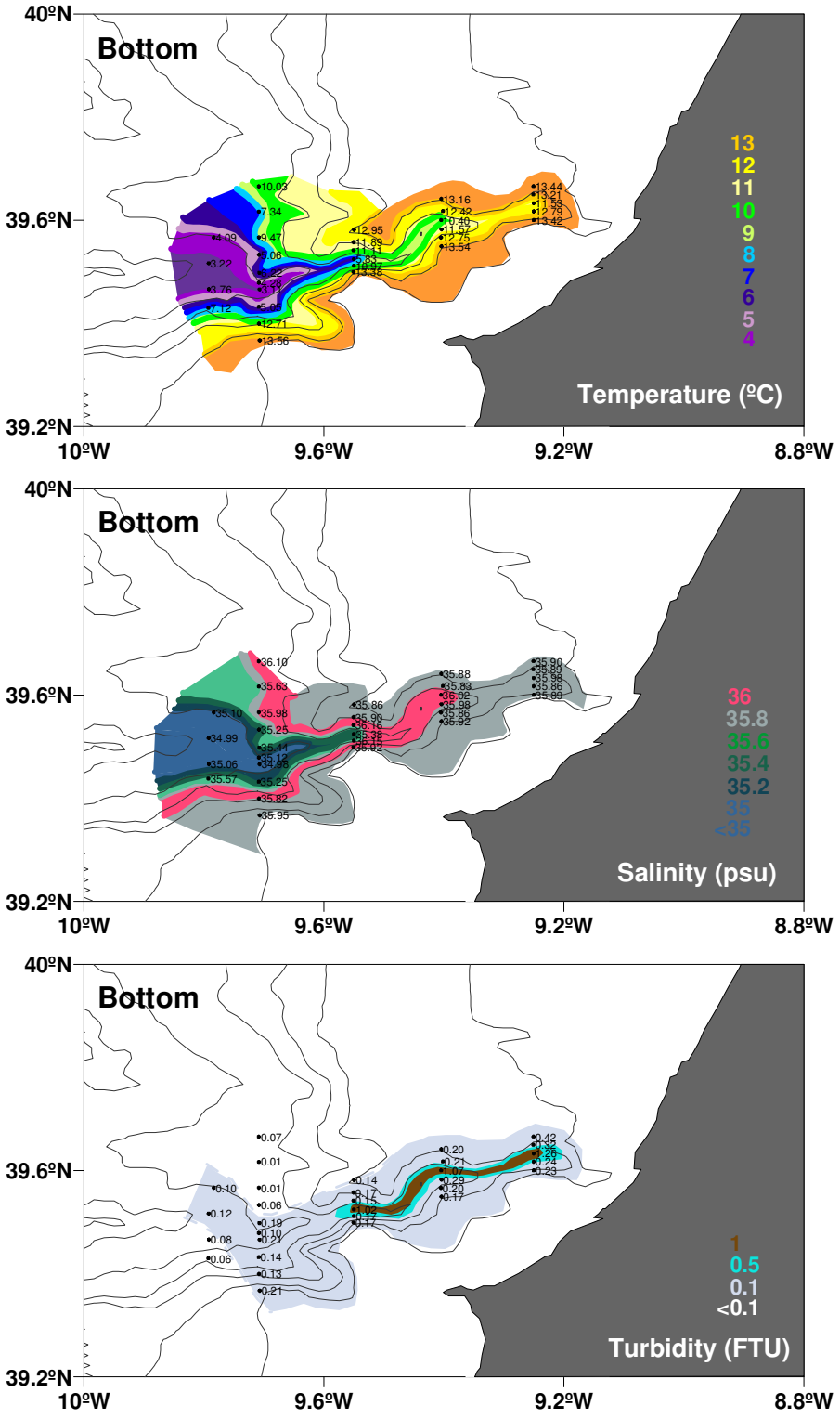

Figure 26 - Horizontal distribution for CTD temperature (ºC), salinity (PSU) and turbidity (FTU) along the bottom layer (1 meter above the bottom for all stations) in the Nazaré canyon during the 2005 cruise.

Figure 26 represents near bottom horizontal distribution for temperature (ºC), salinity (PSU) and turbidity (FTU) measurements in Nazaré canyon area. The values correspond to the last CTD measurement, 1 meter above the bottom, for each station. The pattern of the temperature and salinity distributions represents well the water channelization along the canyon axis, where the warmer and saltier MW reaches almost 700 m depth. This may increase the bottom velocities what may be in the origin of the higher bottom turbidity values observed in the narrow part of the canyon axis, being the highest values (above 1 FTU) found between the 1500 m depth and the canyons head.

These features are well patent in Figure 27 and Figure 28, that represent the vertical distribution of temperature (top) and salinity (bottom) in Figure 27 and turbidity (contours) and density (solid lines) in Figure 28, along the canyon axis section. These observations are identical to the two previous cruises. Once again, a continuous turbid layer is found from the canyon head down to the level of the bottom of the MW with 3 maximums (1.2 FTU) found around the 1500 m, the 1000 m and the 300-400 m depth. Notice once more the relation between the isopycnals and the location and spreading of the nepheloid layers.

As in 2003 the higher concentrations observed below the MW level around the 3000 m depth, may be resuspended sediment being transported down-canyon as a BNL, or may be a result of an intensification of the resuspension processes due to the strong spring tide current.

Suspended sediment concentrations are again of the same order of magnitude (around 1 FTU) than those in 2002, what indicates that in 2003 there was an intensification of the processes responsible for sediment resuspension.

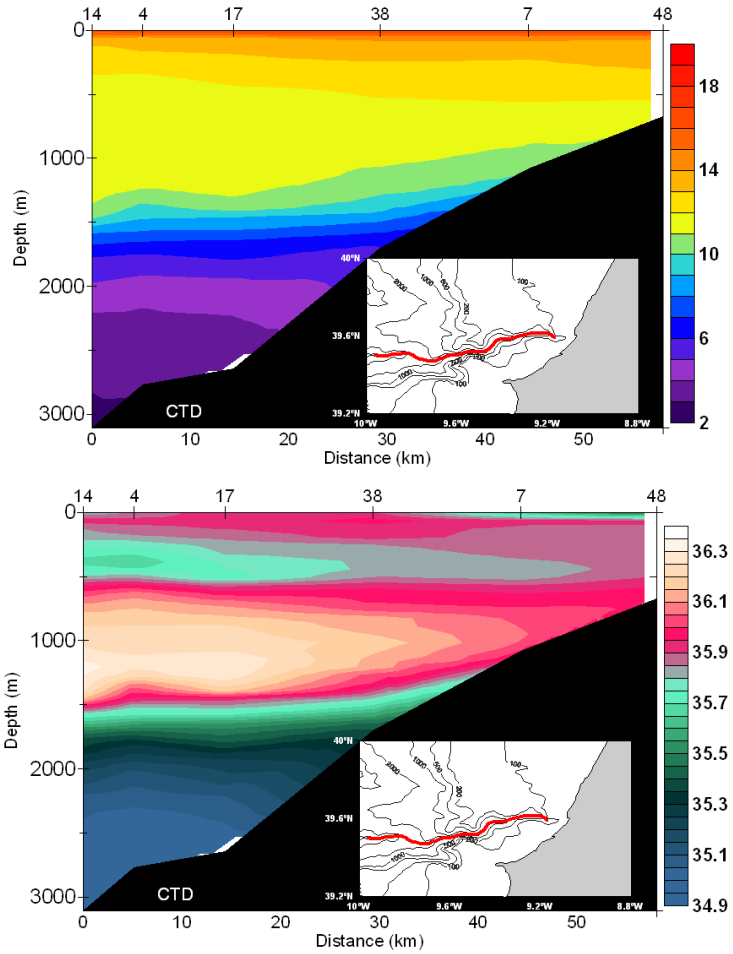

Figure 27 - Vertical distribution of the Salinity (bottom) and Temperature (top) along the canyon axis section, during the 2005 cruise and the respective location.

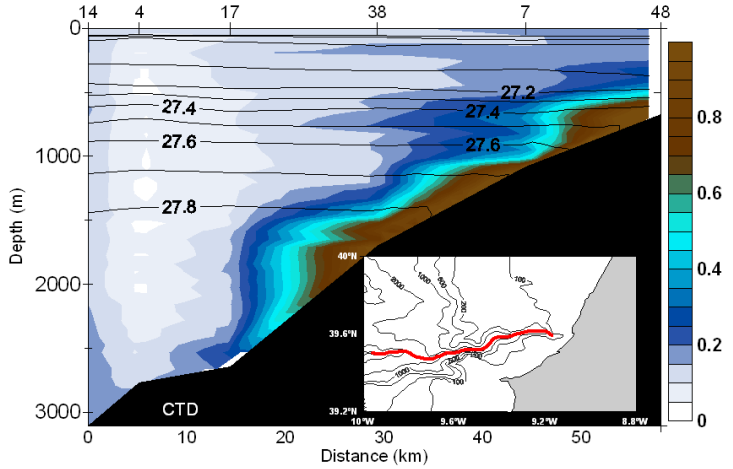

Figure 28 – Vertical distribution of the Density (solid lines) and Turbidity (contours) along the canyon axis section, during the 2005 cruise and the respective location.

PE252 Cruise (2006)

The main goal of the 2006 cruise was the characterization of the slopes adjacent to the Nazaré Canyon, so most of the work was done outside the canyon. Results from an along slope vertical profile will be shown and discussed in chapter 5 of this thesis in order to compare the observations inside the canyon with the open slope.
As referred previously, during this cruise 4 stations in the canyon were sampled for a tidal cycle (Figure 11).

In order to have an idea of the hydrographical conditions for the cruise period when the tidal cycles were performed Figure 29 shows the SST AVRHH (left side) and Modis (right side), 7 day composite images.
This figure reveals upwelling conditions, with colder coastal water, around 15º/16ºC (Modis) in the Nazaré area and warmer oceanic waters with temperatures around 19º/20ºC (Modis).

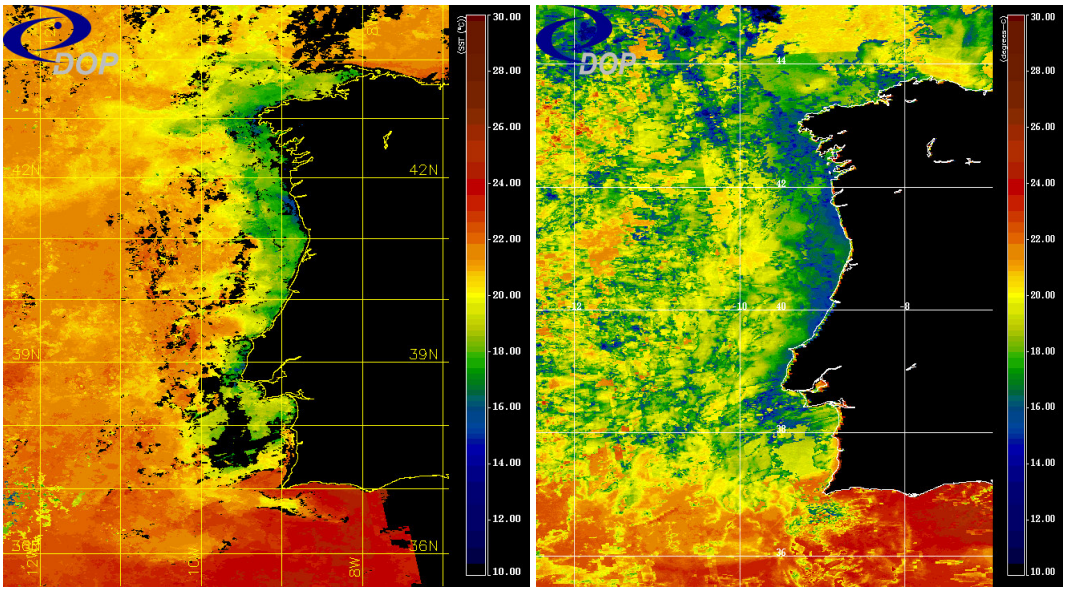

Figure 29 - SST AVHRR (left) and Modis (right) images. 7 day average for the CTD Tidal cycle sampling period during the 2006 cruise (06 to 13 September 2006). (http://oceano.horta.uac.pt/detra/) (DOP - Department of Oceanography and Fishery, Azores University).

In 2006 the effort on the canyon was to observe the tidal effect on the water column structure, because the experiments done in 2002 were not conclusive.

For this reason during the 2006 cruise CTD vertical profiles were repeated for station 41 and 42 (Figure 11) every 30 minutes during 13 hours. In Figure 30, hourly results for salinity (dashed lines) and turbidity (solid lines) are shown for a tidal cycle for station 41 at 800 m depth. In Figure 31 the same is represented for station 42 at 300 m deep. Both stations are on the canyon axis. Contrary to the 2002 observations, there is no relevant turbidity associated to the SML. Nevertheless, in both figures it can be observed that the sinking of the minimum salinity during flood tide was followed by a decrease in the intensity of the BNL that progressively increased during the ebb tide. In both stations it can be observed the 100 m vertical displacements in salinity (see the minimum of salinity in station 41). These results not only reveal the existence of an internal tide with the period of the semidiurnal tide, but also that near bottom the concentration of sediment varies along a tidal cycle having higher values during ebb tide periods. During ebb tide the SPM concentrations may double the values found during the flood tide period. The changes in the thickness of the BNL are also variable with tide being usually thicker during ebb tide than during flood tide, accompanying the maximum in concentration values.

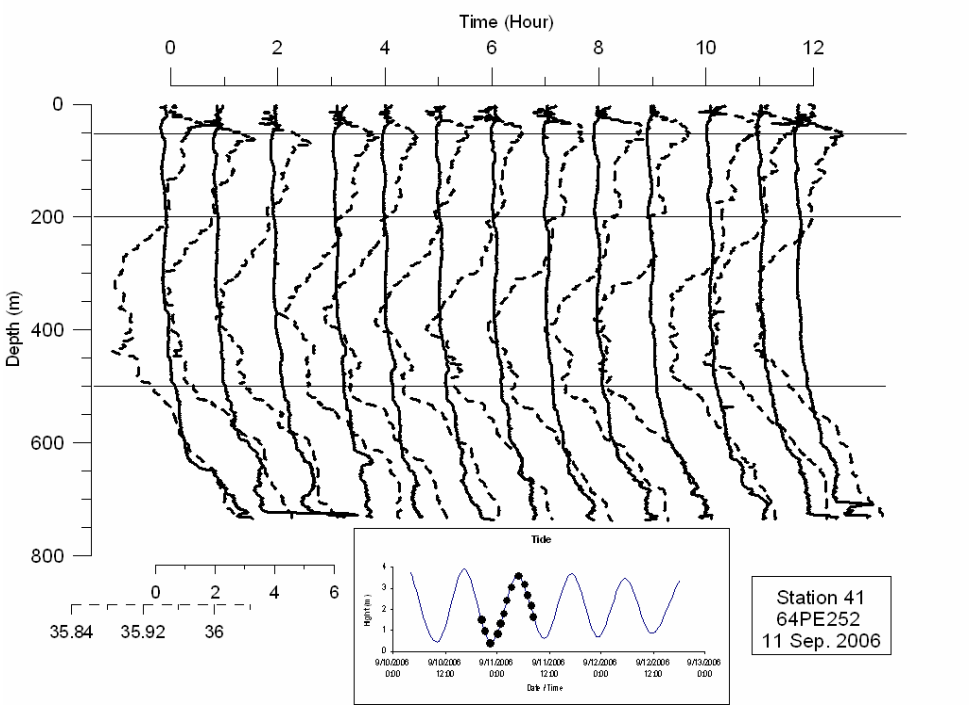

Figure 30 - CTD results for salinity (dashed lines) and turbidity (solid lines) from station 41 repeated for a tidal cycle during the 2006 cruise.

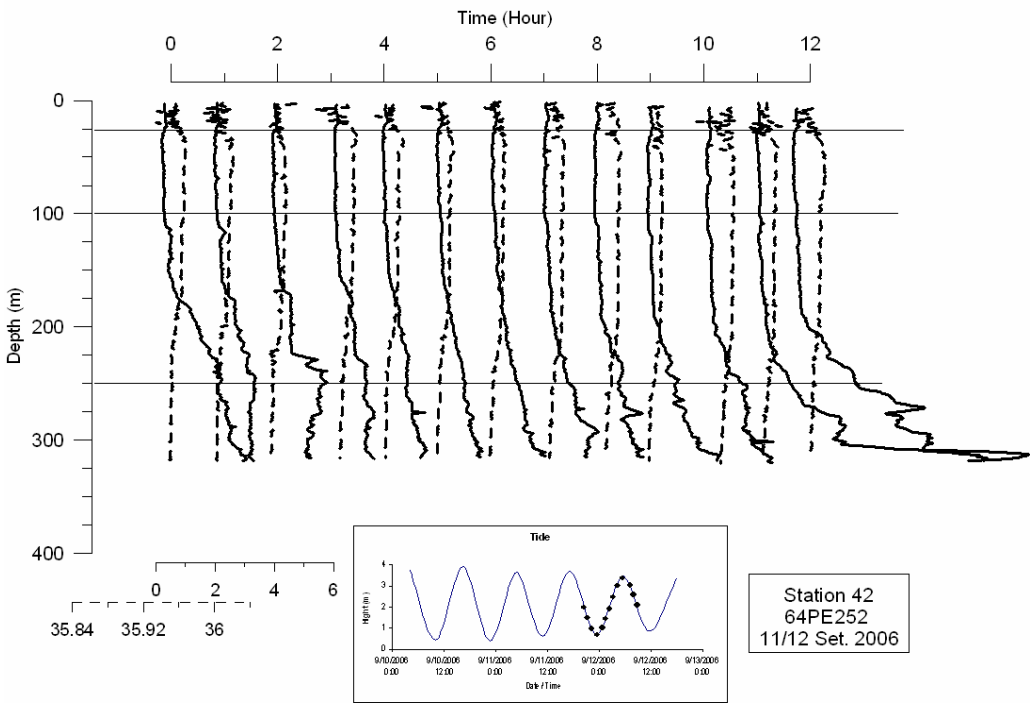

Figure 31 - CTD results for salinity (dashed lines) and turbidity (solid lines) from station 42 repeated for a tidal cycle during the 2006 cruise.

This variation of bottom concentrations, which depends on the tide, may be due to three factors (1) increase and decrease in near bottom velocity and consequently increase or decrease in resuspension, (2) horizontal transport, with the turbid layer being transported up-canyon and down-canyon with tide, (3) both of the factors.

4.4 CONCLUSIONS

Different stations were occupied during each cruise so it is not possible to compare results obtained from one year to the other, in the same location. Also the fact that sediment concentration varies with the semi diurnal tidal cycle, as show in Figure 30 and Figure 31 makes this task difficult. Nevertheless, some overall conclusion may be taken.

Resuspension processes are more intense and important in the upper canyon than in the middle canyon. Concentrations near the bottom in the deeper stations below 2500 m depth show values near two orders of magnitude lower than those found in the

upper narrower canyon. Here, a permanent BNL is found all along the canyon axis from the 1600 m depth (bottom of the MW) up to the canyon head, with maximum concentrations at three depths: (1) around the 1500 m, (2) at 1000 m and (3) between the 300-400 m.

These results indicate that the upper canyon seems to act as a temporary catchment area and as a sediment trap for the material which is reworked and transported over the shelf, until they are flushed to the deep sea via the canyon.

This BNL along the upper canyon axis, in most places is at least 200 m tick, and at the level of the bottom of the MW it may extend seaward, along the 27.8 Kg m^{-3} isopycnal, as an INL for more than 10 km. Several studies (e.g. McPhee-Shaw & Kunze, 2002; McPhee-Shaw, 2006) concluded that depending on the stratification and on the mixing layer these nepheloid layers could spread seaward as far as 16 to 25 km away from the margin. They also concluded that the thickness of the suspended layer depends on vertical diffusion.

Relatively higher concentrations found at 3000 m depth on the middle canyon may be due to the down-canyon transport as a BNL of resuspended sediments, or may be a result of an intensification of the resuspension processes due to strong spring tide currents.

Another important conclusion is the observation in the upper canyon of an internal tide with the period of the semi-diurnal tide. The permanent vertical stratification below the surface layer (Figure 12) is known as favourable to the development of internal tides.

This internal tide is responsible for the variation of the suspended sediments concentration near the bottom depending on the tidal cycle, with higher values during ebb tide periods. Also the thickness of the turbid layer varies with the tide, being usually thicker during ebb than during flood tide.

Internal tides seem to play an important role in sediment dynamics in Nazaré canyon. Nevertheless, the data do no allow to clearly establishing a connection between the internal tides and the nepheloid layers. For that reason the MOHID model was applied to the Nazaré canyon in order to check if internal tides were responsible for the high turbidity observed in the upper narrow canyon area. The results obtained will be presented and discussed in the next chapter.

Chapter 5

MODELLING INTERNAL TIDES IN NAZARÉ CANYON

5.1 METHODS

5.1.1 The MOHID Model

The development of the MOHID model started back in 1985, suffering since then updates and improvements due to its use in the framework of many research and engineering projects. Initially MOHID was a bi-dimensional tidal model by Neves (1985). The first three-dimensional model was introduced by Santos (1995), which used a vertical double Sigma coordinate (MOHID 3D). The limitations of the double Sigma coordinate revealed the necessity to develop a model that could use a generic vertical coordinate, this way allowing the user to choose from several coordinates, depending of the main processes of the area of study. Due to this necessity the concept of finite volumes was introduced with the version *Mesh 3D* by Martins (2000). In the *Mesh 3D* model, a 3D eulerian transport model, a 3D lagrangian transport model (Leitão, 1996) and a zero-dimensional water quality model (Miranda, 1999) were included. This version of the model revealed that the use of an integrated model based on a generic vertical coordinate is a very powerful tool. However it was verified that the model was difficult to maintain and to be extended due to the limitations of the FORTRAN 77 language.

In 1998 the whole code was submitted to a complete improvement using ANSI FORTRAN 95 language and an object oriented strategy like the described in Decyk *et al*. (1997). The main goal of this rearrangement was to turn the model more robust, reliable and also to protect its structure against involuntary programming errors, this way it would be easily extendable.

The new MOHID philosophy (Miranda, *et al*., 2000), allows to use the model in any dimension (as one, two or three-dimensional). Actually the MOHID is composed by

over 60 modules which complete over 280 thousand code lines. Each module is responsible for managing certain kind of information. In terms of processes simulated some of the main modules are listed in Table 5.

Another important feature of MOHID is the possibility to run nested models. This feature enables the user to study local areas, obtaining the boundary conditions from the "father" model. The number of nested models is only limited by the available computer power.

Presently the MOHID system is divided in two main groups (i) MOHID Water, and (ii) MOHID Land. MOHID Water permits the simulation of hydrodynamic processes, dispersion processes (lagrangian and eulerian approach), sediment transport, water quality/Biogeochemical processes in the water column and interaction with the bottom (Fernandes, 2005). MOHID Land is a watershed comprising surface run-off, infiltration, soil water fluxes through a porous media and interaction with the aquifer.

Table 5 – Main modules of the MOHID model.

Module name	Module description
Hydrodynamic	Full 3D dimensional baroclinic hydrodynamic free surface model. Computes the water level, velocities and water fluxes.
Water Properties (Eulerian Transport)	Eulerian transport model. Manages the evolution of the water properties (temperature, salinity, oxygen, etc.) using a eulerian approach.
Lagrangian	Lagrangian transport model. Manages the evolution of the same properties as the water properties module using a lagrangian approach. Can also be used to simulate oil dispersion.
Turbulence	One-dimensional turbulence model. Uses the formulation from the GOTM model. Manages the turbulent flow properties, such as viscosities, diffusivities, turbulent kinetic energy, in a eulerian referential
Interface SedimentWater	Bottom boundary conditions
Interface WaterAir	Atmospheric forcing (wind, temperatue, solar radiation, etc…)
Water Quality	Zero-dimensional water quality model. Simulates the oxygen, nitrogen and phosphorus cycle. Used by the eulerian and the lagrangian transport modules. Based on a model initially developed by the Environmental Proctection Agancy (Bowie, et. al., 1985).

The MOHID Water Modelling System has been applied in different systems for different proposes true the years. As examples we have the case of applications in the North Atlantic for the study of the general circulation (Neves *et al.*, 1998; Coelho *et al.*, 2002; Santos *et al.*, 2002) and oil spills (Leitão, 2003), the study of circulation,

eutrofization and residence time in estuaries (Cancino & Neves, 1998; Martins, 1999; Villarreal *et al*., 2002; Braunschweig *et al*., 2003; Vaz *et al*., 2007; Saraiva *et al*., 2007) and dams (Braunschweig, 2001) and studies of water quality in coastal lagoons (Trancoso *et al*., 2005; Santos *et al*., 2008).

In this section a brief description of the main modules used for implementing the hydrodynamic and sediment transport model for Nazaré Canyon will be done. More detailed information can be found in Coelho *et al*. (2002), Leitão (2003), Fernandes (2005) or in the model web site (www.mohid.com).

5.1.1.1 Hydrodynamic Module

The Hydrodynamic model consists in a three-dimensional baroclinic model which solves a primitive equation in orthogonal horizontal coordinates for incompressible flows assuming Boussinesq and hydrostatic equilibrium.

The spatial discretization of these equations is performed using the finite volume technique (Martins *et al*., 2001) allowing the use of a generic vertical coordinate system, becoming the model independent from the vertical discretization. This means that the model can be easily used in different places with different geometries.

Temporal discretization is based on a semi-implicit ADI (Alternate Direction Implicit) algorithm with two time levels per iteration. Two numerical schemes are currently implemented: the 4-equation S21 scheme (Abbott *et al*., 1973), and the 6-equation Leendertsee scheme (Leendertsee, 1967).

The hydrodynamic module has as main goal to compute the evolution of the flow properties. Horizontal velocities components (X and Y) are properties which are calculated based on Eq. 1:

$$\frac{\partial}{\partial t}\int_V P dV = -\oint_A \vec{F}\cdot dA + FPA\ (sources - sinks) \qquad \text{(Eq. 1)}$$

Where, *A* is the surface which defines the boundary of the control volume (*V)*, where the surface of integral $\vec{F}$ corresponds to the flux of property (*P)* true (*A)*, admitting that:

$$P = \rho \cdot \vec{v} \wedge \vec{F} = P \cdot \left(\vec{v} \cdot \vec{n}\right) = \rho \cdot \vec{v} \cdot \left(\vec{v} \cdot \vec{n}\right) \quad \text{(Eq. 2)}$$

$$Sources - Sinks = \sum Forces = Gravitic + Pressure + Viscous \quad \text{(Eq. 3)}$$

ρ is the volumic mass, $\vec{v}$ is the 3D flow velocity vector and $\vec{n} = (n_x, n_y, n_z)$ is the vector normal to the boundary surface (A) of the control volume (V).

Gravity forces include Earth$\left(g \int_V \rho dV \right)$, Moon and Sun attraction forces over the control volume.

Pressure and viscosity forces are the result from the interaction of the control volume with the evolving environment. Pressure forces are normal to the boundary surface $\left(-\oint_A p \cdot \vec{n}\, dA\right)$ while viscous forces may be subdivided in tangential or normal.

For tangential viscous forces is necessary to define surface and bottom boundary conditions. At bottom, a quadratic law is used where the shear stress is equal to the Chezy coefficient plus the velocity square. At surface if the forcing agent is wind the shear stress is the wind shear stress, if it isn't its null.

Free surface elevation is obtained by integrating the equation (Eq. 1) over the whole water column. In this case the terms of the equation may be written like:

$$P = \rho \wedge \vec{F} = \rho \cdot \vec{v} \quad \text{(Eq. 4)}$$

$$Sources - Sinks = Discharges + Precipitation - Evaporation \quad \text{(Eq. 5)}$$

Eq. 1 becomes a 2D mass conservation equation:

$$\frac{\partial}{\partial t} \int_V \rho dV = -\oint_A \rho \vec{v} \cdot d\vec{n} + Discharges + Precipitation - Evaporation \quad \text{(Eq. 6)}$$

In this case the transported property is known (ρ) and the incognita is the control volume.

Since it is a 3D approach it is necessary to introduce an equation to compute vertical fluxes, which are obtain from Eq. 6 taking into account the hydrostatic hypothesis.

5.1.1.1.1 Assumptions

Eq. 1 when applied to the momentum conservation law is only valid for a fix referential. Nevertheless the natural referential, Earth, is in permanent rotation being the effect of the rotation in the flow usually considered as an inertial force known as the Coriolis Force.

Another assumption is done when applying the momentum conservation law to oceanic and coastal flows, by considering that in these cases the variation of density in the water is less than 3%. The density can then be considered constant for the computation of the inertial forces and mass, except for the forces depending on gravity. This simplification is known as Boussinesq approximation.

A third assumption, has in consideration that in the ocean and coastal waters the vertical scales are small; as a consequence of that the flow has lower velocities in that direction. Beside that, small differences in density also tend to inhibit the vertical movement. Vertical accelerations are small as well as viscous forces. The fluid behaves like being in static equilibrium. Under these conditions the hydrostatic hypothesis is valid; this meaning that it is possible to neglect the inertial terms and to admit that the vertical pressure gradient is in equilibrium with the gravity force. In the case of the hydrostatic hypothesis, pressure is only depending on the depth and vertical density gradient.

The pressure term, may be discretized considering the two components, barotropic and baroclinic. The first considers the effect of the vertical gradient over the pressure and the second considers the effect of the density gradient. This separation permits to relate the variation of the free surface with pressure (barotropic). Free surface can be used to compute the control volume has well as to estimate the barotropic pressure. Also distinct numerical methods may be applied at each term.

The previous assumptions give rise to the following equation (Eq. 7),

$$\frac{\partial}{\partial t}\int_V \vec{v}dV = -\oint_A \left(\vec{v}\cdot\vec{v}\right)d\vec{n} + \oint_A \upsilon_T \frac{\partial\left(\vec{v}\right)}{\partial n}d\vec{n} - \underbrace{g\oint_A(\eta - z)\cdot d\overrightarrow{n_x}}_{\text{Barotropic Force true X}} - \underbrace{g\oint_A\left(\int_z^\eta \frac{\rho-\rho_0}{\rho_0}dz\right)\cdot d\overrightarrow{n_x}}_{\text{Baroclinic force true X}}$$

$$\underbrace{-g\oint_A(\eta - z)\cdot d\overrightarrow{n_y}}_{\text{Barotropic force true Y}} \underbrace{-g\oint_A\left(\int_z^\eta \frac{\rho-\rho_0}{\rho_0}dz\right)\cdot d\overrightarrow{n_y}}_{\text{Baroclinic force true Y}} - \underbrace{\oint_A p_{atm}d\overrightarrow{n_x}}_{\text{atmospheric pressure X}} - \underbrace{\oint_A p_{atm}d\overrightarrow{n_y}}_{\text{atmospheric pressure Y}}$$

$$\underbrace{+\int_V 2\vec{\Omega}\times\vec{v}\,dV}_{\text{Coriolis Force}} + \text{Tide Potential} \qquad \text{(Eq. 7)}$$

Where, ρ is the volumic mass , ρ_0 is the reference volumic mass, $\vec{v}$ is the 3D flow velocity vector, $\vec{n} = (n_x, n_y, n_z)$ is the vector normal to the boundary surface (A) of the control volume (V), Ω is the angular velocity, η free surface level, z depth, υ_T turbulent viscosity and p_{atm} atmospheric pressure.

The hydrodynamic module solves the 3D momentum conservation equation (Eq. 7) to compute the horizontal components of the velocity and a 2D mass conservation equation (Eq. 6), to compute the free surface variation in time. Finally it solves again equation (Eq. 6) for a 3D environment, to compute the vertical velocity components.

5.1.1.2 Turbulence Module

The numerical resolution of the equations of the hydrodynamic module is discrete in space and time. For this reason the hydrodynamic module computes the previous equations based on Reynolds decomposition.

This decomposition may be seen as a time filtering, where the instantaneous values of the properties (f) are substituted by average quantities ($\overline{f}$) plus turbulent fluctuations (f').

Temporal integration of equation (Eq. 7) permits to write it in terms of average values, appearing, due to non linear effects, additional terms (Reynolds tensors). These terms represent the contribution of the turbulent transport for the average field and can be seen as the transport of the variable field fluctuations by the velocity field fluctuations.

This introduces another issue known as turbulence closure theory. There are several methods to solve this problem being normal to admit that this new term is proportional to the gradient of the average property transported:

$$\overrightarrow{v}'\overrightarrow{v}' = \upsilon_T \frac{\partial \vec{v}}{\partial n} \quad \text{(Eq. 8)}$$

The variable, υ_T is known as turbulent viscosity. If the fluid is considered isotropic we can admit that υ_T is constant. If not it is needed to compute a value for each direction, $\upsilon_T = (\upsilon_x, \upsilon_y, \upsilon_z)$.

In most cases it is admitted that $\upsilon_x = \upsilon_y$, once the processes may be considered horizontally homogeneous. The major difference is in the characteristic scales of the horizontal and vertical directions. In this perspective the turbulent viscosity coefficient may be divided in horizontal and vertical turbulent viscosity, $\upsilon_T = (\upsilon_H, \upsilon_H, \upsilon_V)$

As it was assumed that the new term has a mathematical nature similar to the viscous forces term, their units are easily comparable. The scales usually computed by the hydrodynamic models are in the order or meters, what corresponds to a turbulent viscosity several orders higher than molecular viscosity, reason for which the viscous forces can be neglected.

Vertical eddy viscosity/diffusivity is determined by using a turbulence closure model selected from those available in the General Ocean Turbulence Model (GOTM) (Burchard *et al.*, 1999) incorporated in MOHID. All models use the turbulent viscosity principle that permits to obtain the turbulent exchange coefficients as function of the average flow properties. In this study we used a turbulence model, calculating turbulence kinetic energy (TKE), length scale and stability functions. Further and more detail information on the GOTM model may be found at (http://www.gotm.net).

5.1.1.3 Water Properties Module

It is also necessary to study the transport and evolution of the water properties (salinity, temperature, cohesive sediments, etc). This transport considering a eulerian referential it is computed by the Water Properties module. A 3D model that solves Eq.

7, solving explicitly the horizontal advection and diffusion terms and implicitly the vertical advection and diffusion terms. The advection term may be solved by using one of the following schemes: first, second and third order upwind centred differences and TVD (Total Variation Diminishing).

Density is calculated as a function of temperature, salinity and pressure by the UNESCO equation of state (UNESCO, 1981).

Temperature and salinity evolve due to the combined effect of the flow, of punctual discharges, surface fluxes, heat exchanges (solar radiation, infrared radiation, latent and sensible heat) and mass exchanges (evaporation, precipitation).

5.1.1.3.1 Eulerian transport of particulate properties

Particulate properties transport is governed by a 3D advection-diffusion equation where the vertical advection includes the particle settling velocity.

$$u_z = u_{z'} + w_s \qquad \text{(Eq. 9)}$$

Where u_z is the overall vertical velocity of the particulate property, $u_{z'}$ is the vertical current velocity, and w_s is the property settling velocity. This methodology enables to compute the transport of particulate properties, like particulate contaminants or particulate organic matter, likewise and dependent of cohesive sediments (Fernandes, 2005).

To compute settling velocity it is considered that each particle can have its specific and constant settling velocity, which can be derived from literature (depending on its size and biogeochemical characteristics).

5.1.1.4 Sediment-water Interface module

The sediment-water interface handles processes occurring between the water and the sediment column. This interface is abstract, because physically it is very difficult to define. In the model, it can be seen as a thin sediment layer (fluff-layer) with transient characteristics, depending basically on temporal scales associated with hydrodynamics and transport on the water column, namely erosion and deposition. This layer has a

separation function, which allows dissociating processes that occur on the sediment deposit, at a very slow scale, "filtering" the high frequencies of erosion/deposition fluxes that shape it, therefore leading to consolidation.

Dissolved properties can be produced in the interface but their mass is not part of it, becoming part of the water column by means of a boundary flux condition. On the contrary, particulate properties are acquainted in the sediment-water interface. This can be the case when sediment deposition occurs, but the sediment is not yet consolidated. Thus, a particulate property deposited mass is tracked in order to know how much of it is available when erosion conditions occur. Following this concept, it is considered that dissolved properties can exchange fluxes directly between the water column and the sediment interstitial water. In erosion conditions, if this transient layer is completely eroded, then scouring is made from the sediment compartment upper layer, where consolidated sediment is present. When this happens, interstitial water is dragged along with the sediment, therefore constituting a flux to the water column. The same happens when the fluff-layer consolidates and becomes part of the sediment column, there is an input of overlaying water (and its properties) to the sediment compartment (Fernandes, 2005).

5.1.1.4.1 Cohesive sediments fluxes

For bottom cohesive sediments, a flux term, F_b, (mass of sediment per unit bottom area per unit time) can be defined, corresponding to a source or sink for the suspended particulate matter in conditions of erosion or deposition, respectively. Consequently, at the bottom:

$$F_b = F_E - F_D \qquad \text{(Eq. 10)}$$

where F_E and F_D are the erosion and deposition fluxes, respectively.

It is assumed that when bottom shear stress is smaller than a critical value for deposition, there is addition of matter to the bottom. Conversely, when the bottom shear is higher than a critical value, erosion occurs. The erosion algorithm used is based on the classical approach of Partheniades (1965). The flux of eroded matter is given by:

$$\begin{cases} F_E = E\left(\dfrac{\tau}{\tau_E} - 1\right) & for \quad \tau_b > \tau_{CSE} \\ F_E = 0 & for \quad \tau_b < \tau_{CSE} \end{cases} \qquad \text{(Eq. 11)}$$

where τ_b (Pa) is the bed shear stress, τ_{CSE} (Pa) is a critical shear stress for erosion and E is the erosion parameter (kg $m^{-2}s^{-1}$). This erosion algorithm is computed at the sediment-water interface.

The deposition flux can be defined as:

$$\begin{cases} F_D = (CW_S)_B\left(1 - \dfrac{\tau}{\tau_{CSD}}\right) & for \quad \tau_b < \tau_{CSD} \\ F_D = 0 & for \quad \tau_b > \tau_{CSD} \end{cases} \qquad \text{(Eq. 12)}$$

Where Ws is the near-bottom settling velocity (according to Stokes law); and C the near-bottom cohesive sediment concentration, τ_b (Pa) and τ_{CSD} (Pa) are the bottom shear stress and the critical shear stress for deposition, respectively. This concept reflects the fact that the deposition of aggregates is controlled by near-bottom turbulence. The deposition algorithm (Krone, 1962), like the erosion algorithm, is based on the assumption that deposition and erosion never occur simultaneously, e.g., a particle reaching the bottom has a probability of remaining there that varies between 0 and 1 as the bottom shear stress varies between its upper limit for deposition and zero, respectively.

5.1.1.5 Lagrangian Module

Lagrangian transport models are based on the simulation of tracer's movements in a lagrangian referential. They use the concept of tracers being referred as particle tracking models. The main characteristic is to avoid the explicit resolution of the advective term of the transport equation, avoiding the instability problems. The major advantage of these models is in the applications with marked gradients since the lagrangian approach does not take with it the numerical diffusion problems that characterize the eulerian transport models.

In the MOHID Lagrangian module the tracers are characterized by there spatial coordinates (x, y, z), volume and a list of properties (in the case of sediment particles, Critical Shear Erosion, Critical Shear Deposition, Settling velocity, etc.). Each tracer has associated a time to perform the random movement. The movement of the tracers can be influenced, for example, by the velocity field of the hydrodynamic module, by the wind from the Atmospheric module, by the spreading velocity from oil dispersion module and by random velocity.

The tracers are "born" at origins. Tracers which belong to the same origin have the same list of properties and use the same parameters. Origins may differ in the way they emit tracers.

There are three different ways to define origins in space:

• a "Point Origins" that emits tracers at a given point;

• a "Box Origins" that emits tracers over a given area;

• a "Accident Origins" that emits tracers in a circular form around a point (used for example for oil spills)

There are two different ways in which origins can emit tracers in time:

• Continuous Origins - emits tracers during a period of time;

• Instantaneous Origins - emits tracers at one instant;

Origins can be joined together in Groups. Origins which belong to the same group are grouped together in the output file, so it is easier to analyze the results.

The major factor responsible for particle movement is generally the mean velocity. The spatial co-ordinates are given by the definition of velocity:

$$\frac{dx_i}{dt} = U_i(x_i, t) \qquad \text{(Eq. 13)}$$

where u stands for the mean velocity and x for the particle position. Equation 13 is solved using a simple explicit method:

$$x_i^{t+\Delta t} = x_i^t + \Delta t . u_i' \qquad \text{(Eq. 14)}$$

Higher order accuracy requires the use of an iterative procedure. The Heun scheme adopted by Monteiro (1995) uses second order accuracy. Costa (1991) concluded that higher order schemes are important whenever the curvature of the flow exists and a

large time step is used. For most of the natural flows the explicit method is accurate enough. Velocity at any point of space is calculated using a linear interpolation (Figure 32) between the points of the hydrodynamic model grid. The lagrangian module permits to divide the calculation of the trajectory of the tracers into sub-steps of the hydrodynamic time step.

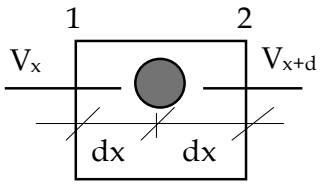

Figure 32 – Average tracers velocity calculation (Adapted from Leitão, 1996).

To velocities Vx and Vx+dx, at 1 and 2 faces can still be added a drift velocity due to wind, a velocity representative of the diffusive/turbulent transport or in the case of an oil spill the velocity of the oil spreading.

Turbulent transport is responsible for dispersion. The effect of eddies over particles depends on the ratio between eddies and particle size. Eddies bigger than the particles make them move at random as explained in Figure 33. Eddies smaller than the particles cause entrainment of matter into the particle, increasing its volume and it's mass according to the environment concentration, like shown in Figure 34.

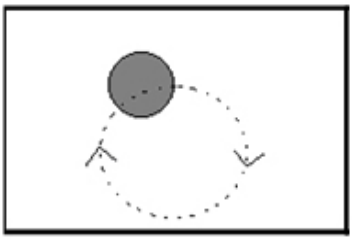

Figure 33 - Random movement forced by an eddy larger than the particle.

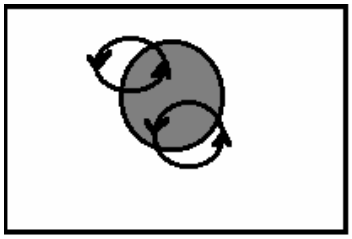

Figure 34 - Volume and Mass increasing forced by an eddy smaller than the particle.

The random movement is calculated following the procedure of Allen (1982). The random displacement is calculated using the mixing length and the standard deviation of the turbulent velocity component, as given by the turbulence closure of the hydrodynamic model. Particles retain the velocity during the necessary time to perform the random movement, which depends on the local turbulent mixing length.

The lagrangian module permits to monitor the distribution of particles inside "monitoring boxes". This feature is very useful to compute, for example the residence time of water inside these monitoring boxes and the origins of the water present inside each box at each moment (Braunschweig *et al*., 2003). The lagrangian module "monitors" the boxes the following way:
In every instant the volume of each box b, *InstBoxVol(b)* is calculated:

$$InstBoxVol(b) = \int (h + Z)dxdy \qquad \text{(Eq. 15)}$$

In every instant the origin "o" of the water inside each monitoring box "b" is identified and the volume of the water from each origin is stored in the variable

$$InstVolumeByOrigin\ (b, o) = \sum_{o} Vol_j^b$$

In case of instantaneous emissions in boxes, these contributions are integrated over the time, *IntgVolumeByOrigin(b, o)*

$$IntgVolumeByOrigin(b, o) = \int InstVolumeByOrigin(b, o)dt \qquad \text{(Eq. 16)}$$

A measure of the residence time of the water emitted into box "o" in monitoring box "b" is given by:

$$ResidenceTimePerBox(b, o) = IntgVolumeByOrigin(b, o) / IntialVol(o) \quad \text{(Eq. 17)}$$

These values also permit to compute how each monitoring box is influenced by each emitting box:

$$InfluenceOverBox(b, o) = IntgVolumeByOrigin(b, o) / InitialVol(b) \quad \text{(Eq. 18)}$$

In case of a continuous emission, the residence time can be computed as:

$$ResidenceTimePerBox(b, o) = InstVolumeByOrigin(b, o) / Disch\,arg\,eRate(o) \quad \text{(Eq. 19)}$$

The addition of the values of the residence time in each box gives the Residence time inside the system.

5.1.2 Experimental design and forcing

The experimental design and forcing that follows and that was used for the simulations presented in this chapter is the result of a continuous work on choosing the best design to reproduce the data observations.

5.1.2.1 Geometry

The model was implemented using two spatial domains: the broader domain - level 1 (Figure 35) - encompassing the west coast of Iberia, extending from 37ºN to 40.2ºN and from 8.7ºW to 11.7ºW, and a nested domain - level 2 (Figure 36) - for the Nazaré Canyon area from 38.8ºN to 40ºN and from 8.9ºW to 11.5º W. The horizontal grid spacing in the two domains is 1.5 km in both directions. For level 1 domain the model uses 27 vertical layers (Figure 37) delimited by constant z-levels at surface and depths of 0, 15, 190, 304, 494, 544, 612, 727, 910, 1166, 1416, 1468, 1489, 1528, 1551, 1593, 1649, 1697, 1746, 1881, 1988, 2182, 2530, 2930, 3430, 4030 and 4800m. The bottom topography for this domain was derived from ETOPO2* by means of an interpolation for the model grid followed by smoothing with a five-point Laplacian filter. The bottom cells are

* U. S. Department of Commerce, Natural and Atmospheric Administration, National Geophysical Data Center, 2006, 2-minute Gridded Global Relief Data (Etopo2V2).

defined using a "partial step" approach, instead of the traditional "full step" or "staircase" approach. Adcroft *et al*. (1997) shows that this approach minimizes the traditional problems associated with the staircase topography of z-level models.

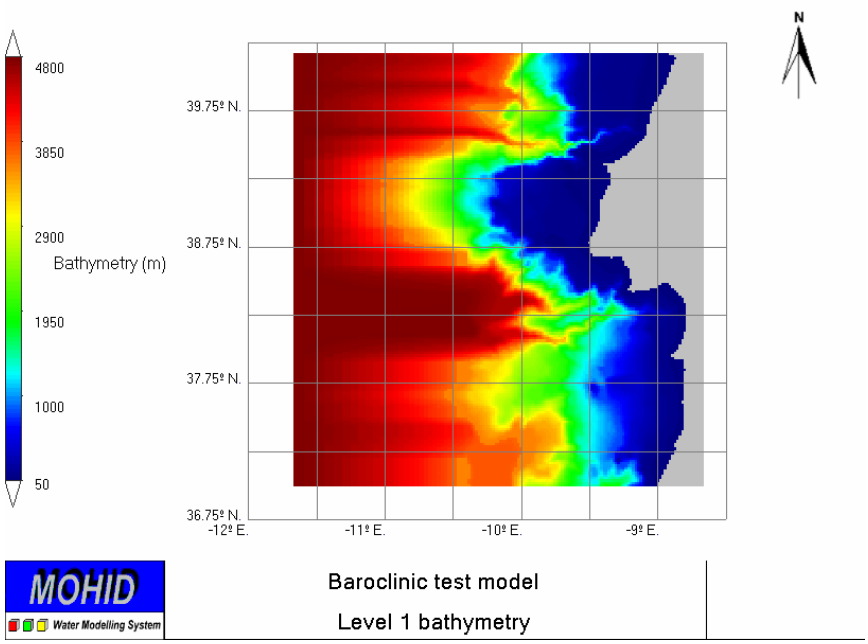

Figure 35 – Level 1domain and the respective bathymetry (from ETOPO2).

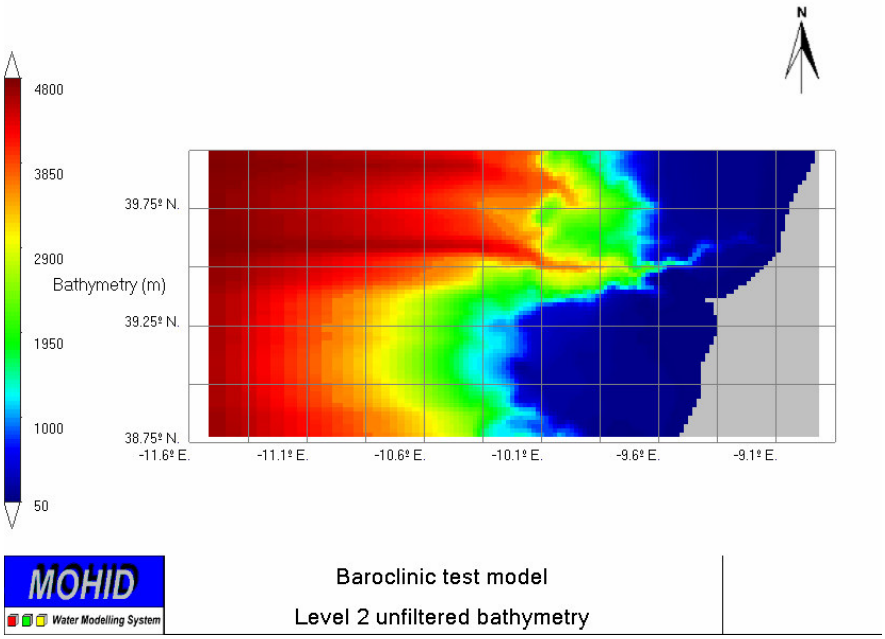

Figure 36 – Level 2domain and the respective bathymetry.

Level 2 domain vertical discretization (Figure 38) is composed from bottom to surface by a set of fixed depth layers, having depths 1.7, 5.1 and 10.2m, chosen for better modelling the sediment dynamics (high resolution of the bottom layers), and an upper domain with 15 sigma coordinate layers having relative thicknesses of 0.01, 0.03, 0.05, 0.08, 0.14, 0.20, 0.12, 0.1, 0.16, 0.05, 0.01, 0.01, 0.01, 0.01 and 0.02. This sigma coordinate discretization was chosen to reproduce adequately in the Nazaré Canyon the annual mean density vertical gradient observed at the Iberian Margin. Level 2 bottom topography, was obtained as a simple extraction of the level 1 topography and filtered afterwards for the slope parameter between adjacent topography cells, calculated by $\frac{\Delta h}{2\bar{h}}$ where Δh is the topography change and $\bar{h}$ is the average topography of the two cells, to be 0.2 maximum, following the results of Beckmann & Haidvogel (1993) for sigma coordinates models. Biharmonic momentum diffusion coefficients are set to $1x10^9$ $m^4 s^{-1}$. A constant turbulent diffusion of 10 $m^2 s^{-1}$ was considered for heat and salt transport. The model was initialised from a rest state with a null horizontal sea level gradient. The temperature and salinity fields are horizontally homogeneous. The vertical profile of these properties corresponds to the annual mean conditions observed along the Iberian Margin. The baroclinic forces are connected gradually in a time span of 3 inertial periods starting at the beginning of the simulation, so that model dynamics can smoothly adapt to the imposed initial stratification.

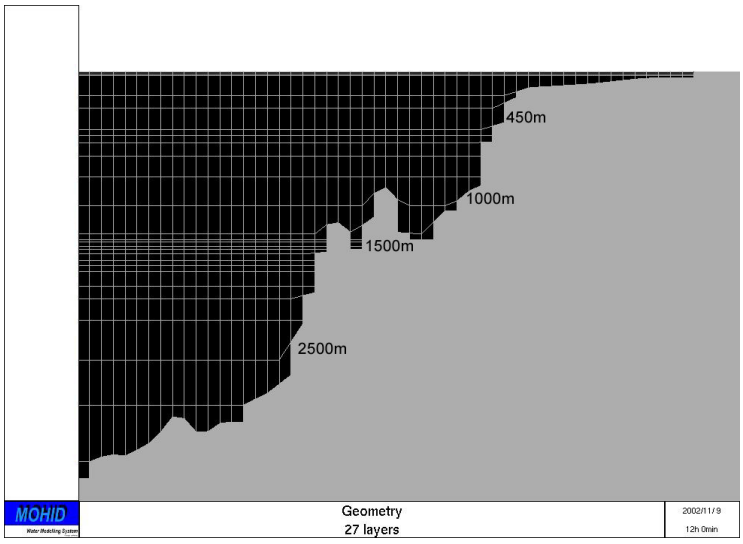

Figure 37 – Domain 1 vertical discretization

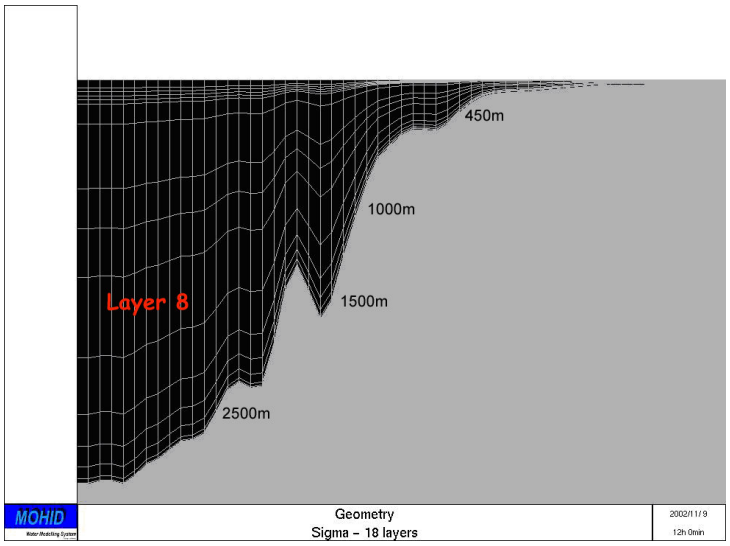

Figure 38 – Domain 2 vertical discretization with indication of layer 8.

5.1.2.2 Lateral Boundary Conditions

In level 1 domain the normal and tangential components of the velocity were set to zero at land boundary and the fresh water river input at coastal boundaries was not considered in this study. The western, southern and northern boundaries are open. A Blumberg & Kantha (1985) radiation boundary condition was applied to the sea level. According to Leitão (2003) this is the best boundary condition for the tide.

$$\frac{\partial \eta}{\partial t} + \left(\sqrt{gh} \cdot n\right)\left(\frac{\partial \eta}{\partial x}, \frac{\partial \eta}{\partial y}\right) = \frac{1}{T_d}(\eta_{ref} - \eta) \qquad \text{(Eq.20)}$$

where η corresponds to the sea level, η_{ref} is the reference sea level , T_d is decay time and h is depth.

The reference sea level was assumed equal to the sum of the contributions of the 26 locally most important tidal constituents deduced from the global model FES95 (Le Provost *et al.*, 1998). The reference sea level is increased gradually until its full value in a period of 57 hours (corresponding to 3, 19 hours' inertial periods) at the beginning of the simulation, so that the model could adjust its dynamics. For salinity and temperature a null gradient boundary condition was assumed.

In level 2 lateral boundary conditions are taken from the level 1 domain solution in the following way. A Flather (1976) radiation boundary condition is applied for the sea level (Eq. 21). Once again Leitão (2003) demonstrated this to be the better option for linking nested domains.

$$(q - q_{ref}).n = (\eta - \eta_{ref})\left(\sqrt{gh}.n\right) \quad \text{(Eq.21)}$$

where q and q_{ref} are, respectively, the barotropic flux of the level 2 domain and the reference barotropic flux; the reference sea level and barotropic flux for this radiation condition are taken from the level 1 solution.

For the horizontal velocity zonal and meridional components, temperature, salinity and cohesive sediment, a relaxation scheme by Martinsen & Engedahl (1987) was considered for the 11 near lateral boundary cells:

$$\frac{\partial \Phi}{\partial t} = -\frac{\Phi - \Phi_{ref}}{\tau} \quad \text{(Eq.22)}$$

where Φ is the relaxed variable, Φ_{ref} is the reference solution for that variable, taken from the level 1 solution, and τ is the relaxation time constant. This relaxation time constant changes gradually from $9x10^2$s at the boundary cells to $7.2x10^6$s at the 11th cell band. The use of these boundary conditions is consistent with the conclusions of the review by Blayo & Debreu (2005).

Since the vertical discretization are not the same in level 1 and level 2 domains the solution of level 1 is vertically interpolated to the level 2 discretization prior being considered as reference for the level 2 lateral boundary conditions.

For simulating cohesive sediments the values used for settling velocity (Ws), critical shear deposition (CSD), critical shear erosion (CSE) and erosion rate were respectively 0.00015 m s^{-1}, 0.18 Pa, 0.17 Pa and 0.5 kg m^{-2} s^{-1}. These are average values for the canyon area obtained by the team of Prof. Laurenz Thomsen from the International University of Breman, also partners in the Eurostrataform project.

5.2 MODEL SIMULATIONS

Our objective with the model simulations was to investigate if the internal waves could be the process responsible for resuspension and transport of fine particles within the Nazaré submarine canyon.

Field observations indicated the presence of internal tides in the canyon, and high current activity, which could be in the origin of the permanent BNL, along the canyon axis, mainly from the 1600 m depth up to the canyon head.

The model was forced exclusively by the tide. Salinity and temperature profiles obtained with the CTD during the 2002, 2003 and 2005 cruises, representative of the water masses in the area and real bathymetry, were used to verify if in such conditions it is possible to reproduce the observed patterns.

The knowledge of the system and the available data are insufficient for a complete model validation, nevertheless some basic aspects can be verified. One of these aspects is the barotropic tide propagation, by comparing the hourly results of the simulated water level with the tide values obtained from tide gauge tidal components at coastal sites of Cascais (38.69ºN and 9.42ºW, using 59 tidal components), near Lisbon, and Peniche (39.35ºN and 9.37ºW, using 9 tidal components), close to the Nazaré canyon. The statistical results of this model validation are presented in

Table 6.

Table 6 - Statistical analysis parameters for comparison between 2D barotropic model MOHID results and tide predictions at tidal gauge locations. RMSE corresponds to the Root Mean Square Error.

		Tidal gauge location	
		Cascais	Peniche
Correlation coefficient (r)	Total results 14/11/02-30/11/02	0.9986	0.9869
	Neap tide results 17/11/02-23/11/02	0.9986	0.9963
	Spring tide results 23/11/02-29/11/02	0.9993	0.9818
RMSE (cm)	Total results 14/11/02-30/11/02	5.6	13.1
	Neap tide results 17/11/02-23/11/02	5.1	5.9
	Spring tide results 23/11/02-29/11/02	6.6	16.3

The model is strongly correlated with the tidal observations (r>0.99) in neap and spring tide conditions, and a root mean square error (RMSE) below 7 cm at Cascais and 17 cm at Peniche. What seemed to be the worst performance in Peniche, both in correlation and RMSE, is thought to be related with the use of a tidal prediction obtained with a small number of tidal components.

Simulations were performed for the same periods of the 2002, 2003, 2005 and 2006 cruises, to better compare data and model results.

5.2.1 Hydrographic data and Nephelometry

In order to compare if the model could reproduce the water masses structure for the west Portuguese Margin (Figure 12) a Temperature/Salinity diagram was plotted considering the same stations as those from the November 2002 cruise, after 7 days run (Figure 39). Data is from Domain 2 (sigma coordinates).

This result indicate that the model reproduces very well the main water masses for the west Portuguese Margin, the SML, the NACW, the MW and the NADW.

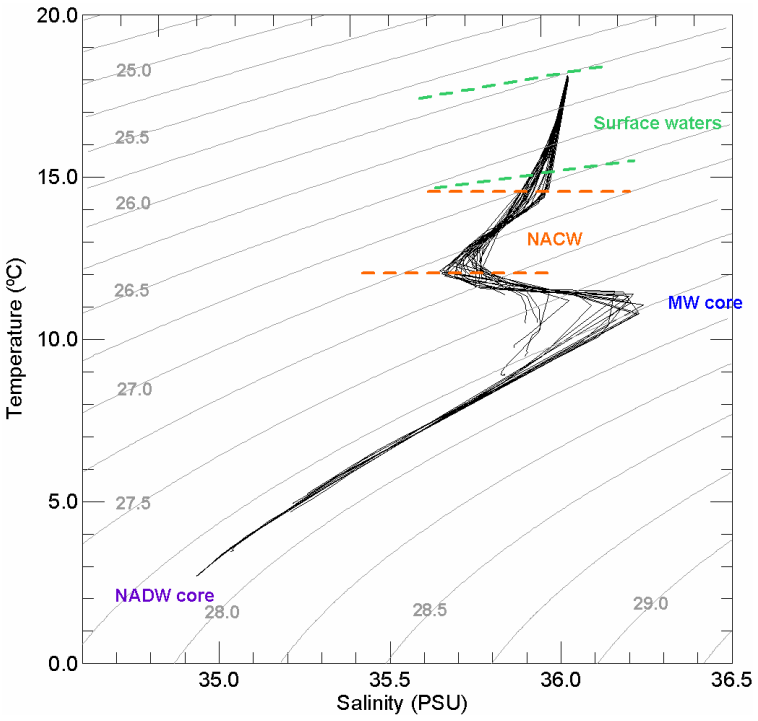

Figure 39 –Temperature /Salinity profiles from Domain 2 model results after 7 days run, for November 2002 simulation. Although the SML is not has evident as in the data (Figure 12), the presence of the SML, NACW, MW, NADW is well reproduced.

Figure 40 and Figure 41 represent model results, for the bottom layer, for Domain 2 of temperature (left side) and salinity (right side), for the year 2002 and 2005, respectively. When compared these results with the observed data (Figure 16 and Figure 26, respectively), it can be identified a very similar pattern with the water masses flowing up canyon. Notice how well the model reproduces de saltier MW (right side of the figures).

The importance of using temperature and salinity profiles from the period of the simulations is patent when looking, for instance, to the differences in the temperature field (left side of the figures) of Figure 40 and Figure 41. The near coast warmer waters observed in 2002 (also confirmed in the data, Figure 16), were not observed in 2005 neither in the model neither in the in situ data (Figure 25).

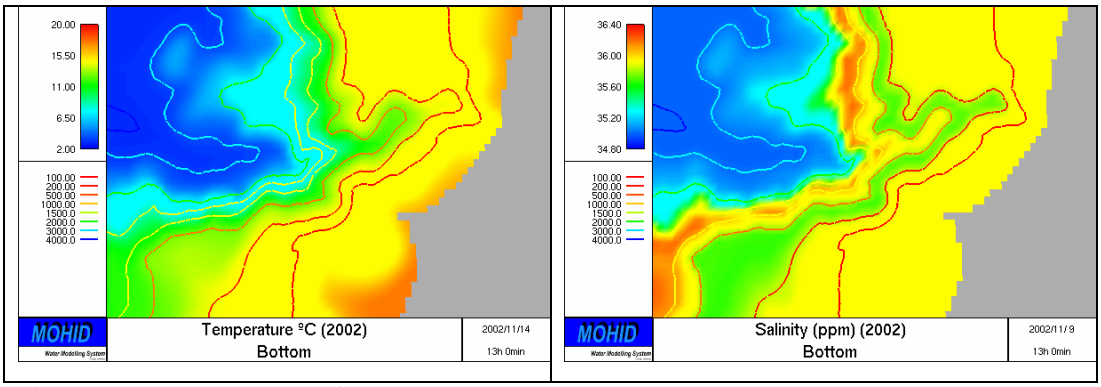

Figure 40 – Model results for near bottom temperature and salinity distribution along the Nazaré Canyon for 2002.

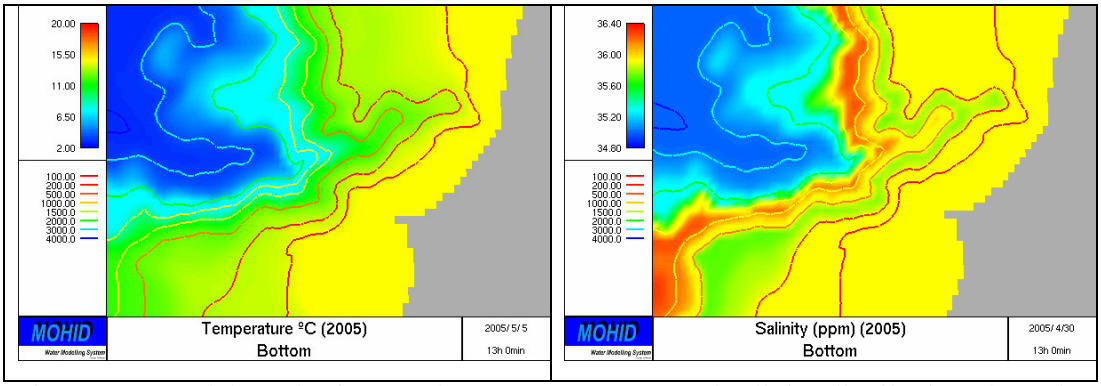

Figure 41 – Model results for near bottom temperature and salinity distribution along the Nazaré Canyon for 2005.

At the surface the model results do not compare very well the in situ data, mainly temperature. As referred previously, in the beginning of the simulation, we considered that temperature and salinity were horizontally homogeneous in the entire domain and since the model does not have any atmospheric forcing (it was not under the scope of this work), meaning that there is not any heat or radiation input or any exchanges from the surface water with the atmosphere, the water gets progressively colder. This discrepancy observed at surface is not relevant for this work since we are dealing with deeper processes, where the model reproduces well the observed data.

Model results for the Domain 2, after 15 days run, show a very similar residual circulation pattern, for the 2002, 2003 and 2005 simulations at the surface (Figure 42), at an intermediate layer (layer 8, see Figure 38) (Figure 43) and at the bottom (Figure 44).

Once more the residual currents at surface do not take into account any atmospheric effect, and so they are not representative of the circulation during the cruises period. So, it will be analysed in the perspective of a model result.
At surface (Figure 42) the most relevant features are a stronger (between 2 and 5 cm s^{-1}) southward current located along the continental slope. In the coastal area over the Estremadura Plateau there is the formation of two eddies over the plateau for 2002 and 2003 and a larger anticyclonic vortex in 2005. Near the coast the current flows northward, in the canyon direction. Another anticyclonic eddy is formed in the northern margin of the canyon in the coastal area, with a prevailing southward direction.

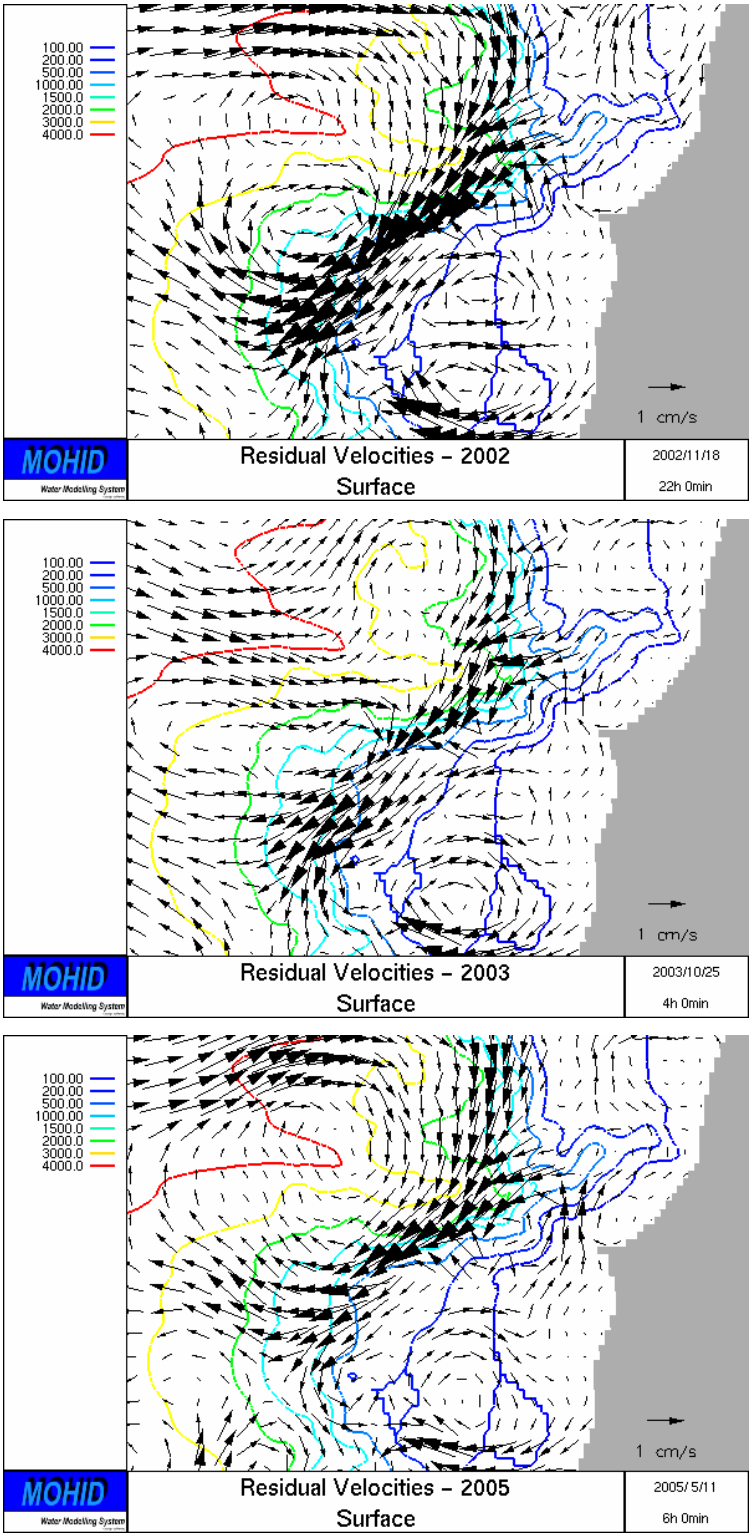

Figure 42 – Residual circulation for Domain 2 at surface. Results after 15 days run for the period of the 2002, 2003 and 2005 cruises.

Layer 8 is a middle water layer (Figure 38), centred in the deeper parts around the MW level. Once more the residual circulation pattern is very similar for the 3 simulated periods (Figure 43). The Along slope MW northward current is well defined in the 3 simulations, with higher velocities (between 2 and 5 cm s^{-1}) in the slope southern of the canyon, contouring the Estremadura Plateau. This current is then diverted and flows up-canyon reaching almost the 500 m depth; this shows the channelization of the flow along the canyon axis. These results are according with what is known for the circulation in this area (Chapter 2 and Chapter 3), and have also been observed by other authors as for example Xu *et al*. (2002) at Monterey Canyon (West Coast of USA), Puig *et al*. (2000) at the Foix Canyon (NW Mediterranean) and Lafuente *et al*. (1999) at La Línea Canyon (Western Alborean Sea). According to these last authors these along canyon currents are forced by the internal pressure gradients associated with the baroclinic tide that is generated in the surrounding areas.
In the southern canyon rim, over the Estremadura plateau (between the 200 m and the 500 m isobath) a stronger southwestward current is present.
Over the northern shelf a cyclonic eddy is present, while in the southern shelf an anticyclonic eddy can be observed.

As in the previous Figures there are no significant differences in the residual bottom circulation (Figure 44) for the 2002, 2003 and 2005 simulations. Bellow the 3000 m depth a southward residual current, with velocities around 1 cm s^{-1} is observed. Along the slope until the 500 m depth the residual current, is more intense south of the canyon and flows northward. The intensification of the upward current inside the canyon is visible in all images. At shallower depth the current flows southward being intensified in the Estremadura plateau region.

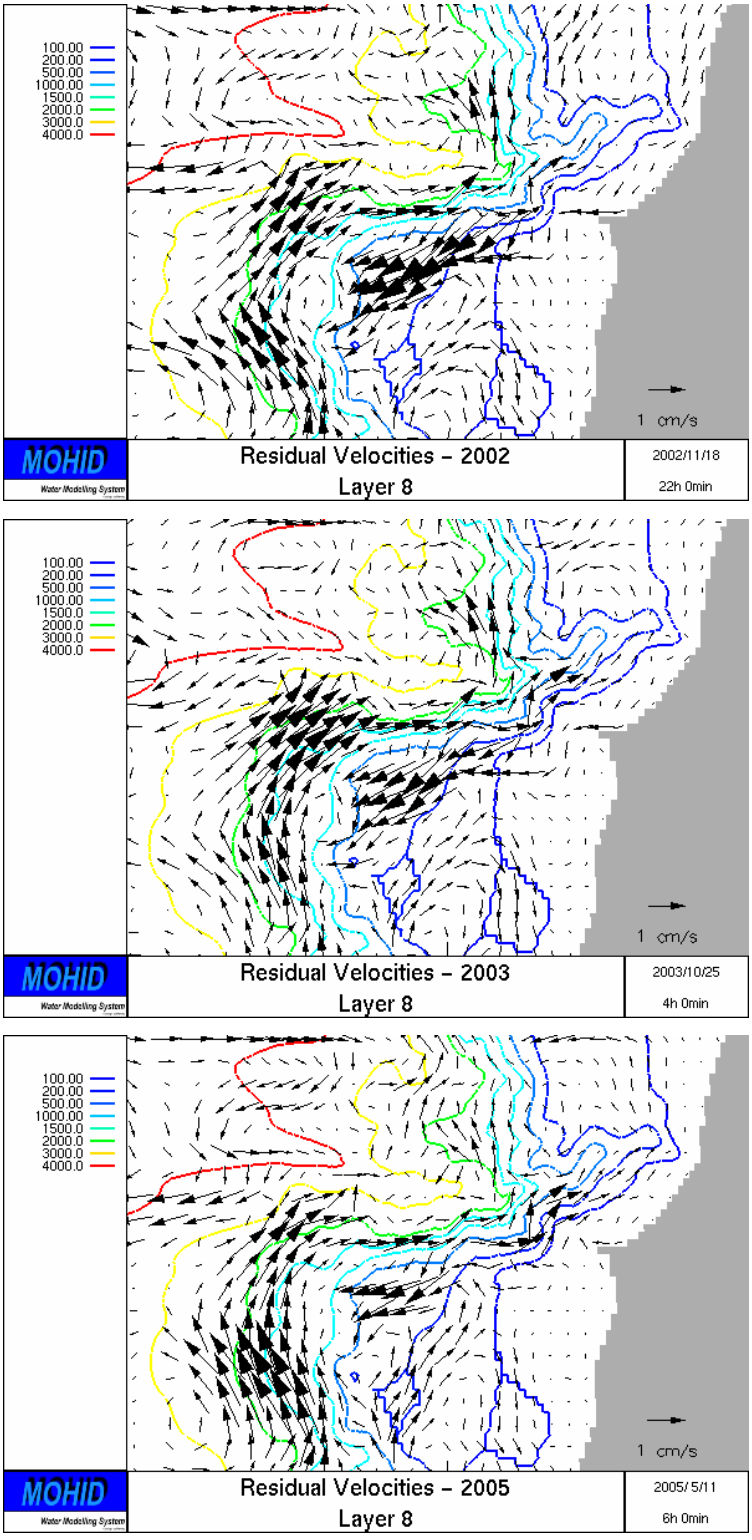

Figure 43 - Residual circulation for Domain 2 at an intermediate layer (Layer 8). Results after 15 days run for the period of the 2002, 2003 and 2005 cruises.

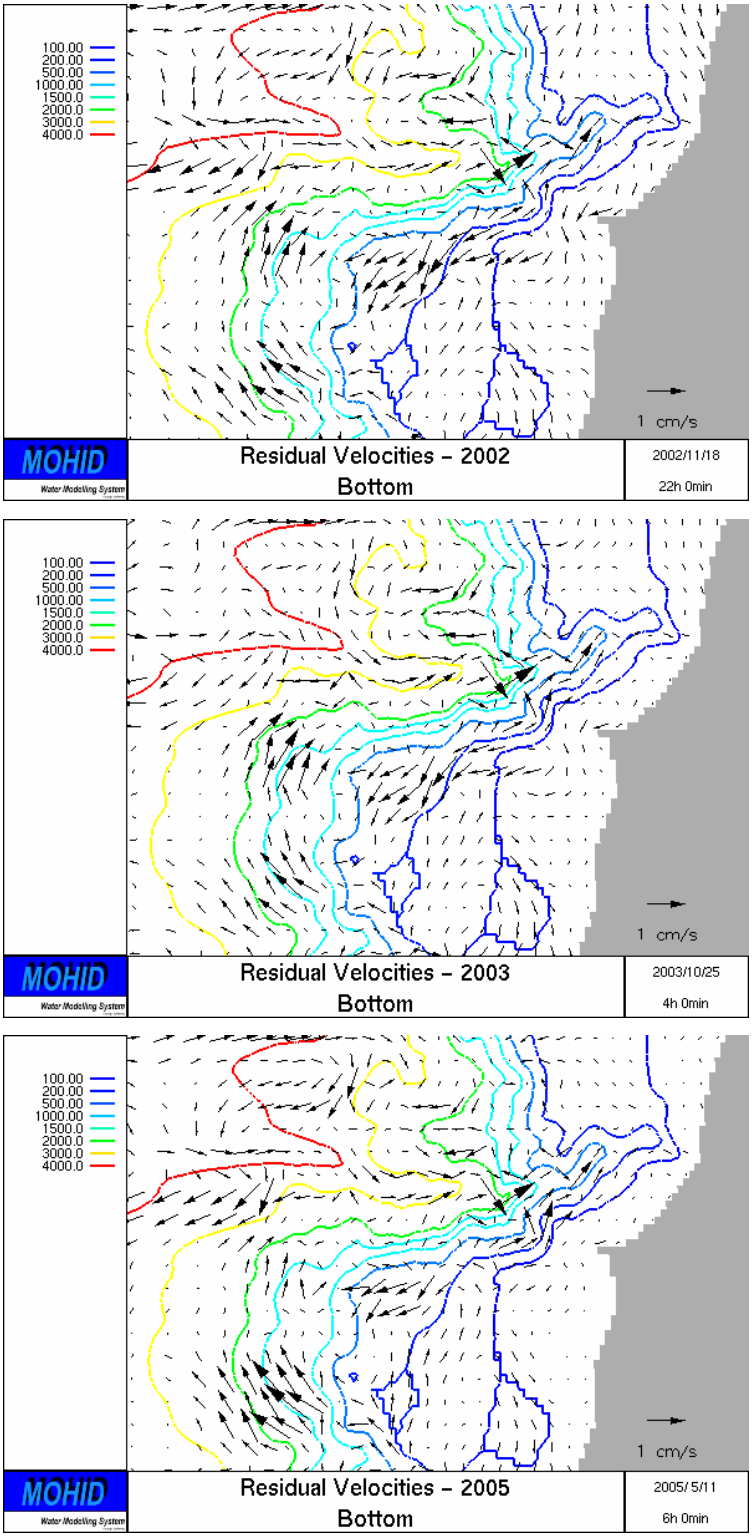

Figure 44 - Residual circulation for Domain 2 at Bottom. Results after 15 days run for the period of the 2002, 2003 and 2005 cruises.

Model velocities are lower than those measured in this area (see chapter 2 and chapter 3). For the deeper layers, where the effect of wind and waves is irrelevant, the model results are according with what in known for the general circulation in this region (chapter 2) and inside the canyon (chapter 3). So we can consider that the model reproduces well the major current patterns for this area.

The channelization and intensification of the bottom current in the canyon axis is an aspect to retain.

Since the model was able to reproduce the water masses structure and the circulation pattern for this area, the next step was to verify if forcing the model with tide could reproduce the nepheloid structures observed during the 2002, 2003 and 2005 cruises, due to the generation and propagation of internal tides at specific levels.

Model results were analysed for cross sections A, B and C referred in Figure 15 for 2002 and cross sections D, E, F and G referred in Figure 25 for 2005 and also the along canyon axis sections for 2002, 2003 and 2005 (Figure 18, Figure 22 and Figure 28, respectively).

Although quantitatively there are differences between model and data (see for example Figure 18 and Figure 47), qualitatively the model reproduces most of the observed patterns. The model is able to reproduce in the same locations the INLs and BNLs observed with the CTD. One thing that must be kept in mind is that for model simulations bottom topography was interpolated and smoothed (as explained in Section 5.1.2.1). This procedure is responsible for the differences seen in the shape of the canyon, particularly in the upper middle canyon sections, as for example sections B, E and F.

Quantitatively in most cases the model gives higher SPM values than those found locally. There are several variables that may influence these differences. One is the initial concentration of the sediments in the entire water column that it was set to 0.1 mg l^{-1} (for example, for the 2002 cruise values measured in the clear water column were 10 times lower). Another is the bottom layer initial concentration that it was set to 5 Kg m^{-2} for the entire domain, value that we found probably a bit exaggerated for some parts of the canyon. Although the values of CSE, CSD, Ws considered in these

simulations were an average value calculated for this area (see also de Jesus Mendes *et al*., 2007) they may also be an error factor.
Several attempts were made to find the best initial conditions combination, although that did not improve the results obtained. Further work must be done in this area.

Analysing the model results in what concerns suspended sediment concentrations for the 2002 cruise (Figure 45 - 3rd column), for section A the model reproduces the maximum in sediment concentration at the shelf break at the southernmost stations following the same N-S gradient observed in field data.
The model also reproduces de INL at the southern wall around the 1500 m, but although it spreads northward no connection is seen with the northern rim.
The model was able to reproduce also the small BNL at the canyon axis just as in section A.

In section B, the model reproduces well the patterns observed with field data, with higher reuspension at the northern canyon rim and wall. The model reproduces the INL below the SML, the BNL at the canyon axis, with more than 200 m thickness and the BNL at the northern shelf break, spreading southward.

For cross-section C, the results match with those already obtained for sections A and B. Once again the model is able to reproduce the nepheloid layers below the SML. Although field data does not show continuity between the BNLs at the shelf break and the BNL at 300-400 m depth, this continuity is observed in model results. In the model there is a continuous high turbid layer starting on the shelf going along both flanks until the canyon axis. This results seem, nevertheless, very realistic. The differences in field data and model results may be due to sampling procedure. Section C has only 3 sampling stations; this spatial distribution may have influence in the sediment distribution patterns, since there is no continuity as there is in the model. As in field data the concentration of sediment is higher in the northern canyon wall than in the southern canyon wall. A well developed BNL at the level of the shelf break in the northern rim is visible in both field data (Figure 15) and model simulation (Figure 45).

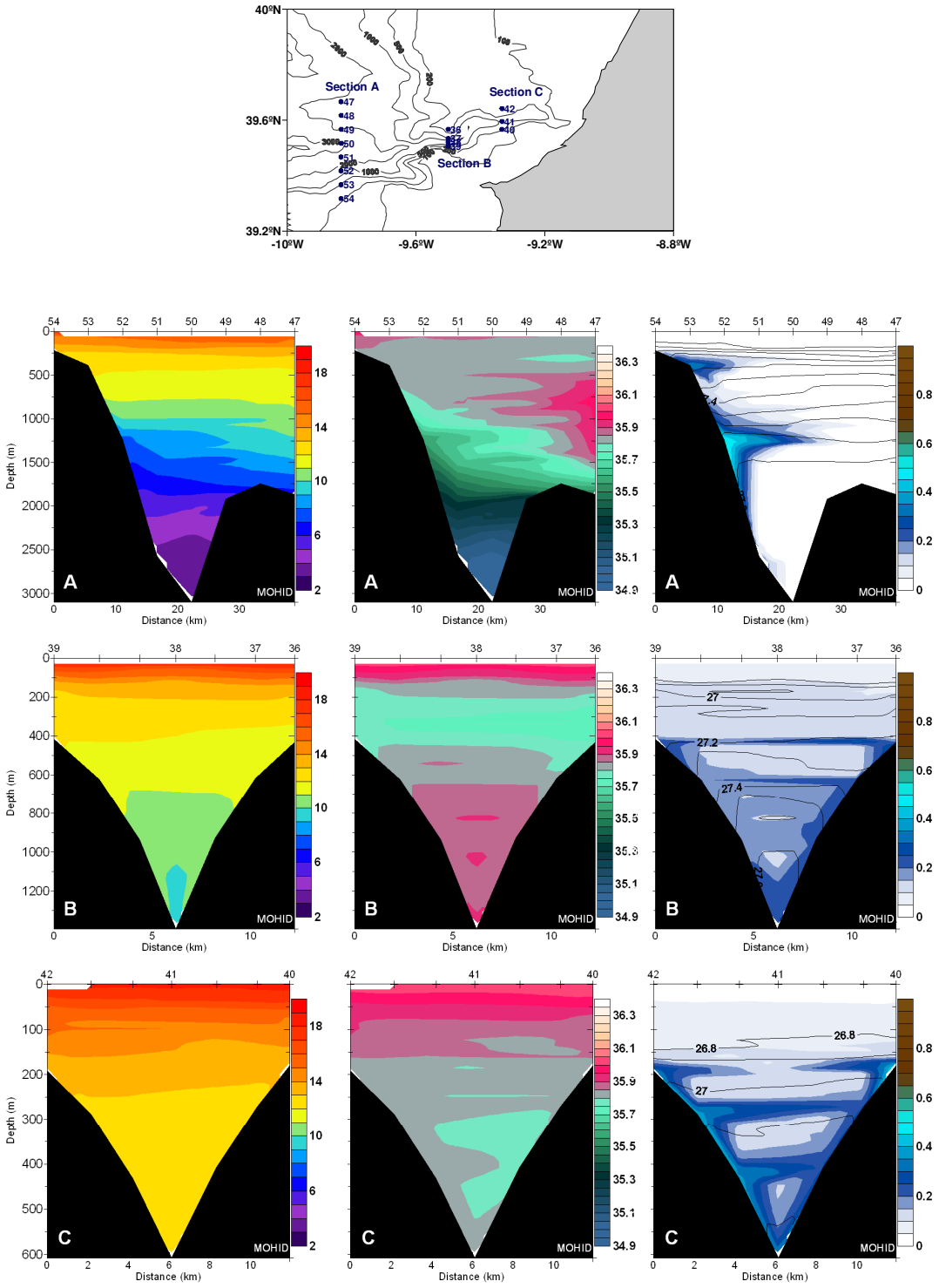

Figure 45- Model results for the period of the 2002 cruise, of the vertical distribution at 3 cross sections A, B and C, of Temperature (ºC) (1st column), Salinity (PSU) (2nd column) and Turbidity (FTU) and Density (kg m-3) (3rd column), where contours represent turbidity and solid lines density.

The model simulations, for 2002, reproduced qualitatively well field data. When analyzing cross sections D, E, F and G performed during 2005 (Figure 46) the evidence is even higher.

As in field observations (Figure 25) for section D resuspension events are observed mainly at the southern wall of the canyon. Although the model results show resuspension all along the southern wall, higher values can be found forming a BNL at the level of the shelf break and an INL around 1500 m deep with a S-N gradient. The BNL at the northern rim, not as developed as in field data, is also present. A small BNL at the canyon axis is also present. As in field data clear water at the northern area of the section may indicate there is no canyon influence in this area.

Once more results for both upper middle canyon sections (E and F) are very similar as in observations (Figure 25). As in field data resuspension is higher at the southern rim and wall with a continuous BNL from the shelf break, along the canyon wall down to the axis. The BNL at the canyon axis is present in both stations, being the only difference the higher thickness of this BNL in section E when compared with field data.

In the model results, sediment concentration patterns for section G (Figure 46) are also very similar to the observations (Figure 25). A continuous BNL along the entire northern canyon wall (where concentrations are higher) merges with the BNL at the canyon axis. A small BNL at the level of the shelf break in the southern rim is also present. The major difference is in the superficial turbid layer that is not visible in the model results. In the model it was considered an initial homogeneous concentration of suspended sediments in the water column and at the bottom, but no extra source for sediments. This may explain the absence of the superficial turbid layer.

Apart from suspended sediment concentration values, the model reproduced the main patterns observed in field data. Higher resuspension in the southern canyon wall at the canyon mouth section, and a small BNL at the canyon axis when compared with the upper middle canyon and the canyon head stations, is observed.

Results from field observations and from the model are also very similar for the section near the canyon mouth and canyon head in 2002 and in 2005. The differences observed between the two years in the intermediate canyon sections may be due to their location. Comparing section locations for both years (Figure 45 and Figure 46), section B is in the middle of sections E and F.

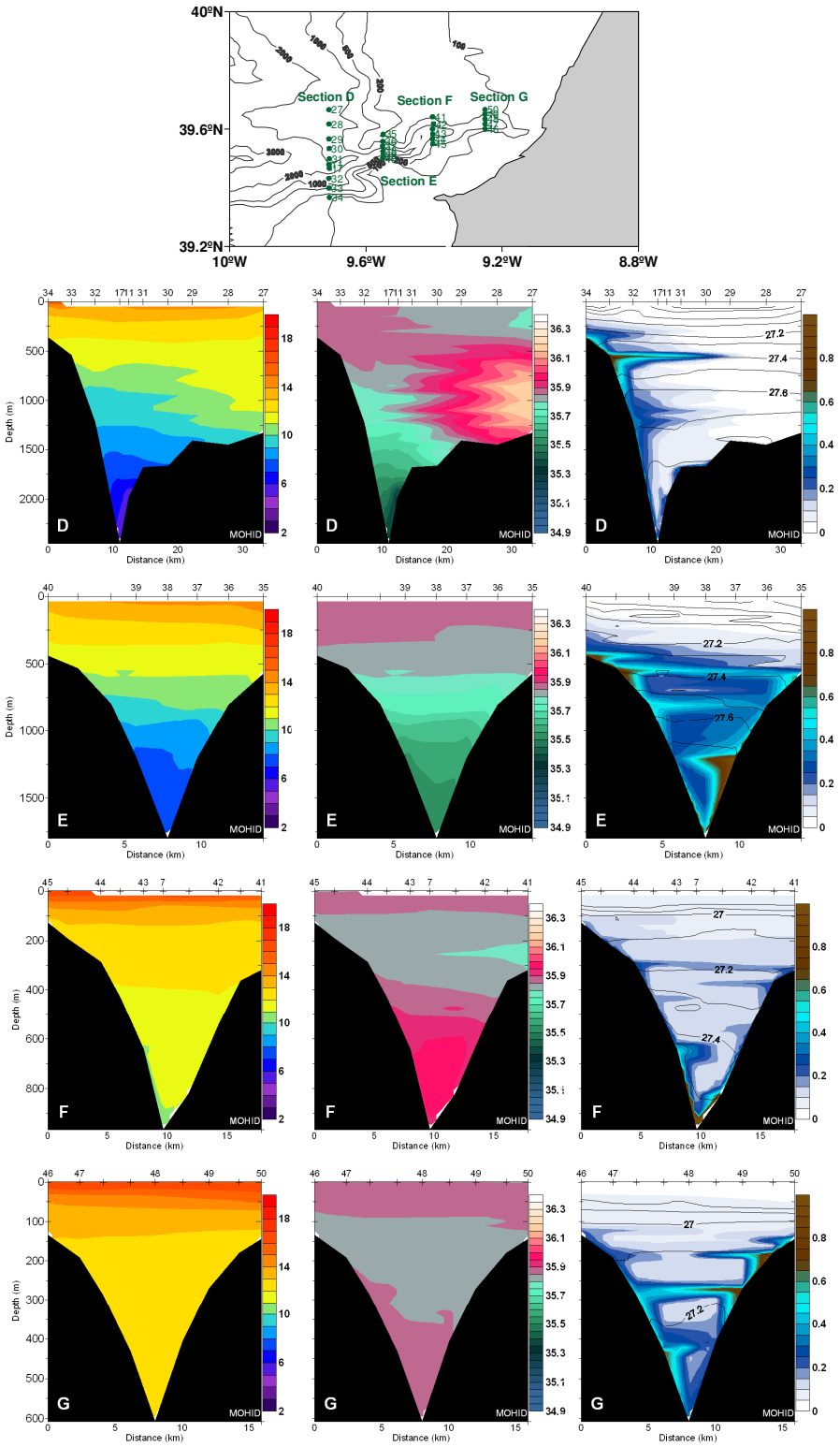

Figure 46- Model results for the period of the 2005 cruise, of the vertical distribution for 4 cross sections D, E, F and G, of Temperature (ºC) (1st column), Salinity (PSU) (2nd column) and Turbidity (FTU) and Density (kg m-3) (3rd column), where contours represent turbidity and solid lines density.

All three sections are located in meanders, but while in section E and F the concavity of the meander is in the northern margin in section B it is in the southern margin. This may create a different effect on the flow pattern and different resuspension conditions.

Suspended matter concentrations produced by the model along the canyon axis, for the 2002, 2003 and 2005 simulations for the period of the cruises are shown in Figure 47, Figure 48 and Figure 49, respectively. Maximum concentrations near the bottom at the canyon head are only reproduced for the 2002 simulation (Figure 47). The concentration maximums observed in field data for the 2002, 2003 and 2005 cruises at 1500 m depth at the level of the bottom of the MW are well reproduced by the model, which also shows relative maximums at the canyon floor around 1500 m depth (bottom limit of the MW). These sediments resuspended at this level are trapped in this mixing layer and tend to extend seaward as an INL. The larger extension in the seaward direction of the nepheloid layers in the model results, compared with field data, may be due to numeric diffusion. As in field data a small maximum is also present around 2500 m deep for all the simulations.

Beside these local maximums, high sediment concentrations can be observed up-canyon along the canyon axis, in agreement with field observations performed during the Eurostrataform project (Figure 18, Figure 22 and Figure 28).
Qualitatively the observed patterns in both situations (model and field data) are very similar, mainly the INLs at the canyon axis that are very realistic and in accordance with field data.

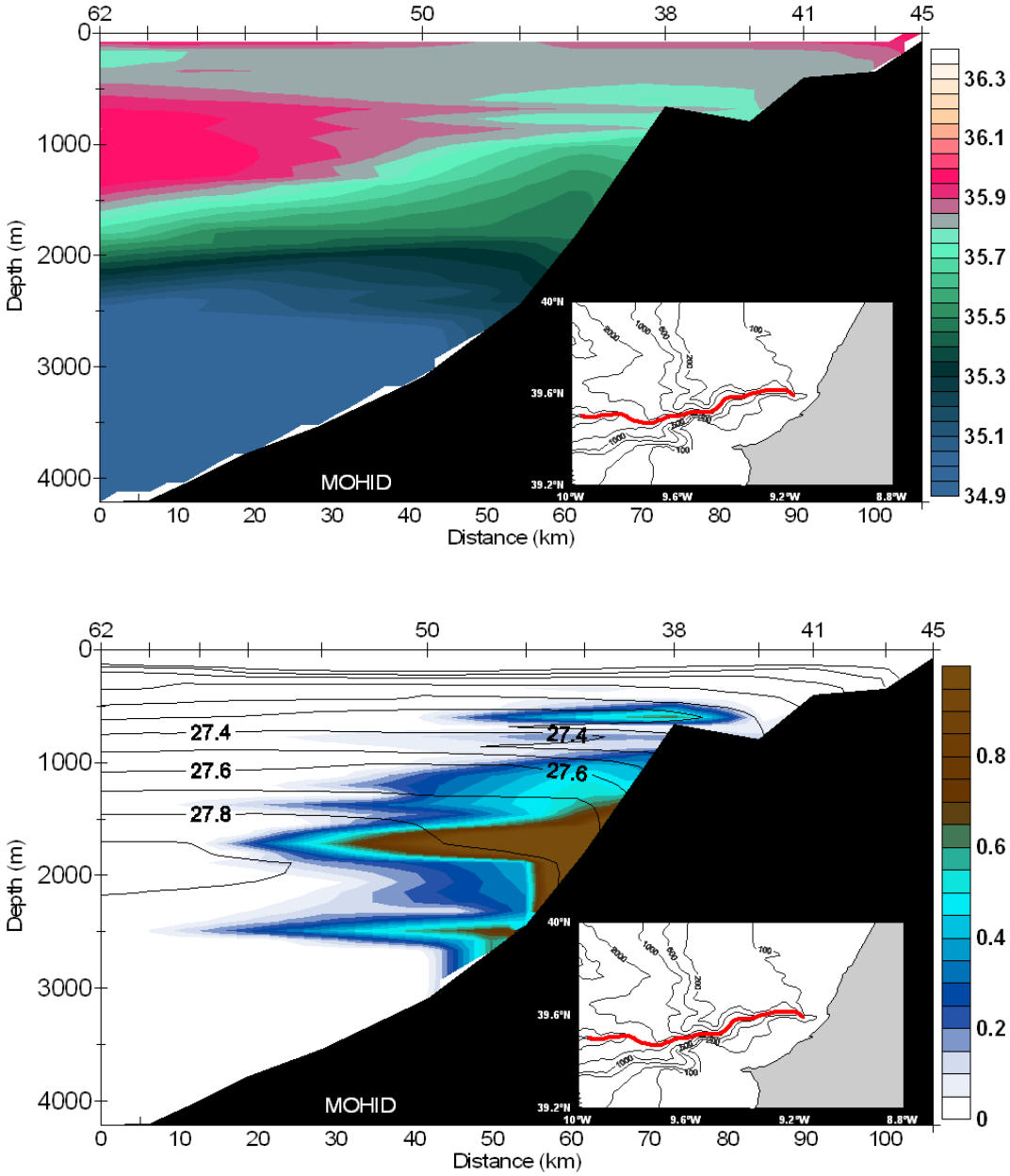

Figure 47 - Model results for Salinity (top) and Turbidity (contours) and Density (solid lines) (bottom) profiles in the along canyon axis section, for the period of the 2002 cruise.

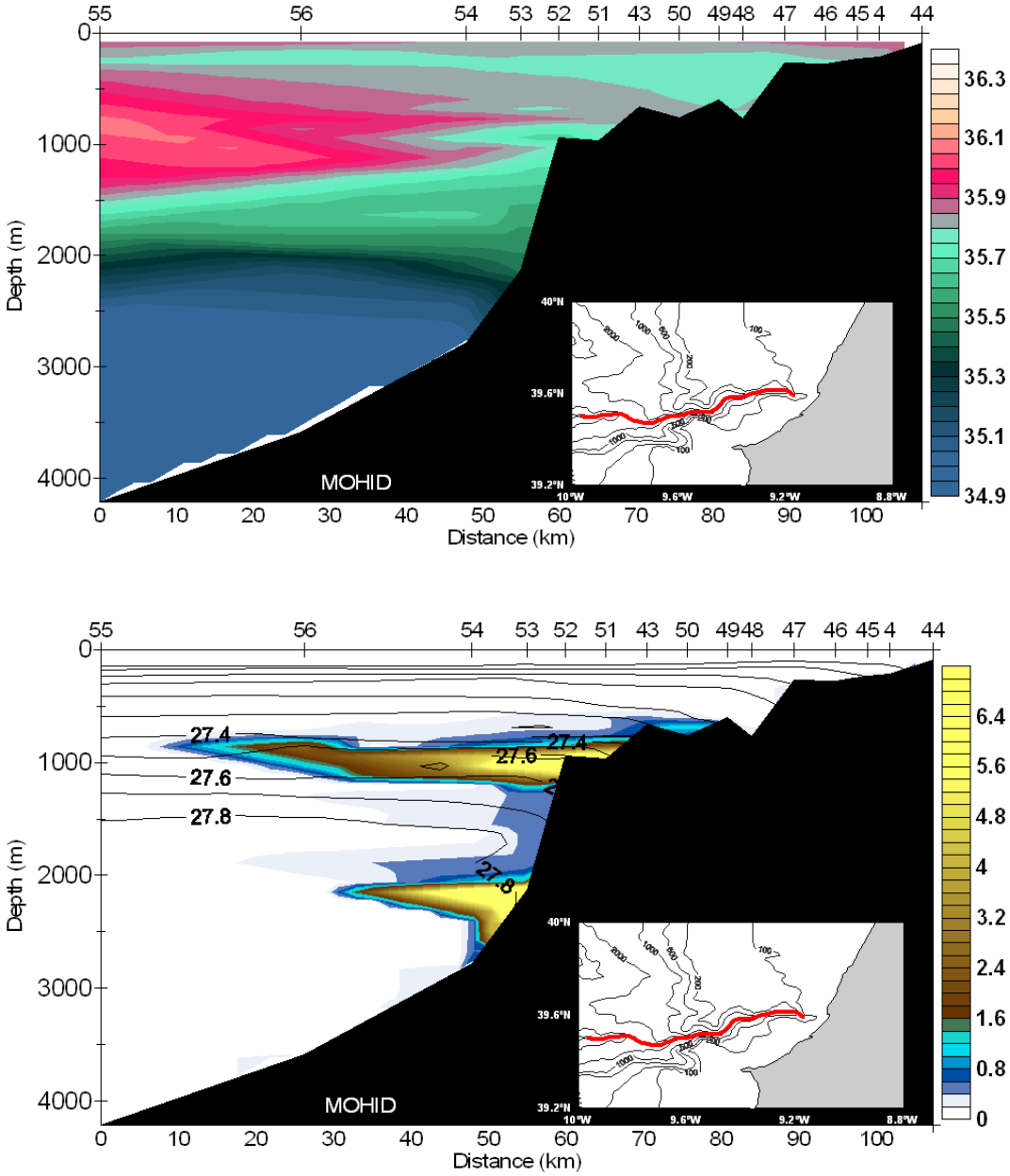

Figure 48 - Model results for Salinity (top) and Turbidity (contours) and Density (solid lines) (bottom) profiles in the along canyon axis section, for the period of the 2003 cruise.

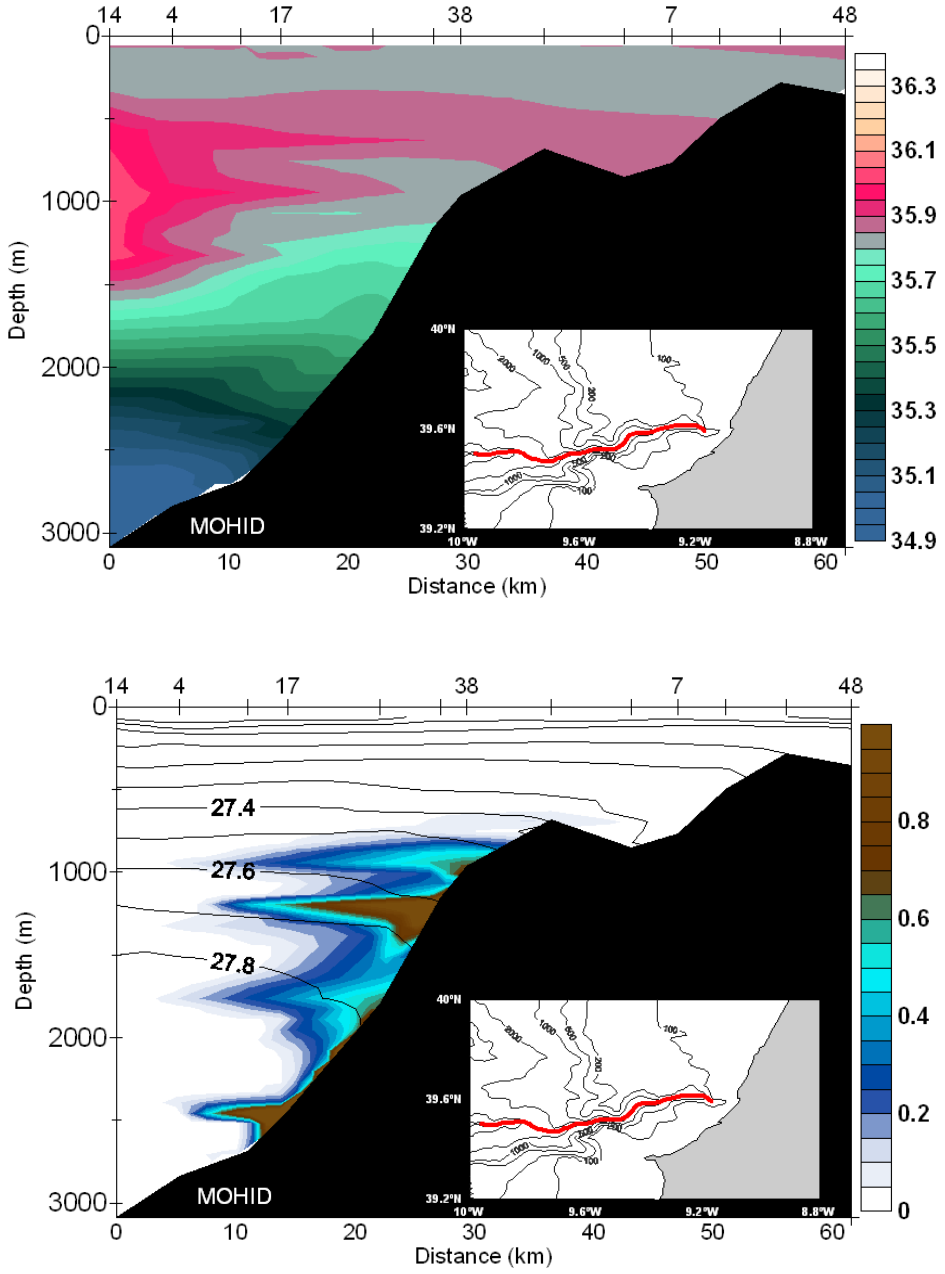

Figure 49 - Model results for Salinity (top) and Turbidity (contours) and Density (solid lines) (bottom) profiles in the along canyon axis section, for the period of the 2005 cruise.

After verifying that the model forced only with tide was capable to reproduce the observed nepheloid layers, it was also checked if the model could reproduced the changes in the nephelometry concentrations in the water column during a tidal cycle.

Figure 50 and Figure 51 represent the evolution of the water column sediment concentration with time (during a tidal cycle) for a station at 800 m deep (Figure 50) and 350 m deep (Figure 51), both in the canyon axis. Results are comparable with Figure 30 and Figure 31, for stations 41 (Figure 30) and 42 (Figure 31) respectively. Results are similar for both stations. The model is able to reproduce sediment concentration variability due to tide, with higher concentrations during ebb tide diminishing during flood tide.

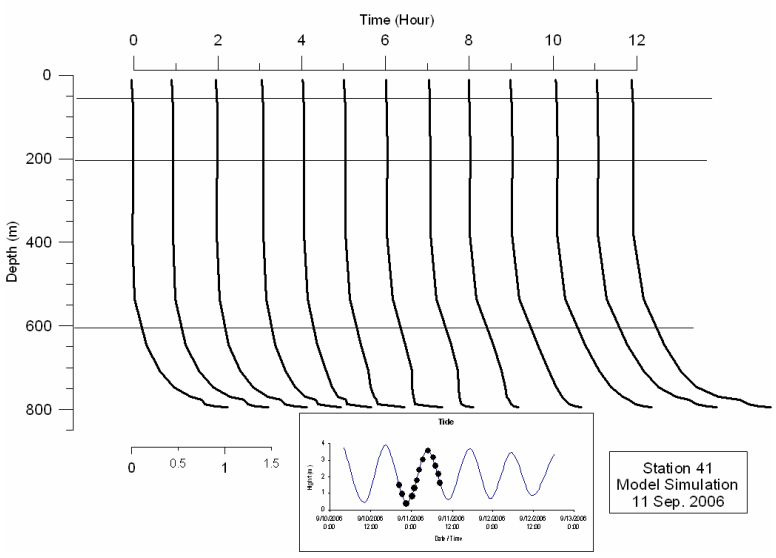

Figure 50 – Model results for turbidity at station 41 (2006 cruise) repeated for a tidal cycle.

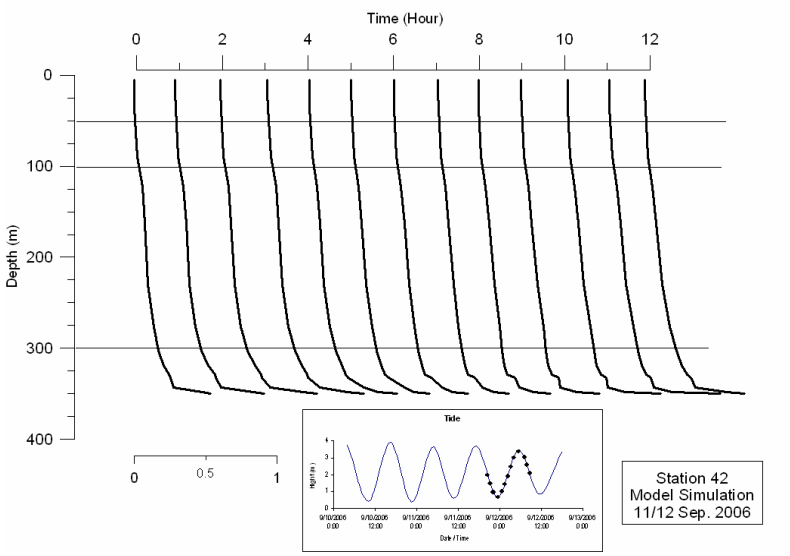

Figure 51 – Model results for turbidity at station 42 (2006 cruise) repeated for a tidal cycle.

5.2.2 Internal Tides

Internal tides, has referred in Section 3.2.5 can be found nearly everywhere in the world. They are often generated in stratified water through the combined effect of barotropic tides and topography. The generation of the internal tides takes place where horizontal currents impinge on undersea mountains or ridges. The conversion of barotropic to baroclinic tides might be a major sink for the barotropic tidal energy. The obliquely propagating internal waves are in turn subject to reflections and scattering.

The submarine canyons play a special role, as they may concentrate locally internal wave energy (e.g. Gordon & Marshall, 1976; Hotchkiss & Wunsch, 1982; Hunkins, 1988). This concentration of energy may be responsible for an enhancement in turbulence and mixing (Davies & Xing, 2004). Beside this, studies reveal also that internal waves signal may be greatly amplified specially in narrow canyons (in the sense that its width is always less than the internal radius of deformation) as in the Hudson and in La Línea submarine canyons (Hotchkiss & Wunsch, 1982; Lafuente *et al*., 1999).

Cacchione & Southard (1974) had already suggested that bottom shear stresses generated by internal tides could be large enough to ressuspend sediment over continental shelf and slope regions.

To find a relation between internal tides and nepheloid layers we need to consider the linear internal wave theory.

5.2.2.1 Linear internal wave theory

Over sloping topography, bottom intensified flows and high mixing rates associated with internal waves can occur when the slope of the topography ($\alpha = dh/dx$) is similar to the angle that the group velocity vector (ϕ) makes with the horizontal. This angle is determined by $tan\ \phi = s = \pm\sqrt{(w^2 - f^2)/(N^2 - w^2)}$, where w is the wave frequency, f the Coriolis parameter, and N the buoyancy frequency. Such slopes are termed critical slopes (e.g. Holloway & Bernes, 1998). These intensified flows may be the dominant process contributing to bottom shear stresses on continental slopes and hence be important in determining sediment resuspension.

The ratios α/s (Figure 52) will determinate how the internal wave energy will propagate along the bottom slope. If the characteristic angle (CA) of the beam is steeper than the slope of the seafloor, internal tidal energy is transmitted landward as it bounces between the seafloor and the base of the mixed layer. If the CA is shallower than the slope, the energy is reflected back toward the deep ocean. When these two angles are equal, the energy is trapped near the seafloor, where it may be sufficient to stir up the sediments or at least to prevent suspended sediments from settling out (Cacchione & Drake, 1986; McPhee & Kunze, 2002).

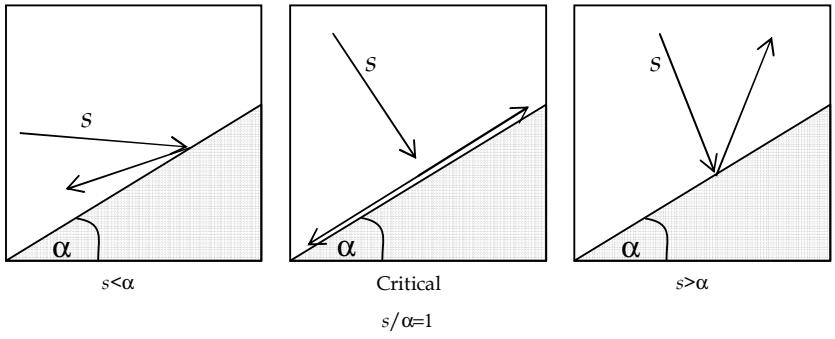

Figure 52 - Schematic illustrating (a) subcritical ($s/\alpha < 1$), (b) critical ($s/\alpha = 1$), and (c) supercritical ($s/\alpha > 1$) internal-wave reflection. Arrows show the direction of characteristic angle propagation. (Adapted from McPhee & Kunze, 2002)

5.2.2.2 Internal waves in Nazaré Canyon

Having in consideration the ratio α/s defined in the previous section, a map for critical conditions was drawn (Figure 53) taking into account the ratio α/s for Nazaré canyon and adjacent areas. To compute α/s we need to know the density field and the bathymetry. In order to keep consistency the calculation was made by using the same data used for the high resolution model calculations. Many near critical areas are found along the continental slope to the north and to the south of Nazaré Canyon mainly between the 500 m and 1500 m isobaths. Near the canyon mouth several critical areas are found. To notice that in particular the bottom slope is critical for M_2 tide at the southern end of cross-section A previously referred. Along the Nazaré Canyon rims, all way up to the canyon head, near critical areas are found.

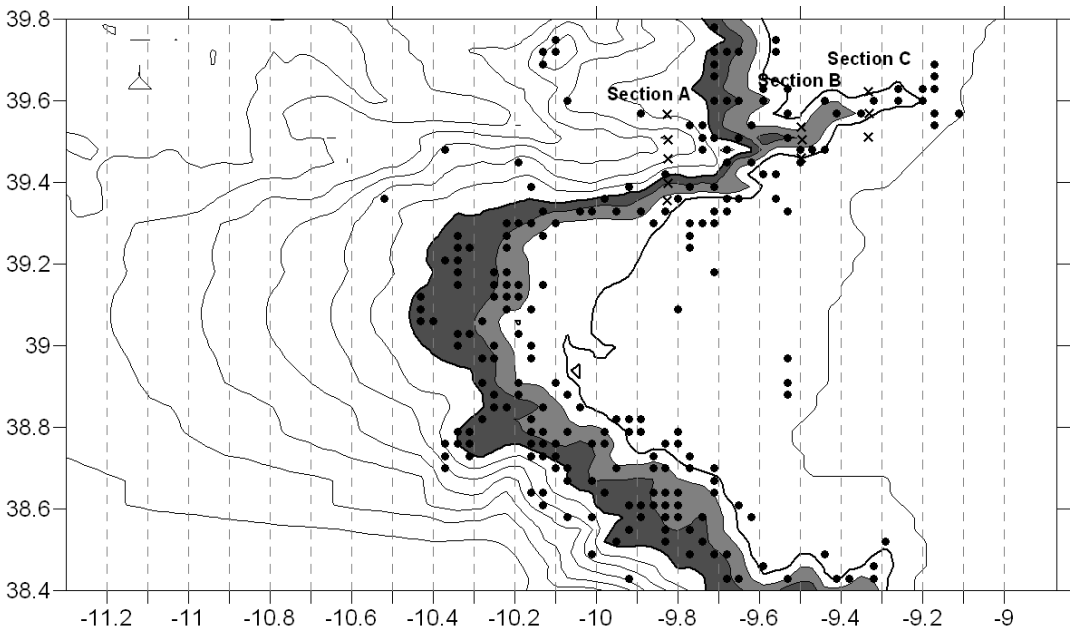

Figure 53 – Critical areas (marked with dots) for the Portuguese Continental shelf and slope around Nazaré Canyon. Isobaths are represented every 500 m. Additionally, we represent the 200 m isobath. The area between 500 and 1500 m is coloured with grey. The Sections A, B and C, are marked with (x) to serve as a reference.

When analysing the CTD results for the cross-sections of the 2002 (A, B, C) and 2005 (D, E, F, G) cruises, it was considered that INLs, were related with critical areas on transects slopes. Taking into account the linear internal wave theory it was calculated, as an example, critical areas (ellipses) (α/s =1) for section A (Figure 54). Comparing this results with those from section A in Figure 15, it can be observe that the critical areas are located according with the places with higher values of turbidity in the CTD cats that lead to the formation of the INLs.

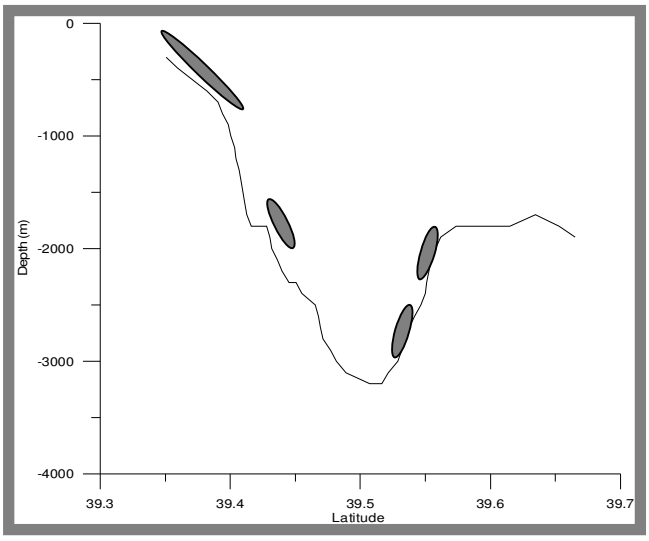

Figure 54 – Critical areas (marked with ellipses) for section A (south is to the left). Results are in agreement with the previous figures and with the CTD data shown for Section A in Figure 15.

Figure 55 and Figure 56 show the baroclinic component of the instantaneous zonal velocity, calculated with the model. Figure 55 corresponds to a strait line transect along the canyon axis and Figure 56 follows the meandering canyon axis (same transect as in Figure 18, Figure 22 and Figure 28). In both cases is evident that the typical beams are associated to maximums in velocity modulus resulting from the propagation of internal tides. Also Rosenfeld *et al*. (1999) using the Princeton Ocean Model (POM) for simulating the effect of internal waves at Monterey Canyon, observed an intensification of currents near the seabed which occurred for critical or near critical slopes when the topographic slope was comparable to the slope of the internal wave beams.

These beams of internal tides inside the Nazaré canyon were confirmed by direct measurements of tidal currents (see also Chapter 3). The bottom intensification of internal tides was particularly evident in a mooring at the upper canyon (1600m depth), where canyon walls are steep. As referred in Eurostrataform (2006b), the mooring data indicated that "*current variability at semidiurnal tidal periods increases more than one order of magnitude from 250m to the bottom (1600m) and is modulated by the spring*

tides /neap tides cycle. Tidal current ellipses reach amplitudes of 50 cm s^{-1} at 20 m above the bottom during spring tides, and were strongly polarized in the along axis direction. Both higher frequency tidal harmonics as well as diurnal periods become increasingly energetic at near bottom depths, suggesting that important non-linear interactions occur at those depths".

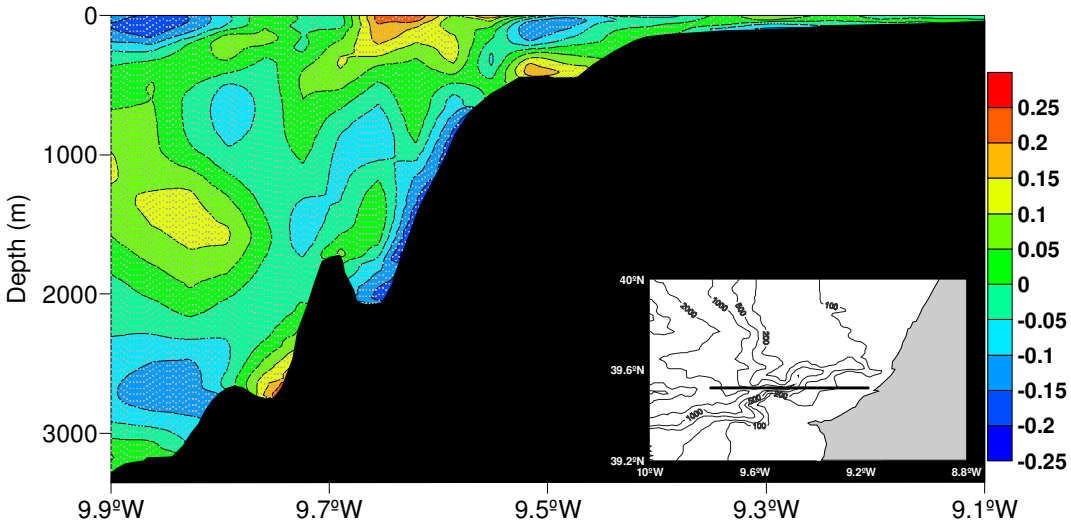

Figure 55 – zonal component of the baroclinic velocity contours in the cross-section depicted at lower right corner of the panel during high tide.

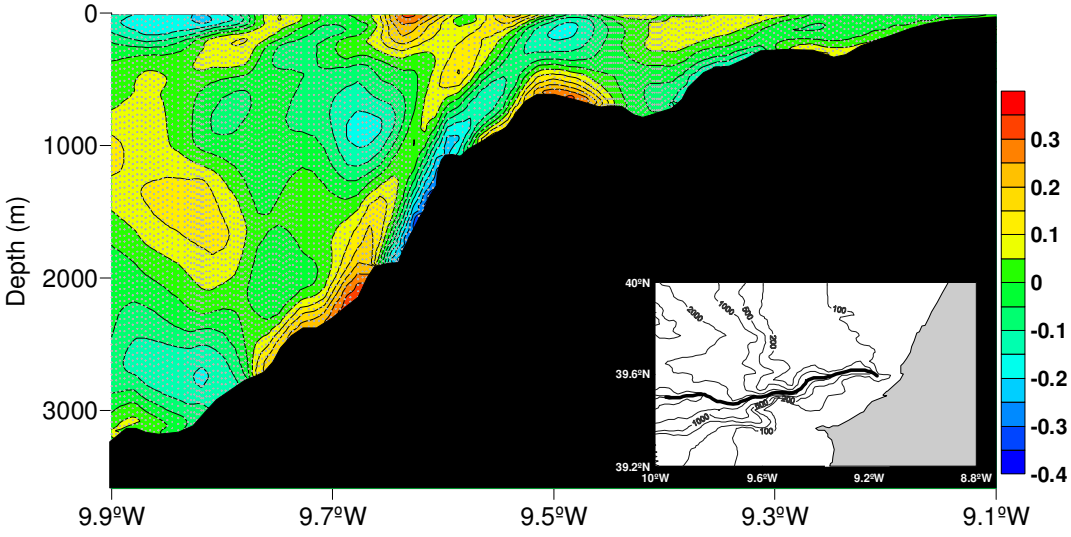

Figure 56 – Zonal component of the baroclinic velocity contours in the along canyon section depicted at lower right corner of the panel during high tide.

The location of these beams (velocity maximums) is in agreement with the location of the critical areas (ellipses) along the canyon axis (Figure 57) drawn based on the linear internal wave theory. In a general way the upper canyon is mostly near critical, what favours the wave propagations along the canyon axis as stated by Petruncio *et al.* (2002). These authors explored the effect of canyon floor slope on internal tide energy generation and found that "*canyons that are near-critical along much of their entire length, …, develop strong internal tides that propagate shoreward.*". Nevertheless, ellipses indicate areas where the ratio $\alpha / s = 1$. These means according to the linear internal wave theory, areas where sediments can be resuspended or at least kept in suspension. These critical areas are located at 1500 m depth, 1000 m depth and 400 m depth, what is in agreement with the CTD observations from Figure 18, Figure 22 and Figure 28, where the turbidity maximums are observed, and are also in the origin of the permanent BNL along the upper canyon axis. Also the results from sediment traps, moorings and Landers deployed during the EUROSTRATAFORM project (Eurostrataform, 2006b) at 1600 m depth, suggested a permanent situation of very high suspended (and resuspended) sediment fluxes near the bottom at this depth, since the sediment traps overfilled soon after each deployment, either in winter as in the summer (along with current meter measurements of 21 cm s^{-1} mean velocity at this depth).

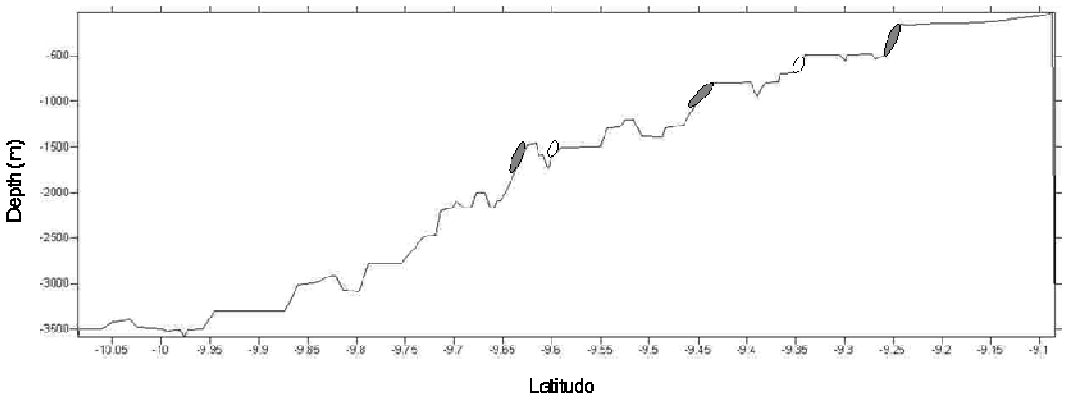

Figure 57 – Bathymetry of the Nazaré Canyon axis. Ellipses indicate areas where the ratio $\alpha/S = 1$, corresponding to areas where resuspension is more favourable to occur.

Similar conclusions, on the relationship between internal wave energy and sloping bottoms, and consequent sediment resuspension, leading to the formation of intermediate and bottom nepheloid layers, and the associated transport, were achieved by several authors. On this subject observations (e.g. Gardner, 1989; Mcphee-Shaw *et al*., 2004; Butman *et al*., 2006), several numerical modelling studies on realistic and idealized bathymetry of different features including canyons (e.g. Ribbe & Holloway, 2001; Davis & Xing, 2002; Xing & Davies, 2003), and laboratory experiments (de Silva *et al*., 1997; McPhee-Shaw & Kunze, 2002) have been performed. They indicate that the slope of the sea bottom, under the influence of internal waves, is determinant for sediment resuspension; that in critical slopes the energy of internal tide beams is high enough to enhance bottom friction velocity and promote resuspension; and that sediment concentrations in these places can be 10 times higher than in the surrounding area.

In order to observe the differences in sediment resuspension between the canyon and the adjacent shelf an along slope transect, performed during the 2006 cruise, at the continental margin north of the canyon (Figure 9) was analysed. CTD observations (Figure 58) indicate high turbidity (0.8 FTU near the coast) over the shelf progressively decreasing in depth and, the presence of an INL located at around 1000 m deep and a less evident one around the 1600 m deep, both with concentrations around 0.1 FTU. Model results are according with field data, reproducing the same nepheloid layers (Figure 59). As seen previously, 1000 m and 1600 m deep are near-critical areas for the semi-diurnal tide. These nepheloid layers at those depths on the slope reinforce the idea that these INLs are the results of near bottom mixing due to the semi-diurnal tide energy trapping in near-critical areas.

Nevertheless ,the higher concentrations found at the same depths inside the canyon, more than 1 FTU in 2002 and 2005 and 7 FTU in 2003, clearly shows that the canyon concentrates the energy associated to the internal tide.

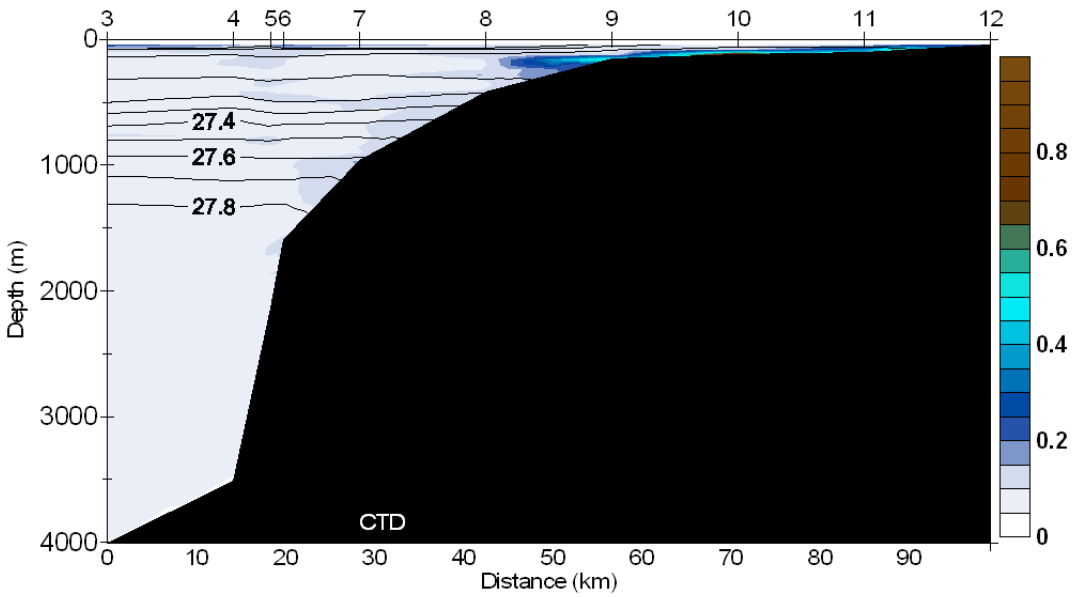

Figure 58 – Vertical distribution of Density (solid lines) and Turbidity (contours) along a slope section located to the North of Nazaré Canyon. CTD Data was obtained during the 2006 cruise.

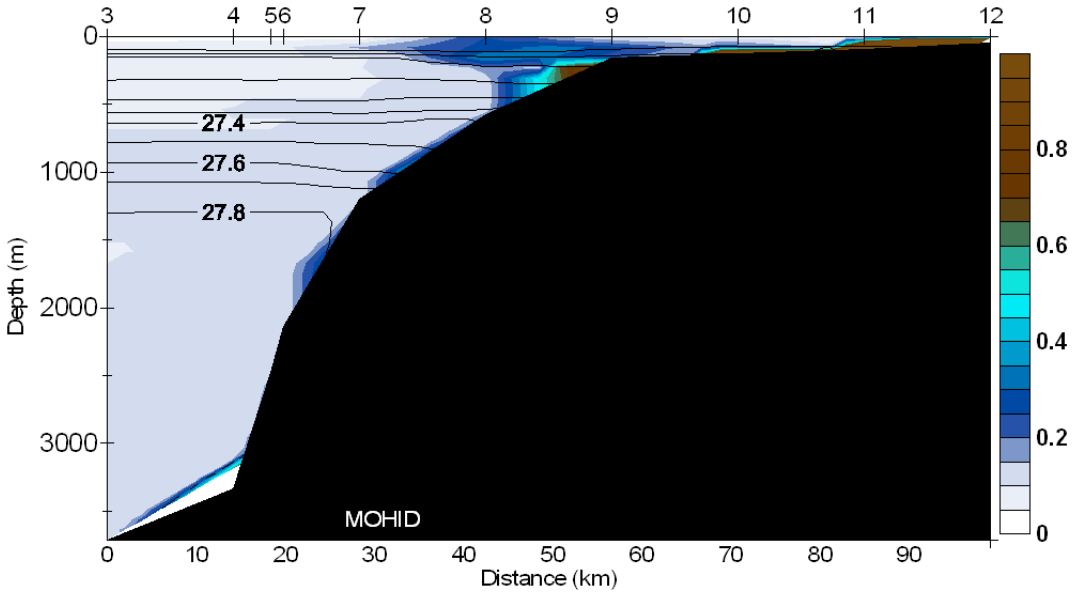

Figure 59 – Model results for the vertical distribution of Density (solid lines) and Turbidity (contours) along a slope section located to the North of Nazaré Canyon, for the period of the 2006 cruise period.

As mentioned earlier submarine canyons play a special role, as they may act as a trap for internal wave energy and by the capacity for channelizing this energy all way up to the canyon head. To better understand the role of the Nazaré canyon in driving this energy the perturbation potential energy (PPE) was calculated from the model results,

according to Gill (1982), which is represented in Figure 60. A large amount of the energy is concentrated near/over the canyon mouth and upper middle canyon – but not over the canyon head, which might explain why in the most seaward cross canyon sections (A and D) higher concentration values are found all along the southern walls. PPE is also higher in the upper canyon meanders with the concavity in the southern rim what also may explain the differences observed at upper middle canyon between sections E and F (Figure 25) and section B (Figure 15). PPE is asymmetrically distributed in the cross canyon direction, with a greater percentage lying along the southern wall. This is particularly evident in the canyon mouth. This kind of asymmetry in energy distribution is likely due to Coriolis rotational effects. Identical features have also been observed by Petruncio *et al*. (2002) in a schematic canyon similar to Monterey Canyon.

In the surrounding areas of the canyon most of the PPE concentrates in shelf break area. Some local maximums of PPE over the shelf, North of the canyon correspond probably to refraction of internal waves that were propagating along the canyon or to waves generated at the shelf break.

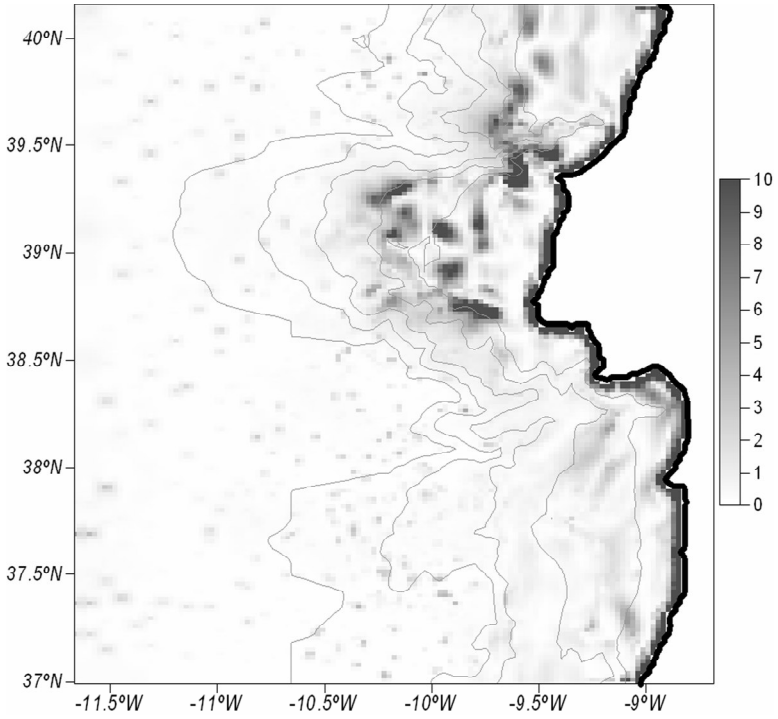

Figure 60 - Model results for the Perturbation Potential Energy for Nazaré Canyon and adjacent areas during flood. Units are Jm^{-3}.

Linear theory states that internal waves are generated where the angle of internal wave ray path matches that of local topography. Steep topographical ridges present effective regions of generation because the bottom slope passes through critically in narrow regions where the vertical momentum is large.

Morphologically the presence of the canyon and the Estremadura Plateau results in the formation of several ridges. In these places internal tide is likely to be generated (similar conclusion had for example Petruncio *et al*., 2002 and Fringer *et al*., 2006) and then funnelled through the canyon.

5.3 CONCLUSIONS

Although there is no major river aligned with the head of the Nazaré Canyon, high values for short -term sediment deposition within the canyon were found, indicating high activity in this canyon (Smith *et al*., 2001; van Weering *et al*., 2002; de Stigter *et al*., 2007; Arzola *et al*., 2008). Important and permanent nepheloid layers were found in deep areas of the canyon, especially between 1000 and 1600 m deep. Both field data and model results indicate that internal tides are the major process for sediment resuspension within the canyon.

The processes in the canyon are much stronger than those in the adjacent margin, inducing higher resuspension of sediments. The near to critical areas in the canyon are in the origin of important nephloid layers and so, sources of sediments to be transported along canyon. Sediment concentration suggest that, while in the lower and middle canyon there was not much energy available, in the upper canyon a considerable portion of the energy was dissipated, probably due to the canyon meandering.

PPE results indicate that this energy propagates along the canyon axis, and it is probably trapped at the upper middle canyon where higher values of suspended material were found. Beside this it was also possible to observe that the southern canyon rims shows higher values of PPE, and this also explains higher concentrations in these areas. These internal tides may be originated in the junction areas between the Estremadura Plateau and the Nazaré Canyon that create special morphological features that may induce the formation of internal tides.

Chapter 6

TRANSPORT AND RESIDENCE TIME OF RESUSPENDED PARTICLES.

6.1 INTRODUCTION

As stated earlier in this work, another objective of the EUROSTRATAFORM project was to define sources of sediments and the sediment transport patterns in submarine canyons, this means, how the sediment is transported along the canyons, and in this specific case, the Nazaré Canyon.

The Nazaré Canyon, as known, cuts the entire shelf collecting and channelling the particulate material derived from the continent and transported laterally from inner and middle shelf to the deep basin.

Oliveira *et al*. (2007) developed a conceptual model of dynamic processes in the Nazaré canyon head area, in the summer and winter, in relation to particle sources. Their studies permitted to conclude that there were several particle sources for the sediments found at the canyon head: (1) the inner and middle shelf north and south of the canyon (where the fine mud deposits are located - Figure 8); (2) beach and cliff erosion and (3) small rivers located south of the canyon.

They concluded that during summer the main source was the resuspension of northern middle shelf deposits by internal wave activity, as confirmed by the studies of Quaresma *et al*. (2007). They observed that this material can be transported as a BNL laterally in suspension to the canyon by upwelling currents. Although during the summer, erosion of the beaches and cliffs north and south of the canyon provides material to be transported to the canyon head by the north-south littoral drift (waves from N-NW); it is during the winter that this process is more intense. In this season, under downwelling conditions, forced by the poleward current, fine sediments carried by southern rivers can reach the canyon area and the middle shelf deposit up to the north. South of the canyon the inner shelf sediments are remobilized by waves that

disturb and inhibit deposition of fines that remain in suspension and tend to disperse northward over the middle shelf region (60–100 m depth) and canyon walls.

Once these sediments are trapped in the upper part of the Nazaré canyon from the coastline to the shelf edge, they will then be, as seen, subject to cyclic resuspension, transport and redeposition under the influence of internal waves.

In this chapter Lagrangian Tracers will be use for simulating sources and the transport of fine sediments resuspended in the Nazaré Canyon and adjacent shelf mud deposits, under different forcing conditions. Will also be used to try to determine how fast the transport of the resuspended particles is by using the concept of residence time.

6.2 METHOD

The simulations were performed using, once more, the MOHID water modelling system. The concepts of the modules used in these simulations, including the Lagrangian module were already presented in section 5.1.1.

Lagrangian tracers simulation were done using the geometry of the Domain 1, already described in section 5.1.2, and considering the same initialization conditions for turbulence and hydrodynamics.
In these experiments we designed 4 scenarios to observe the role of different processes in resuspension and transport in Nazaré canyon and adjacent shelf.
In the first scenario the model was forced with tide, and in order to observe how the vertical density water structure influences resuspension and transport a constant value of temperature and salinity, for the entire domain, was assumed.
In the second scenario the model was again forced with tide but in this case it was used the same salinity and temperature profile as for the 2002 simulations (described in chapter 5). Although temperature and salinity were horizontally homogenous there was a vertical density gradient in this case.

The third and fourth scenarios were also forced with tide, but another forcing condition was added: wind. In the third scenario a persistent constant SW wind with a velocity of 25 km h^{-1} was considered in the fourth scenario it was a constant NW wind. The simulation period was 52 days.

For the lagrangian tracers five boxes were drawn in the Nazaré canyon area (Figure 61); two on the middle shelf, approximately with the same location and dimension of the two mud patches, north and south the Nazaré Canyon (Figure 8); another at the canyon head, and two others on the north and south canyon rim and walls, between the canyon head and the 1000 m deep. The boxes had 1 cm thickness and were full with particles simulating bottom sediments.

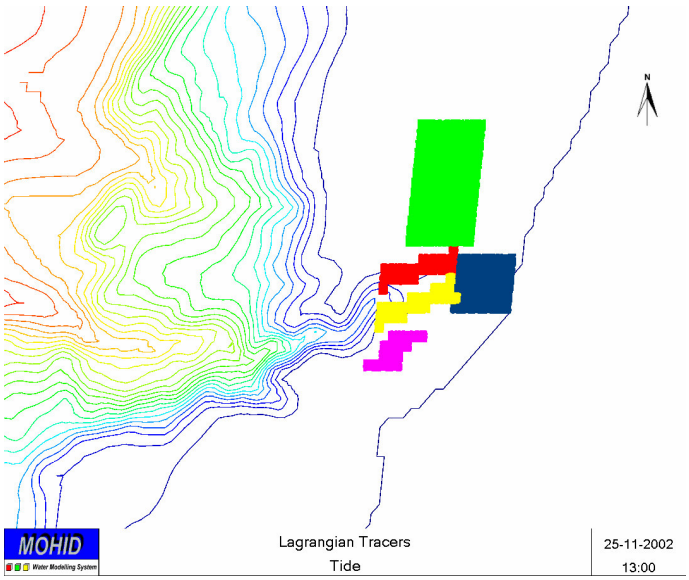

Figure 61 – The 5 boxes (blue, green, violet, yellow and red) considered for the Lagrangian tracers experiments.

Different values of Critical Shear Erosion (CSE), Critical Shear Deposition (CSD) and settling velocity (Ws) were considered for each box. Both boxes on the shelf have values of CSE = 0.1 Pa, CSD = 0.00034 Pa and Ws = 0.0014 m s^{-1}, the boxes on the canyon walls have values of CSE = 0.06 Pa, CSD = 0.00034 Pa and Ws = 0.0014 m s^{-1}, and the box on the canyon head have values of CSE = 0.07 Pa, CSD = 0.00016 Pa and Ws = 0.001 m s^{-1}. All these values are for fine sediments found in each area, during the project. These values were calculated by the team of the International University of Bremen leader by Prof. Laurenz Thomsen, also partner on the Eurostrataform project.

6.3 RESUSPENSION AND TRANSPORT

Since there was no vertical or horizontal density gradient, the main objective on the first experiment was to observe if the particles would respond to tidal forcing. As it can be observed in Figure 62 particles stood still for the period of the simulation. The top of the green particles is in the model boundary, and the movement observed may be due to some instability in this area.

Figure 63 shows the results for the second scenario. Particles are resuspended due to the tidal circulation and internal waves breaking. Has seen in the previous chapter internal waves in the canyon are strong enough to resuspend particles.

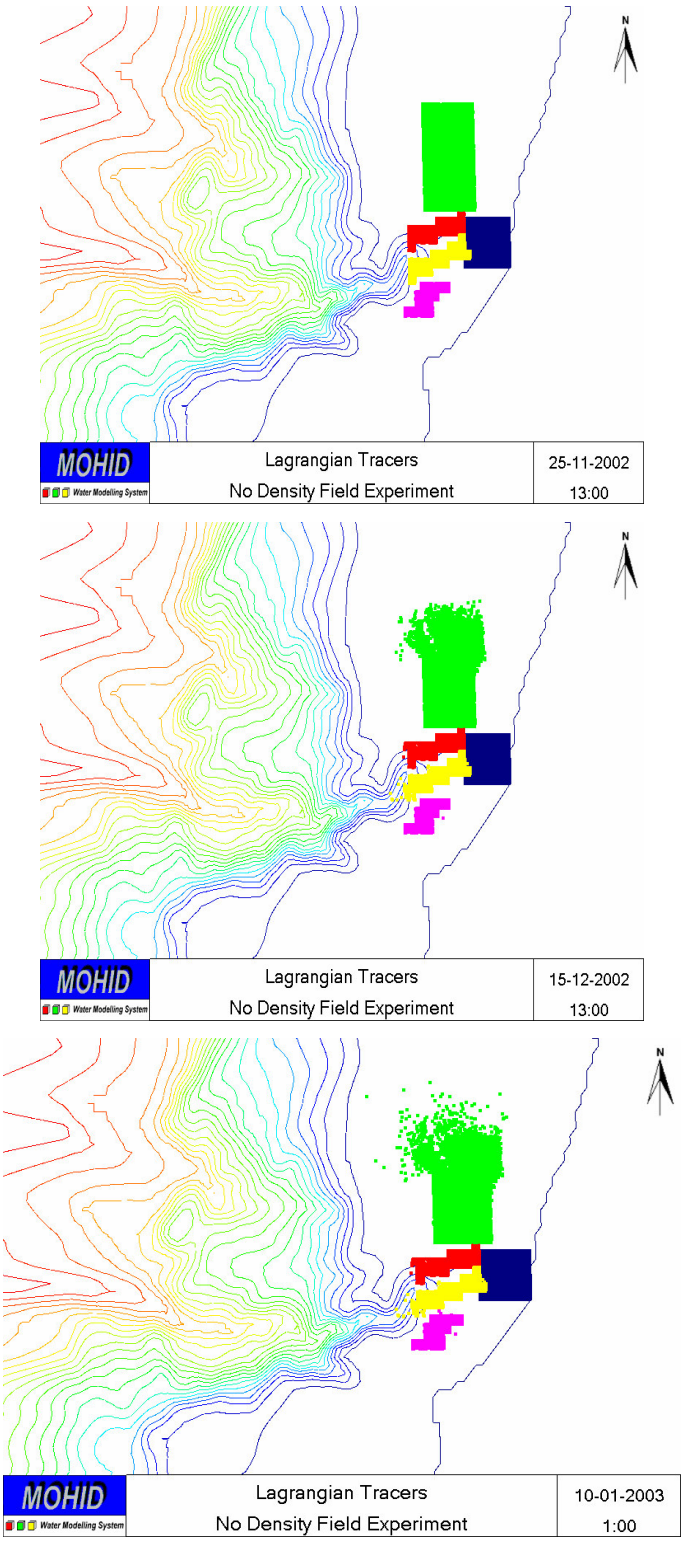

Figure 62 – Three different instants (initial instant, after 20 days and after 47 days run) of the Lagrangian simulation considering no vertical or horizontal gradient and forced only with tide.

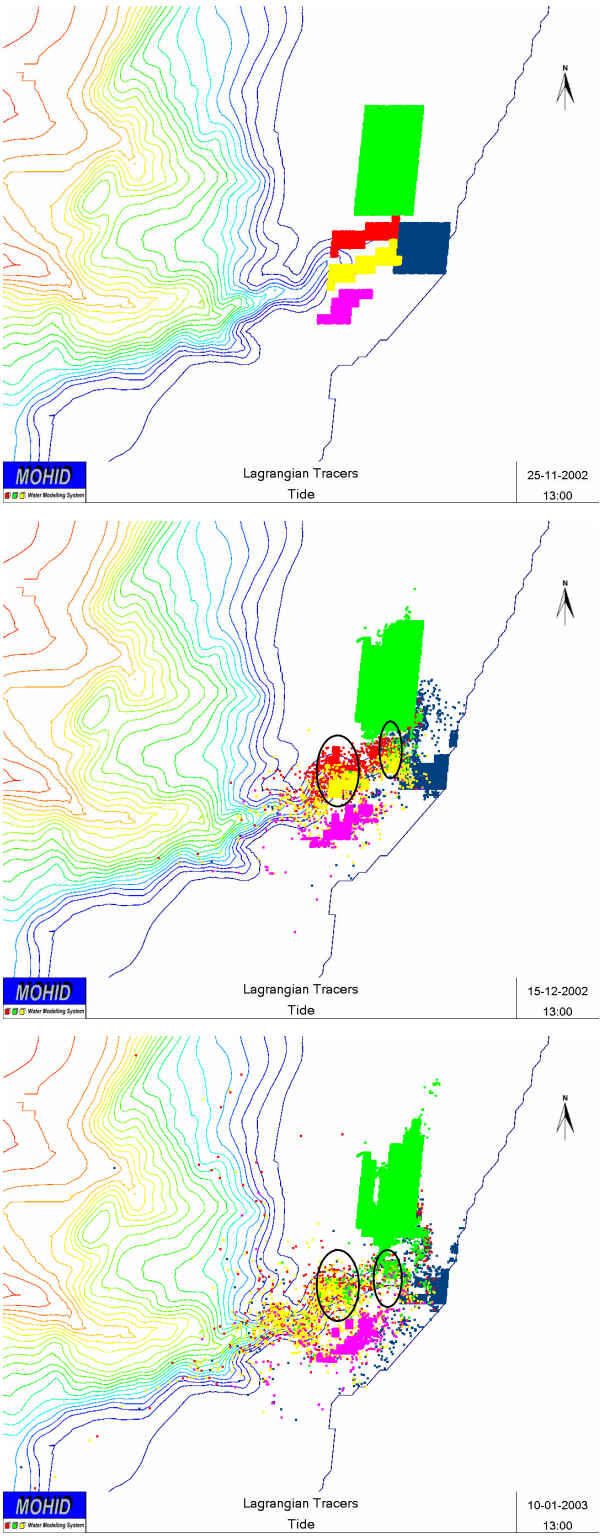

Figure 63 – Three different instants (initial instant, after 20 days and after 47 days run) of the Lagrangian simulation considering a density gradient and forced only with tide. Ellipsis corresponds to depocentre areas.

Only a small part of the shelf sediments are resuspended and transported along the coast, by the effect of tides. Quaresma *et al*. (2007) observed the shoreward propagation of strong nonlinear internal waves (NIW) on the middle shelf around the Nazaré Canyon, generated 25 Km off shore due to the interaction of the northern upper canyon rim with the semi-diurnal current. According to these authors only the stronger NIWs are capable of eroding and suspend the local sediments, nevertheless both the NIW generated at the canyon and the ones generated at the shelf break (Jeans, 1998; Jeans & Sherwin, 2001a,b; Sherwin *et al*., 2002 all in Quaresma *et al*., 2007) induce considerable vertical velocities (0.025-0.1 m s^{-1}), interacting with a permanent BNL observed in this region (Oliveira *et al*., 2007) increasing its thickness even if most NIW do not contain enough bottom shear stress to erode the sediment from the seabed.

Our results seem to be in agreement with the observations from Quaresma *et al*. (2007), since only a small part of the shelf sediment (both the green and violet boxes) are resuspended and transported by the effect of internal waves. Considering the green box (northern shelf) the sediments from the top of the box seem to be transported northward while those resuspended from the lower part of the box seem to be transported southward in the canyon direction. They seem to get trapped in the canyon because no green particles are found in the southern shelf, which is in agreement with the results from Oliveira *et al*. (2007). Considering the violet particles these seem to be transported westward and northward, up to the canyon. This may be the result of an anticyclonic eddy promoted by the coast line topography.

Part of the sediments at the canyon walls and rims seem to be resuspended, but most of the sediments are retained along the upper canyon axis, for the period of the simulation, which goes along with the observations in Chapter 4. The particles are resuspended and transported up-canyon and down-canyon every cycle of the semi-diurnal tide. Once they reach the middle of the upper canyon, part of the sediments seem to flow down-canyon while other part seem to be caught by the slope current and transported northward.

At the canyon head box (blue) the sediments that are inside the canyon are not easily eroded when compared with the shelf ones (see middle image of Figure 63).

The wind affects mainly the shelf sediments. Figure 64 to Figure 67, indicate that shelf particles tend to be transported north or south, depending on the wind direction. SW winds are typical, has referred, of autumn and winter conditions and are, most of the times, connected with storm events and related to downwelling conditions. NW winds predominate during the spring and the summer and are related to upwelling events.
Paying more attention to these figures, some interesting features can be observed. Looking to Figure 64 and Figure 65, referring to SW wind it can be seen that at the shelf north of the canyon the major part of the green particles are transported northward, nevertheless a small percentage is transported southward and is trapped in the canyon (see ellipsis), since once more green particles are not found in the southern shelf. The violet particles (southern shelf) are also transported west and northward, due to the topographic eddy and only a small percentage cross the canyon while the majority gets also trapped by the canyon (mainly in the canyon head area).
Once again, the blue particles at the canyon head seem to be trapped, while the ones at the shelf are also fast transported northward. This is once more in agreement with the observations from Oliveira *et al*. (2007).
The canyon tracers seem to be faster eroded, mainly those from the canyon rims, although the majority of the sediments seem to have the same behaviour as in the previous scenario: a small portion of these particles is transported northward.

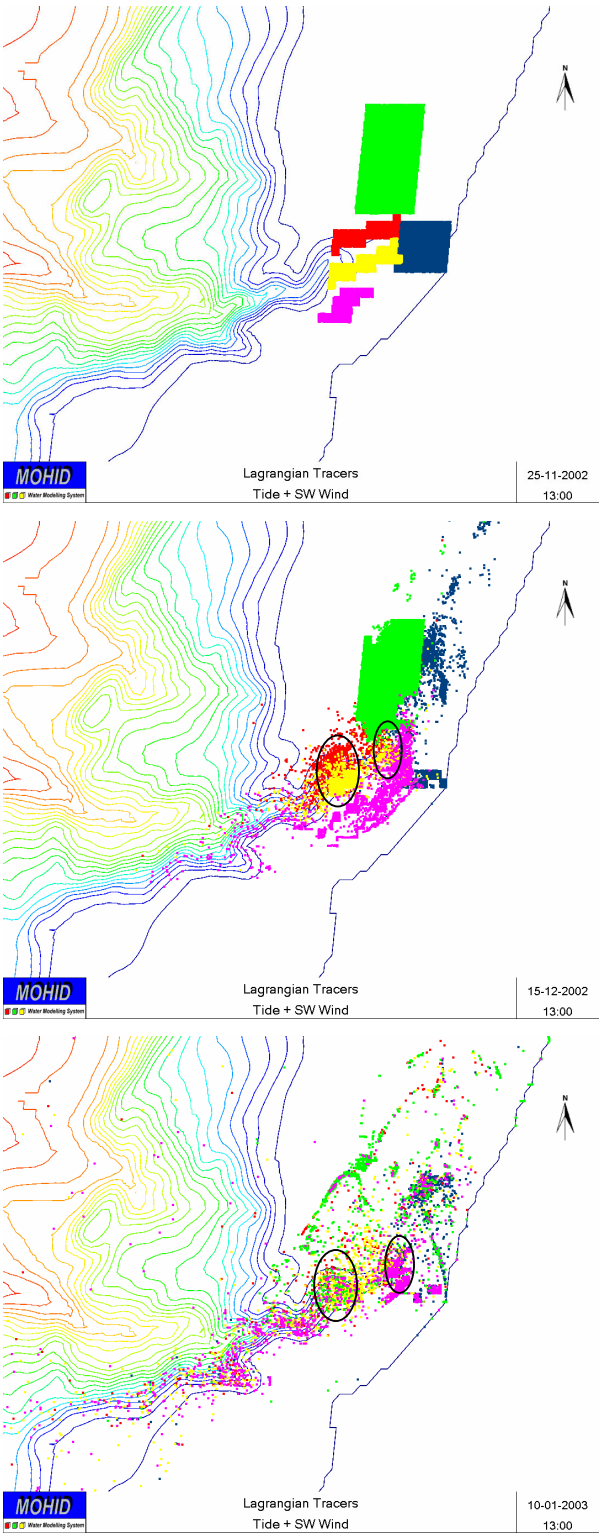

Figure 64 – Three different instants (initial instant, after 20 days and after 47 days run) of the Lagrangian simulation considering a density gradient and forced with tide and 25 Km h^{-1} SW winds. Ellipsis correspond to depocentre areas.

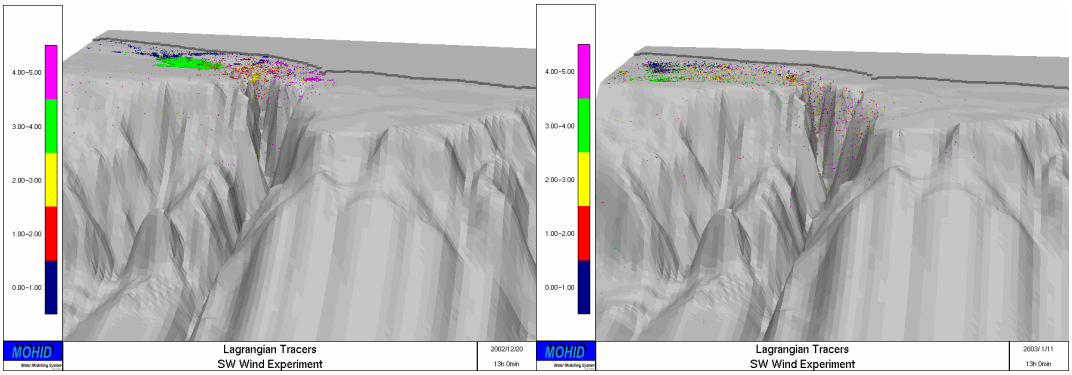

Figure 65 – 3D view of scenario 3 with SW wind, for the same moments as in the horizontal view.

On the case of a NW wind, Figure 66 and Figure 67, the green northern middle shelf particles are not as easily resuspended as in the case of SW winds. As in the second scenario particles from the top of the box tend to be transported northward while the particles at the lower part of the box are transported as a BNL southward, getting trapped at the canyon head (see ellipsis).

The shelf blue particles and the violet particles are once again capture by the topographic eddy and transported, as a BNL, westward and northward into the canyon area, and only a few percentage passes the promontory to the south.

These shelf particles trapped by the canyon will probably feed the BNLs found at the edge of the canyon rims and then entering in the canyon circulation dynamics.

As in the two previous scenarios, the tracers at the canyon walls and rims show the same behaviour being not much affected by the wind currents. Once again, it is interesting to see the capture and the northward transport of the particles by the slope current.

As previously referred in chapter 2, the studies from Magalhães (1999) indicated that under the most frequent wave climate conditions, particles from littoral and fine deposits existent on the middle shelf are remobilized. Under storm conditions, the majority of the shelf and continental slope particles were also remobilized. Oliveira *et al*. (2002) observe that significant wave heights of 6m and periods of 12 s, induce bottom orbital currents over 20 cm s^{-1}, at middle shelf depths, strong enough to resuspend fine bottom material.

Although waves are important when considering resuspension processes in the shelf they don't play any role in the transport of the sediments. For this reason and since our major objective is to define transport patterns in Nazaré canyon area, no simulation was done considering the wave effect.

In Chapter 4 and Chapter 5, it was referred that the side of the concavity of the canyon meanders in the upper canyon seem to have influence in the SPM pattern. In sections E and F (Figure 25), where the concavity is on the northern rim, resuspension is higher at the southern rim and wall and higher concentrations are found along all the canyon section. The contrary was observed in section B (Figure 15), where the concavity is on the southern rim.
If we look at the results from the several scenarios the places where the concavity is to the northern shelf (ellipsis) seem to be preferential depocentres, while the places where the concavity is to the south seem to be erosional areas.

Another curiosity is how the upper part of the canyons head seams to act as an effective trap for sediments, indicating an accumulation area inside the canyon. In this area, most of the internal wave energy has already been dissipated due to the canyon meandering as seen in the previous chapter. This may explain why most of the sediments did not suffer erosion in this area and part of the shelf sediments got trapped.

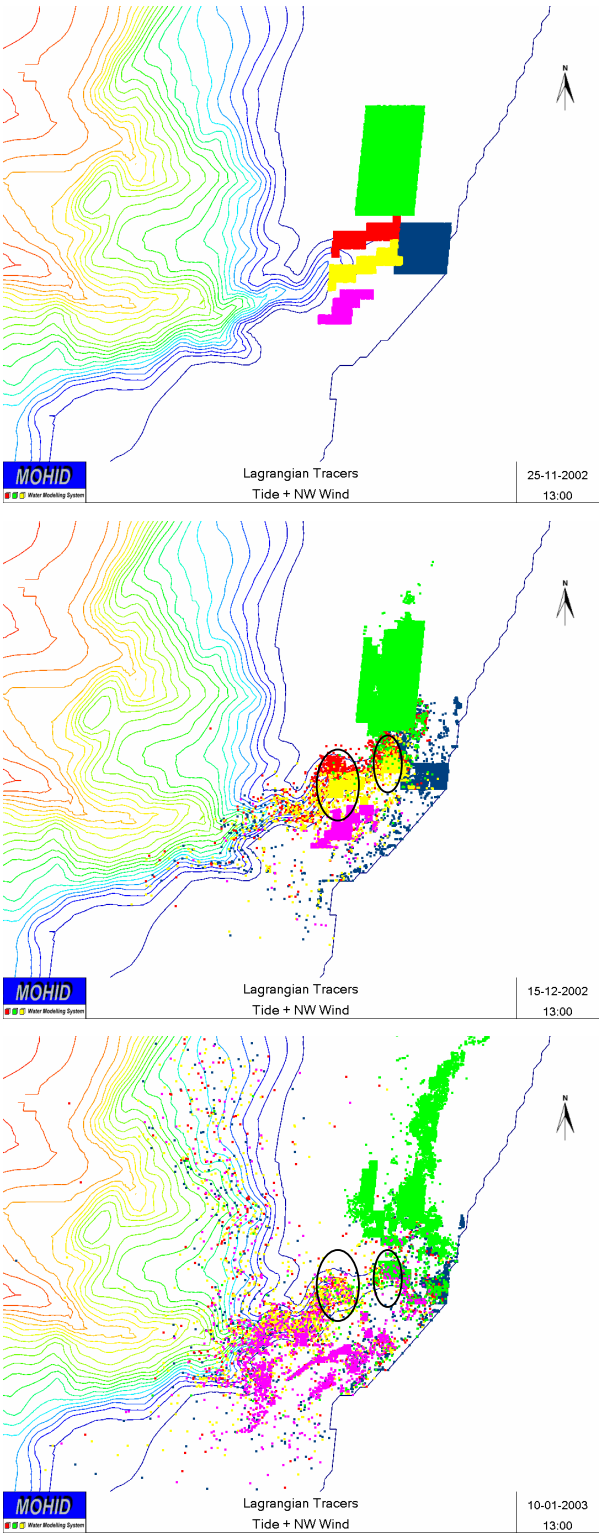

Figure 66 – Three different instants (initial instant, after 20 days and after 47 days run) of the Lagrangian simulation considering a density profile and forced with tide and 25 Km h^{-1} NW winds. Ellipsis correspond to depocentre areas.

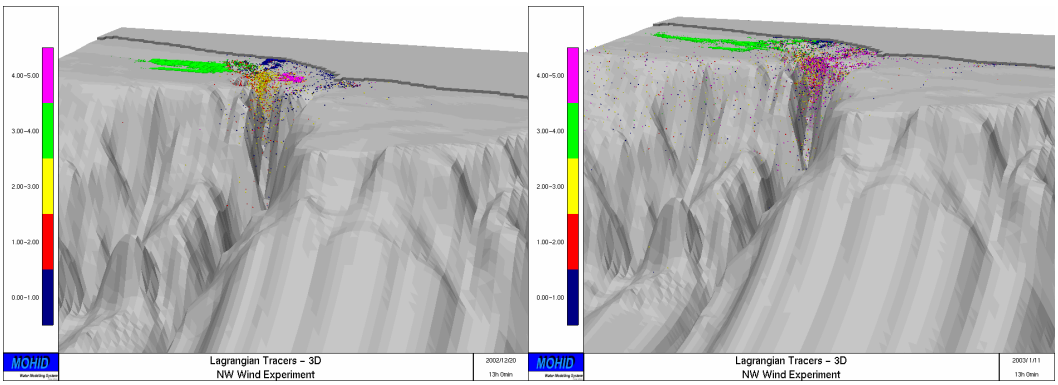

Figure 67 – 3D view of scenario 4 with NW wind, for the same moments as in the horizontal view.

6.4 RESIDENCE TIME

As referred in section 5.1.1.5, the lagrangian module permits to monitor the distribution of particles inside "monitoring boxes". This feature is very useful to compute, for example, the residence time of water inside these monitoring boxes and also the origins of the water inside each box at each moment (Braunschweig *et al.*, 2003).

The residence time concept is mainly used for water bodies and it refers to the time that a specific volume of water takes to be renewed. This concept is of high importance when studding semi-confined water bodies has estuaries or coastal lagoons (Trancoso *et al.*, 2005; Santos *et al.*, 2008).

It would be interesting trying to apply this concept to the sediments. So, as an experiment, monitoring boxes were created by using the same boxes of the lagrangian tracers. At the beginning, the idea was to see how long did it take for the volume of sediments to be resuspended and leave the 1 cm high box. This was not possible because the concept of the monitoring box was designed considering the whole of the box water column. So the sediment volume was integrated in the water column volume and analyse how long did it take for the sediments to abandon the box area. We did this experiment for scenarios 2, 3 and 4, forcing with tide, with tide and SW wind and with tide and northwest winds, respectively.

Figure 68 shows the results after the 52 days run, for the tide forcing scenario. Considering only the tide it can be seen that the area where resuspension and transport is more active is at the two boxes located at the canyon rims and walls. It is interesting to notice that in the red box during the majority of the simulation period the concentration inside the box was constant, which indicates a high residence time for the sediments in the upper part of the canyon. The sediments that left the box at the beginning of the simulation, must be the ones located at the canyon rims. On the southern canyon wall (yellow box) the particles also show high residence time. Nevertheless they seem to be faster transported, which may indicate differences in circulation and current velocities in the two sides of the canyon.

On the northern shelf only 2% of the sediments left the box. Nevertheless it can not be forgotten, that although sediments may be resuspended as long as they are kept in the box area they are written up. At the canyon head box, after 52 days, 80% of the sediments remain in the box which may correspond to the canyon head sediments. At the southern shelf deposit a jump is observed after 32 days simulation, although no reason was found for this jump, particles tend to stay in the area and are not easily resuspended.

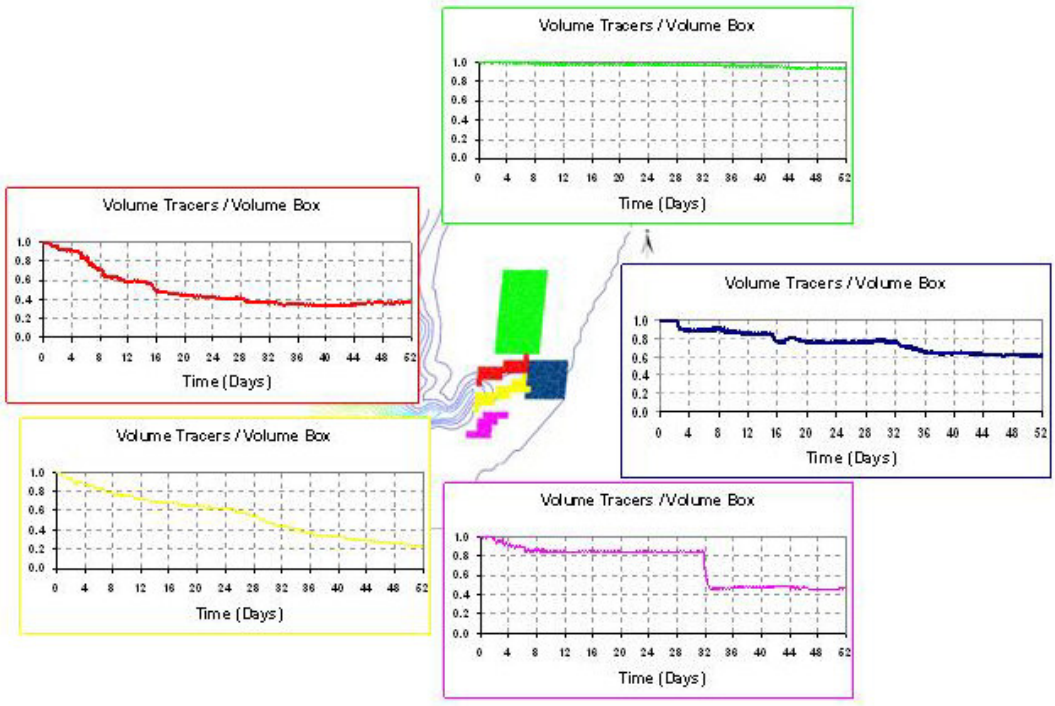

Figure 68 – Residence Time in the 5 monitoring boxes in Nazaré Canyons and adjacent shelf, for the tide forcing scenario.

Figure 69 shows the results after the 52 days run, for the tide and NW wind forcing scenario. In this case once more it can be observed that the area where resuspension and transport is more active is at the two boxes located at the canyon rims and walls. The results are very similar to the first scenario, indicating that the wind seems not to play an important role in resuspension in these areas of the canyon. On the northern shelf, only after 36 days the particles started leaving the area, even then after 52 days only 50% of the SPM left the box. At the canyon head the results were the same of those of the tide scenario indicating that the NW wind does not affect the canyon head sediments.

In the particles from the southern shelf (violet box), once more it can be observed a jump after 32 days, but in this case it was due to the wind effect on the particles. These particles once resuspended seemed to be faster transported outside of the box.

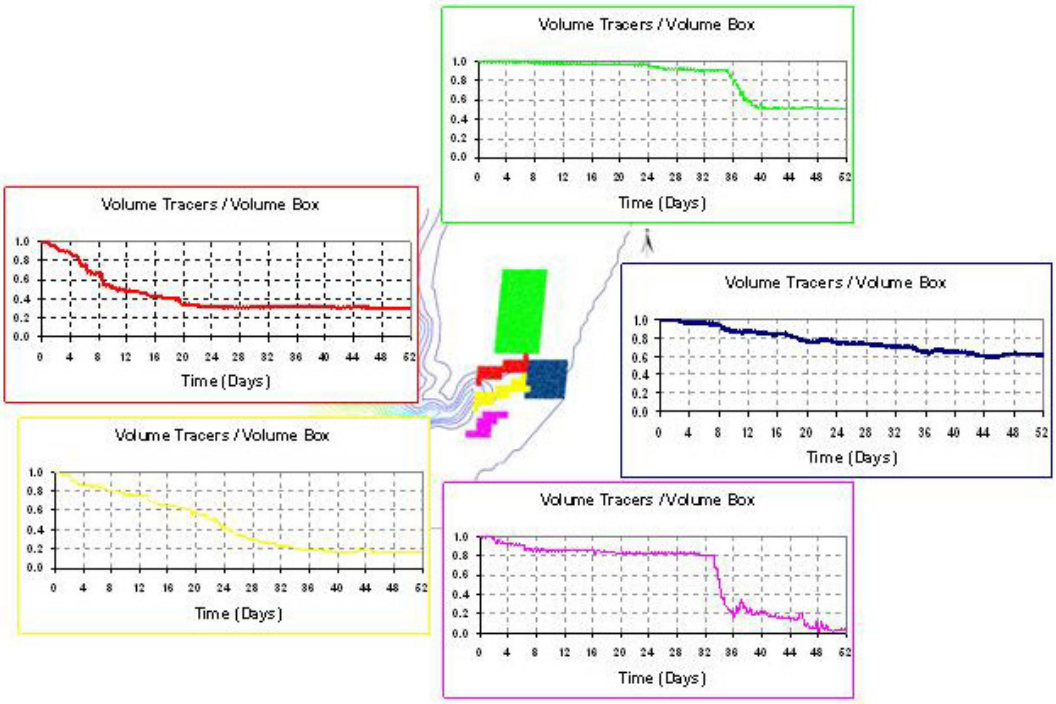

Figure 69 - Residence Time in the 5 monitoring boxes in Nazaré Canyons and adjacent shelf, for the tide and NW wind forcing scenario.

Figure 70 shows the results after the 52 days run, for the tide and SW wind forcing scenario. In this case, once again, it can be observed that the canyon rims and the walls (red and yellow boxes) are not much affected by wind because the results are very similar to the first scenario.

Contrary to the tide and NW wind, SW wind seems to have an effect on the canyon head sediments where after 20 days, 50 % of the sediment had already left the area and by the end of the simulation only 10% of the sediment remained.

In the case of the two shelf deposits (green and violet boxes), after an initial period of 32 days for the green box and 16 days for the violet box, the resuspended sediments are then faster transported outside the box areas.

We must take in attention that the tracers were subjected to a persistent 25 km s^{-1} southwest wind for a 52 days period. As we refer in section 2.3, although southwest winds are frequent during autumn and winter, they usually do not last for more than 5 or 6 days. Although resuspension occurs due to this SW wind, the duration does not favour the transport in the same order of magnitude as we saw in this simulation.

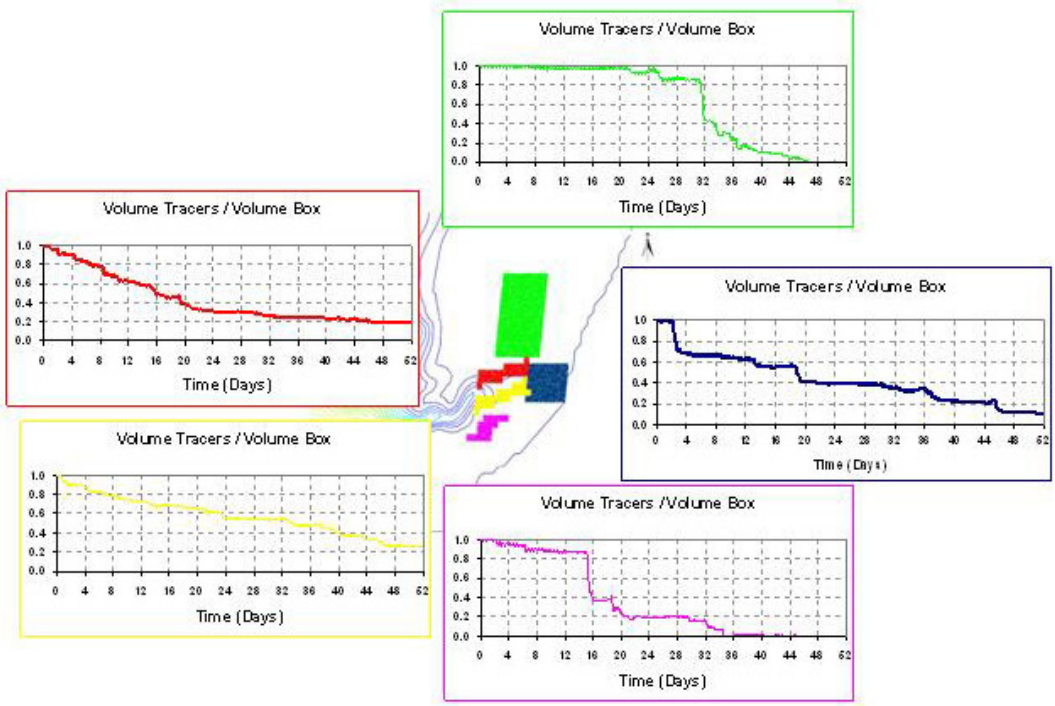

Figure 70 - Residence Time in the 5 monitoring boxes in Nazaré Canyons and adjacent shelf, for the tide and SW wind forcing scenario.

6.5 A CONCEPTUAL MODEL

Gathering in: (1) the information from what is known for the circulation in the Portuguese margin an more specifically in the Nazaré Canyon, described in chapter 2 and 3 of this thesis and; (2) combining this information with what is known on sediment fluxes and sediment rates along the Nazaré canyon (de Stigter *el al.*, 2007) and; (3) on the conceptual model for the dynamic processes acting on the canyon head and adjacent shelf area (Oliveira *et al.*, 2007) and finally; (4) the results obtained in this work, a conceptual model for fine sediment transport along the Nazaré Canyon was drawn.

Since the circulation on the Portuguese continental margin at shallower depths up to the upper slope is conditioned by the prevailing typical winds, two scenarios were taking in consideration. A SW wind (light blue), typical of winter conditions and a NW wind (dark blue), typical of summer conditions.

At the surface the transport depends mainly on the wind forcing.

In the shallow areas where the wind acts, an anticyclonic eddy in the shelf north of the canyon and an anticyclonic eddy at the southern shelf together with the wind direction, influences the dynamics of fine sediments.

During the southwest wind periods (Figure 71 – light blue), sediments from the middle-shelf deposits and surrounding areas of the canyon head tend to be faster transported northward. On the northern shelf, a small percentage of the SPM from the shelf deposits near the canyon seem to be transported southward into the canyon head area.

During northwest wind periods (dark blue), the two eddies north and south of the canyon play also an important role. In the northern shelf, although the net transport may be considered southward some particles caught in the vortex, near the coast, are transported northward and will be trapped in this recirculation cell. At the southern shelf due to the topography the flow is diverted west and northward and the particles are caught in this recirculation cell, tending to be trapped in this area of the shelf. Only a small percentage of the particles will be transported southward (Figure 71 – dark blue).

The northward current between 200 m and 1600 m depth, is disturbed by the canyon presence (Figure 71 – green). While part of the flow continuous North the other part is diverted on the canyon direction and flows along the canyon axis. At the upper canyon axis, the propagation of the internal tide results in sediment resuspension and transport during every cycle of the semi-diurnal tide. Tracer's results confirm that the resuspended particles, due to the tidal movements, remain in the upper canyon axis for a long period. Nevertheless according to de Stigter *et al*. (2007) the net transport is down-canyon.

When reaching the middle upper canyon, below the 1500/1600 m depth, part of the fine sediments will be transported down-canyon as a BNL and or an INL along the canyon axis, another will be caught by the northward slope current.

Durrieu de Madron *et al*. (1999) observations at Cap-Ferret canyon indicated that low frequency currents were important for the lateral transport of the suspended material mainly at the shelf break area and INL's. They also observe that this phenomenon was more intense during winter when the currents were intensified.

Below the 2000 m deep, e the southward deep current is present (Figure 71 – red). One part of the fine sediments that occasionally, during spring tides, may be resuspended at the middle canyon depths, will be transported down-canyon as a BNL and or an INL along the canyon axis. Another part may be caught by the current and transported southward.

The occasional occurrence of sediment gravity flows or even rare turbidity currents as stated by de Stigter *et al*. (2007) and Arzola *et al*. (2008), results in an overall net transport down-canyon.

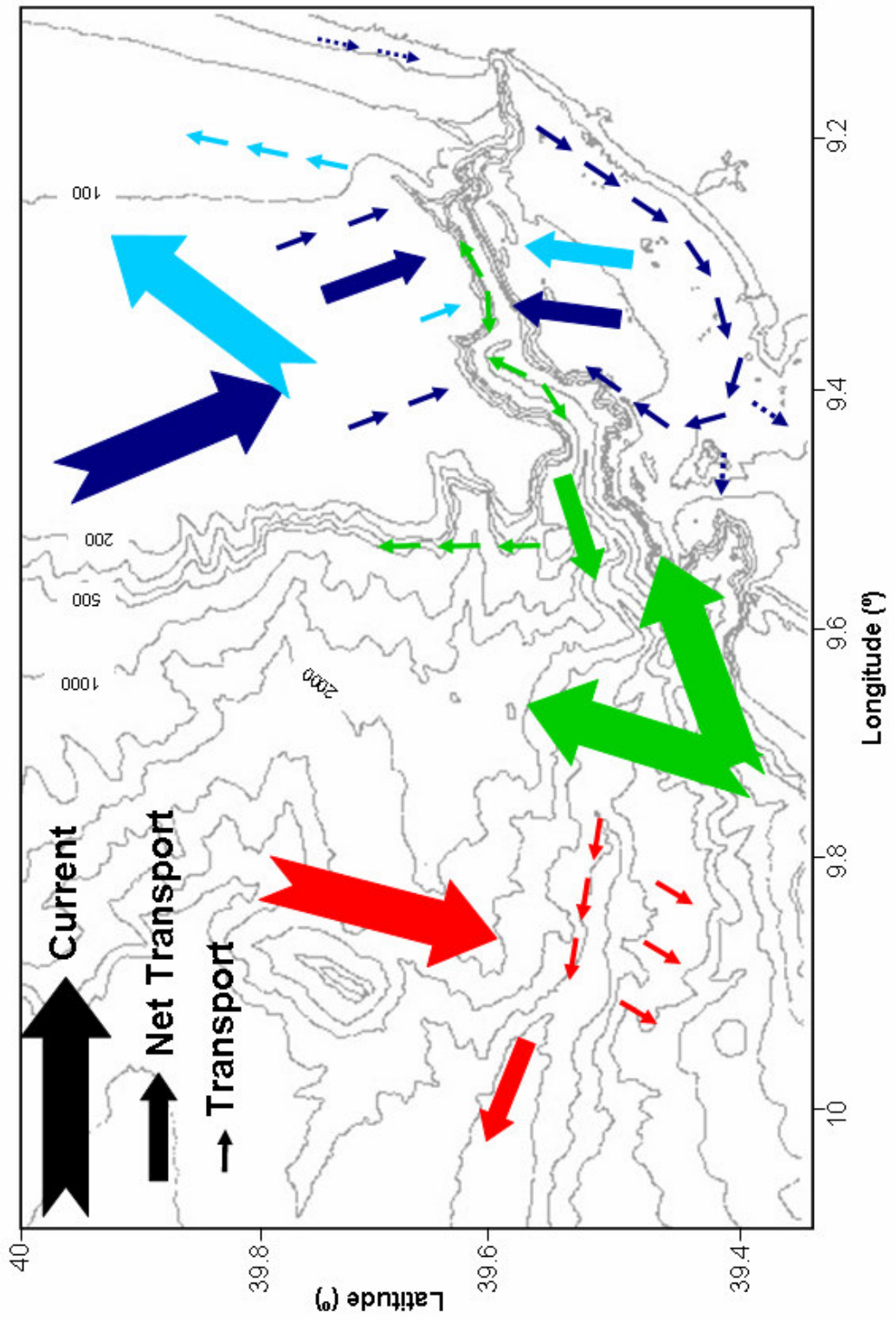

Figure 71 – Conceptual model for fine particles transport in Nazaré canyon. Light and dark blue correspond to the shelf dynamics under NW prevailing winds (dark blue) and SW prevailing winds (light blue). Green is for the slope current and red for deep ocean current.

6.6 ON THE ORIGIN OF FINE PARTICLES

When studying fine sediments dynamics in Nazaré Canyon and adjacent shelf one question still remains without answer: what is the origin of all this fine particles?

Although the origin of the fine particles found in the shelf deposits were not under the scope of this work, some considerations should be done about this subject.

Several authors working in the area like Dias (1987), Magalhães (1999), Duarte (2002), Oliveira *et al.* (2007), Quaresma *et al*. (2007), consider that the mud deposits located on the shelf north and south of the Nazaré Canyon (Figure 8), are a major source of fine sediments in the Canyon. Tracer's results also indicate that part of the fine sediments of the shelf deposits may be suspended and transported into the Canyon, but this raises another question concerning the origin of these deposits.

According to Duarte (2002), the northern deposit is aligned in the NNE-SSW direction; which is in agreement with the direction of the normal faults that occur north of the canyon according to Vanney & Mougenot (1990). To this author, this is a relict deposit because there is not an actual fluvial source of sediments. He then considers, that this deposit may be related with an ancient fluvial source, in a lower sea level stand, or by filling of an ancient paleovalley or by massive sedimentation on an internal shelf environment. This ancient river would have had a NE-SE direction, aligning with the actual location of the Mondego River.

Concerning the deposit south of the Nazaré Canyon according to this author (Duarte, 2002) it is aligned in the same direction of the Nazaré fault (NE-SW) (Vanney & Mougenot, 1990). For this deposit, Duarte (2002) considers two sources for the sediments: the Canyon it self and the small fluvial systems that flush near the area. Tracer's results indicate that the south deposit may contribute with sediments into the canyon although the contrary is not that clear.

Although we also consider that these deposits are probably located in depressed areas tectonically controlled, we believe that these fine sediments found in the area were and still are (although with much lesser frequency, due to the intense damming) supplied by the Tagus River.

Coelho (2001), made a study on the combined effect of river plumes and the wind over the continental shelf, taking as an example the Douro River plume during the 2001 flood. He observed that during floods (when the runoff may reach 10000 m^3s^{-1}) and

South – Southwesterly wind (the typical regime during storms in the Portuguese coast), the river freshwater over the shelf forms a thin layer (less than 10 m), that combined with the winds lead to surface velocities higher than 80 cm s^{-1}, flowing northward along the shelf.

Taking as an example the 1979 Tagus flood (Ramos & Reis, 2001), already after the intense dam construction in the Tagus basin, during this flood the runoff reached values of 14500 m^3s^{-1} and it was estimated an exportation of sediments higher than 1000000 m^3. Having these values in mind we considered that during intense floods and South- Southwest wind regimes the same process observed for the Douro shelf could take place in the shelf off Tagus, inducing a northward transport of the sediments that could probably reach the Nazaré canyon area, nursering the mud deposits.

6.7 CONCLUSIONS

Transport patterns within the Nazaré canyon are very complex, although net transport is downcanyon, cyclic processes of deposition, resuspension and transport occur along the canyon axis.

Results from the lagrangian tracers experiment go in the same direction of the conclusions taken, based on observations, by authors like Oliveira *et al*. (2007) for the canyon head and de Stigter *et al*. (2007) and Arzola *et al*. (2008) for the deeper canyon. These data is fundamental because it make us understand how accurate the model can be. Once the model is validated, the use of this technique is of the maximum interest since it permits to follow the particles from the source to their depositional centers.

Based on these some important conclusion are taken from this chapter

At the upper canyon, the channelization of the northward slope current together with the tidal -forcing keep the resuspended sediments on semi-permanent movement up and down canyon, although the net transport is down-canyon, these particles can stay for a long period trapped in the upper canyon area. Once the particles leave the influence of the narrow canyon channel, some particles will go down-canyon mainly as a BNL while others will be caught by the northward current and transported north.

Particles that reach the deepest part of the canyon or are sporadically resuspended, may be also transported down-canyon as a BNL but part will be caught by the southward deep current and transported south.

At the surface the transport depends very much on the wind. The net transport will be to the south on the shelf north of the canyon and to the north at the shelf south of the canyon (due to the eddy generated by the topography) during persistent north winds and to the north with south winds.

Another important conclusion is that the canyon head works effectively has a catchment area for sediments transported along the shelf, both from north or south depending on wind conditions. Once they are in this area the sediments are not easily resuspended and transported neither by wind or the effect of internal waves.

The lagragian experiments also confirmed that the major process for sediment resuspension in the canyon is the internal tide, since there is no great variation on the resuspension pattern due to the wind effect. The shelf resuspension is much more dependent on the effect of the wind and its duration. For this to occur it is necessary several days of persistent winds both form SW or NW.

Chapter 7

CONCLUSION, SYNTHESIS AND FUTURE WORK

This thesis aimed (1) to verify if the internal tide is a major driver of the observed suspended sediment distribution patterns within and around the Nazaré Canyon; (2) to assess the canyon geometry role on propagation and dissipation of internal waves and (3) to understand the role of the currents generated by internal waves for the resuspension and transport of fine sediments within the canyon.

We can now state that Nazaré canyon is subjected to the influence of internal waves propagating along the upper canyon up to his head. This tidal motion is responsible for the high near bottom velocities that promote resuspension along the upper canyon axis mainly above 1600 m deep, forming a permanent BNL in this region of the canyon. According to the linear internal waves theory the regime is near critical along most of the upper canyon, being critical in areas where topographical slope matches the angles of the high energy beams: at 1500 m, 1000 m, and at 300-400 m deep. Those are also the depths where the maximums turbidity values were found. The critical regime in those regions also explains the intense short -term sediment deposition measured by several authors as referenced in Chapter 3.

The MOHID model results reinforce the hypotheses that internal waves are the major process for resuspension of fine sediments in Nazaré Canyon showing that near bottom concentration vary with the semi-diurnal tidal cycle, usually with higher values during ebb tide and lower values during flood tide (Goal 1). This resuspension is due to the fact that the upper Nazaré Canyon axis is near critical almost along is extension (Goal 2).

After validation of the MOHID model hydrodynamic, using velocity measurements and the thermohaline structures observed with CTD data it was decided to use the velocity to simulate fine sediment transport in Nazaré Canyon using a Lagrangian approach. The results confirmed the conceptual model for fine sediment transport in Nazaré Canyon and adjacent shelf (Goal 3).

At the shelf the hydrodynamics and consequently the transport is much wind driven. During the summer the winds are predominantly from NW inducing southward current and SPM transport. South of the Nazaré canyon the southward general circulation associated to the coast topography create an anticyclonic eddy transporting the sediment west and northward into the canyon. In the winter the SW winds promote northward transport both north and south of the canyon rims.
On the upper canyon the tidal current is the dominant transport mechanism, moving the particles resuspended by internal waves up and down canyon under oscillatory tidal movements. The residence time was also studied by using the model and it was verified that particles can stay for a long period in this part of the canyon feeding the permanent BNL found at the canyon axis between the 1600 m depth and the canyon head. Once these particles leave the narrow canyon, part may be transported northward along the slope current. The net transport in the entire canyon is nevertheless down-canyon, most fine particles being transported as BNLs or INLs to the abyssal plains. Particles reaching the lower part of the canyon tend to be caught by the southward deep current and transported to the south.

The results of this work have scientific and socio-economics importance. Scientifically they contribute for understanding (1) the dynamics of the Nazaré canyon and (2) the exportation of fine particles into the deep ocean. A major socio-economic relevance of this study can be the support to the extension of the Portuguese Continental Shelf beyond 200 nautical miles (according to the United Nations Convention on the Law of the Sea).
The combination of field studies and modelling permitted to get an integrated vision of processes in space and time, it is very important for supporting coastal and ocean managers. An example is the use of lagrangian tracers to locate depocenters for per type of particles which may contribute for searching mineral resources on the ocean bottom.

Future development of this work should be dedicated to model grid refinement and improvement of boundary conditions, e.g. by coupling this model to an ocean operational model. This will improve the quality of the results and will generate results that can be compared with the actual measured data. Also more field data is required

for improving the description of the sediment properties in this area with especial emphasis for critical shear stress for erosion and for deposition and settling velocities.

The use of Lagrangian Tracers reveals to be a powerful tool for the study of sediment transport and residence time.
Although numerical Lagrangian tracers are already being used to model floating "particles" and for calculating residence time of water in coastal areas, with very good results, this is the first study using numerical Lagrangian tracers as bottom sediments, so the work performed in this thesis can be considered an "opening door for the future", and can be used for the most diverse applications.
This approach was already used to study the resuspension, transport and deposition behaviour of two different organo-mineral aggregates, in the Nazaré canyon and adjacent shelf (de Jesus Mendes *et al*., 2007b).

In what concern the use of lagrangian tracers as bottom sediments several tests and inputs can and should still be done to improve it, mainly in what concerns residence time, since the concept is based on a different approach (as referred previously). This concept should be adjusted to the case of the sediments and instead of integrating in the all water column it should integrate only the volume of the sediment box, this could tell us not just how long does it take for that sediments to leave that box but also if sediments from other boxes would be deposit in that area. This would give a more accurate idea of the resuspension and deposition spots on a certain area. Future work will be developed in this sense.

Another important step in the study of sediment resuspension and transport in any system is to couple these modules to fully operational Models. This kind of approach is know started to be tested by a PhD student Sibila Sousa from the International University of Breman, that will couple the lagrangian module to the operational model in order to investigate aggregates and biogenic particles transport and deposition on the Nazaré Canyon and similar systems.

Finally, it can be stated that the goals proposed in the introduction of this thesis were fully accomplished.

REFERENCES

Abbot, M.B., Damsgaardand, A. & Rodenhuis, G.S. (1973). System 21, Jupiter, a design system for two-dimensional nearly-horizontal flows. *J. Hyd. Res.*, 1, pp. 1-28.

Adcroft, A.J., Hill, C.N. & Marshall, J. (1997). Representation of topography by shaved cells in a height coordinate ocean model. *Mon. Weather Rev.*, 125, pp. 2293-2315.

Allen, C.M. (1982). Numerical simulation of contaminant dispersion in estuary flows. *Proc. R. Soc. London*, A 381, pp. 179-194.

Alvarez, I., Gomez-Gesteira, M., de Castro, M. & Prego, R. (2005). Variation in upwelling intensity along the NorthWest Iberian Peninsula (Galicia). *Journal of Atmospheric & Ocean Science*, 10 (4), pp. 309-324.

Arzola, R.G., Wynn, R.B., Lastras, G., Masson, D.G. & Weaver P.P.E. (2008). Sedimentary features and processes in the Nazaré and Setúbal submarine canyons, west Iberian margin. *Marine Geology*, 250 (1-2), pp. 64-88.

Baker, E.T. (1976). Distribution, composition and transport of suspended particulate matter in the vicinity of Willapa submarine canyon, Washington. *Geol. Soc. Am. Bull.*, 87, pp. 625-632.

Beckmann, A. & Haidvogel, D.B. (1993). Numerical simulation of flow around a tall isolated seamount. part I: problem formulation and model accuracy. *Journal of Physical Oceanography*, 23, pp. 1736–1753.

Blayo, E. & Debreu, L. (2005). Revisiting open boundary conditions from the point of view of characteristic variables. *Ocean Modelling*, 9 (3), pp. 231-252.

Blumberg, A.F. & Kantha, L.H. (1985). Open boundary condition for circulation models. *J. of Hydraulic Engineering*, ASCE, 111, pp. 237-2555.

Bowie, G.L., Mills, W.B., Porcella, D.B., Campbell, C.L., Pagenkopf, J.R., Rupp, G.L., Johnson, K.M., Chan, P.W.H., Gherini, S.A. & Chamberlain, C.E. (1985). Rates, Constants and Kinetics formulations in surface water modelling. *United States Environmental Protection Agency – Environmental Research Laboratory* – EPA/600/3-85/040, Athens, USA. 455 p.

Braunschweig, F. (2001). Generalização de um modelo de circulação costeira para albufeiras. *MsC Thesis*, Lisbon Technical University, 84p.

Braunschweig, F., Martins, F., Chambel, P. & Neves R. (2003). A methodology to estimate renewal time scales in estuaries: the Tagus estuary case. *Ocean Dynamics*, 53, pp. 137-145.

Buchard, H., Bolding, K., & Villarreal, M.R. (1999). GOTM, a General Ocean Turbulence Model. Theory, implmentation and test cases. *Report EUR18745 EN*, European Commission, 103 p.

Butman, B., Alexander, P.S., Scotti, A., Beardsley, R.C. & Anderson, S.P. (2006). Large internal waves in Massachusetts Bay transport sediments offshore. *Cont. Shelf Res.*, 26, pp. 2029-2049.

Cacchione, D. & Southard, J.B. (1974). Incipient sediment movement by shoaling internal gravity waves. *J. Geoph. Res.*, 79, pp. 2237–2242.

Cacchione, D.A., & Drake, D.E. (1986). Nepheloid layers and internal waves over continental shelves and slopes. *Geo Mar. Lett*., 16, pp. 147– 152.

Cacchione, D.A., Pratson, L.F. & Ogston, A.S. (2002). The shaping of continental slopes by internal tides. *Science*, 296, pp. 724-727.

Canals, M., Puig, P., Durrieu de Madron, X., Heussner, S., Palanques, A., & Fabrés, J. (2006). Flushing submarine canyons. *Nature*, 444, pp. 354–357.

Cancino, L. & Neves, R.J.J. (1998). Hydrodynamic and sediment suspension modelling in estuarine systems. part I: description of the numerical models. *Journal of Marine Systems*, 22, pp. 105-116.

Cartwright, D.E. (1999). Tides: A Scientific History. *Cambridge Univ. Press*, Cambridge, 292 p.

Carvalho, J.J.R. & Barceló, J.P. (1966). Agitação marítima na costa oeste de Portugal metropolitano. *Memórias do LNEC*, 290, 34p.

Coelho, H.S., Neves, R.J.J., White, M., Leitão, P.C., & Santos, A.J. (2002). A model for ocean circulation on the Iberian coast. *Jour. Marine Systems*, 32 (1-3), pp. 153-179.

Costa, M.D.S. (1992/3/4). Agitação marítima na costa portuguesa. *Anais do Instituto Hidrográfico*, 13, pp. 35-40.

Costa, M.V. (1991). A three-dimensional eulerian-lagrangian method for predicting plume dispersion in natural waters. *Diplôme d'Etudes Approfondies Européen en Modélisation de l'Environnement Marin* - ERASMUS.

Daveau, S., Almeida, G., Feio, M., Rebelo, F., Silva, R. & Sobrinho, A. (1978). Os temporais de Fevereiro/Março de 1978. *Finisterra,* XIII (26), pp. 236-260.

Davies, A.M. & Xing, J. (2002). Processes influencing suspended sediment movement on the Malin–Hebrides shelf. *Cont. Shelf Res.*, 22 (15), pp. 2081-2113.

Davies, A.M. & Xing, J. (2004). Modelling processes influencing wind-induced internal wave generation and propagation. *Cont. Shelf Res.,* 24, (18), pp. 2245-2271.

Decyk, V.K., Norton, C.D. & Szymanski, B.K. (1997). Expressing object-oriented concepts in Fortran90. *ACM Fortran Forum*, 16.

de Jesus Mendes, P.A., Thomsen, L., Holscher, B., de Stigter, H.C. & Gust, G. (2007a). Pressure effects on the biological degradation of organo-mineral aggregates in submarine canyons. *Marine Geology*, 246 (2-4), pp. 165-175.

de Jesus Mendes, PA, Thomsen, L. & Garcia, A.C. (2007b). Transport of organo-mineral aggregates in Nazaré Canyon. *HERMES Annual Meeting*, Faro,26-30 March.

de Silva, I.P., Imberger, J. & Ivey, G.N. (1997). Localized mixing due to a breaking internal wave ray at a sloping bed. *Jour. of Fluid Mech.*, 350, pp. 1-27.

de Stigter, H. & Shipboard Scientific Party (2003). Sediment dispersal in submarine canyons of the Gulf of Lions and the Portuguese Atlantic margin. *Report of cruise 'Canyons 2002' with RV Pelagia Cruise 64PE204*, València - Texel, 2 - 26 November, NIOZ, 55 p.

de Stigter, H. & Shipboard Scientific Party (2004). Sediment dispersal in submarine canyons of the Portuguese Atlantic margin. *Report of cruise 64PE218 with RV Pelagia* València - Lisbon, 11 - 31 October 2003, NIOZ, 43p.

de Stigter, H. & Shipboard Scientific Party (2007a). The sedimentary environment of submarine canyons of the Portuguese continental margin and Gulf of Lions. *Report of cruise 64PE225 with RV Pelagia* Texel - Toulon, 24 April – 25 May 2004, NIOZ, 59 p.

de Stigter, H. & Shipboard Scientific Party (2007b). The benthic environment of submarine canyons of the Portuguese continental margin. *Report of cruise 64PE236 with RV Pelagia,* Vigo - Lisbon, 27 April – 17 May 2005, NIOZ, 47 p.

de Stigter, H. & Shipboard Scientific Party (2007c). Anthropogenic lead on the Portuguese continental margin. *Report of cruise 64PE252 with RV Pelagia*, Cascais - Lisbon, 30 August – 21 September 2006, NIOZ, 57 p.

de Stigter, H.C., Boer, W., de Jesus Mendes, P.A., Dias de Jesus, C.C., Thomsen, L., van den Bergh, G.D. &. van Weering, T.C.E. (2007). Sediment transport and deposition in Nazaré Canyon, Portuguese continental margin. *Mar. Geol.,* 246, pp. 144–164.

Dias, J.M.A. (1987). Dinâmica Sedimentar e Evolução Recente da Plataforma Continental Portuguesa Setentrional. *PhD Thesis*, Lisbon University, 500p.

Dias, J.M.A., Jouanneau, J.M., Gonzalez, R., Araújo, M.F., Drago, T., Garcia, C., Oliveira, A., Rodrigues, A., Vitorino J. & Weber, O. (2002a). Present Day Sedimentary Processes on the Northern Iberian Shelf. *Progress in Oceanography*, 52, (2-4), pp. 249-259.

Dias, J.M.A., Gonzalez, R., Garcia, C. & Diaz-del-Rio, V. (2002b). Sediment distribution patterns on the Galicia-Minho continental shelf. *Progress in Oceanography*, 52, (2-4), pp. 215-231.

Díaz del Rio, G., Alonso, J., Garcia Fernández, M.J., Cabanas, J.M. & Molinero, J. (1992). Estudios dinámicos en la plataforma continental del norte de Galicia (Abril-Junio 1991). *Informes Técnicos, Inst. Español de Oceanog.,* 134, 23p.

Duarte, J., Dias, J.A., & Taborda, R. (2000). Cabeceira do canhão da Nazaré: erosão versus sedimentação. In J. Dias, O. Ferreira (Eds), Proceedings of the Third Symposium on the Atlantic Iberian Continental Margin, Faro, 25-27 September, pp. 227-228.

Duarte, J.F. (2002). Distribuição espacial dos sedimentos do canhão da Nazaré e plataforma adjacente. *Proceedings of Assembleia Luso-Espanhola de Geodesia e Geofísica, Valência, Tomo III*, pp. 1162–1666.

Duarte, J. & Taborda, R. (2003). Multibeam analysis of the Nazaré Canyon head. *Thalassas*, 19 (2b), pp. 45-46.

Durrieu de Madron, X. (1994). Hydrography and nepheloid structures in the Grand-Rhône canyon. *Cont. Shelf Res.*, 14 (5), pp. 457-477.

Durrieu de Madron, X., Castaing, P., Nyffeler, F. & Courp, T. (1999). Slope transport of suspended particulate matter on the Aquitanian margin of the Bay of Biscay. *Deep-Sea Res. II,* 46, pp. 2003–2027.

Eurostrataform Team, (2004). Deliverable 9 – Forcing conditions governing particle transport along transects from the shallow shelf via canyons to the deep sea. Compiled by Royal NIOZ & WP2 partners, 23p.

Eurostrataform Team, (2006a). Final Project Synthesis – 1 November 2002 - 31 October 2005, sections 5&6, 108p.

Eurostrataform Team, (2006b). Year 3 (Final) Annual Report – 1 November 2004 – 30 October 2005, sections 1-4, 172p.

Feio, M. & Almeida, G. (1978). O porto de Sines: prejuízos dos temporais e reparações (I). *Finisterra,* XIII (26), pp. 1-4

Fernandes, L.D.F. (2005). Modelling of arsenic dynamics in the Tagus estuary. *MsC Thesis*, Lisbon Technical University, 97p.

Fiúza, A.F.G., Macedo, M.E. & Guerreiro, M.R. (1982). Climatological space and time variation of the portuguese coastal upwelling. *Oceanol. Acta,* 5 (1), pp. 31–50.

Flather, R.A. (1976). A tidal model of the northwest European continental shelf. *Mem. Soc. R. Sci. Liege*, 6(10), pp. 141-164.

Fringer, O.B., Gerritsen, M. & Street, R.L. (2006) An unstructured-grid, finite-volume, nonhydrostatic, parallel coastal ocean simulator. *Ocean Model*, 14, pp. 139–173.

Frouin, R., Fiúza, A., Ambar, I. & Boyd, T.J. (1990). Observations of a poleward surface current off the coasts of Portugal and Spain during the winter. *J. Geophys. Res.,* 95, pp. 679– 691.

Garcia, C. (1997). Dispersão e deposição da matéria particulada transportada em suspensão para a plataforma continental adjacente aos rios Tejo e Sado. *MsC Thesis*, Lisbon University, 186p.

Gardner, W.D. (1989). Baltimore Canyon as a modern conduit of sediment to the deep-sea. *Deep-Sea Res.*, 36 (3), pp. 323-358.

Garrett, C. & Kunze, E. (2007). Internal tide generation in the deep ocean. *Annu. Rev. Fluid Mech.*, 39, pp. 57–87.

Gill, A.E. (1982). Atmosphere-Ocean Dynamics. *International Geophysics Series*, 30, Academic Press, 662 p.

Gomes, A. (2001-2002). Análise Morfológica dos canhões submarinos da Nazaré e de Setúbal. Revista da Faculdade de Letras – *Geografia XVII-XVIII*, pp. 65-135.

Gordon, R.L. & Marshall, N.F. (1976). Submarine canyons internal wave traps? *Geophys. Res. Lett.*, 3, pp. 622–624.

Haynes, R. & Barton, E.D. (1990). A poleward flow along the Atlantic coast of the Iberian peninsula. *J. Geophys. Res.,* 95, pp. 11141–11425.

Haynes, R., Barton, E.D. & Pilling, I. (1993). Development, persistence and variability of upwelling filaments off the Atlantic coast of the Iberian Peninsula. *J. Geophys. Res.,* 98, pp. 22681–22692.

Heezen, B.C. & Ewing, M. (1952). Turbidity currents and submarine slumps, and the 1929 Grand Banks earthquake. *American Journal of Science*, 250, pp. 849–873.

Hickey, B., Baker, A. & Kachel, N. (1986). Suspended particle movement in and around Quinault Submarine Canyon. *Marine Geology*, 71, pp. 35-83.

Holloway, P.E. & Barnes, B. (1998). A numerical investigation into the bottom boundary layer .ow and vertical structure of internal waves on a continental slope. *Cont. Shelf Res*., 18, pp. 31–65.

Hotchkiss, F.S. & Wunsch, C.H. (1982). Internal waves in Hudson Canyon with possible geological implications. *Deep-Sea Res*., 29, pp. 415–442.

Hunkins, K. (1988). Mean and tidal currents in Baltimore Canyon. *Jour. Geophy. Res*., 93, pp. 6917-6929.

Ivanov, V.V., Shapiro, G.I., Huthnance, J.M., Aleynik, D.L. & Golovin, P.N. (2004). Cascades of dense water around the world ocean. *Progress in Oceanography,* 60, pp. 47–98.
Joint, I. & Wassmann, P. (2001). Lagrangian studies of the Iberian upwelling system—an introduction. A study of the temporal evolution of surface production and fate of organic matter during upwelling on and off the NW Spanish continental margin. *Progress in Oceanography,* 51 (2-4), pp. 217-220.

Jouanneau, J.M., Garcia, C., Oliveira, A., Rodrigues, A., Dias, J.A. & Weber, O. (1998). Dispersal and deposition of suspended sediment on the shelf off the Tagus and Sado estuaries, SW Portugal. *Progress in Oceanography*, 42, pp. 233-257.

Jouanneau, J.M., Weber, O., Drago, T., Rodrigues, A., Oliveira, A., Dias, J.M.L., Garcia, C., Schmidt S., & Reyss, J.-C. (2002). Present day sedimentation and sedimentary budgets on the northern Iberian shelf. *Progress in Oceanography*, 52 (2-4), pp. 249–259.

Krone, R. (1962). Flume studies of the transport in estuaries shoaling processes. *Hydr. Eng. Lab*., University of Berkeley, California, USA.

Lafuente, J.G., Sarhan, T., Vargas, M., Vargas, J.M. & Plaza, F. (1999). Tidal motions and tidal induced fluxes through La Línea submarine canyon, western Alborean Sea. *Jour. Geophy. Res*., 104 (C2), pp. 3109-3119.

Leendertsee, J. (1967). Aspects of a computational model for long water wave propagation. *Memorandum RH-5299-RR Rand Corporation*, Santa Monica.

Le Provost, C., Lyard, F., Molines, J.M., Genco, M.L. & Rabilloud, F. (1998). A hydrodynamic ocean tide model improved by assimilating a satellite altimeter-derived data set. *J. Geophys. Res*., 103 (C3), pp. 5513-5529.

Lewis, K.B. & Barnes, P.L. (1999). Kaikoura Canyon, New Zealand: active conduit from nearshore sediment zones to trench-axis channel. *Marine Geology*, 162, pp. 39−69.

Leitão, P.C. (1996). Modelo de dispersão lagrangeano tridimensional. *MsC Thesis*, Lisbon Technical Institute, 141p.

Leitão, P. (2003). Integração de Escalas e de Processos na Modelação do Ambiente Marinho. *PhD Thesis*, Lisbon Technical Institute, 297p.

Liu, J.T., Liu, K-j., Huang, J.C. (2002). The effect of a submarine canyon on the river sediment dispersal and inner shelf sediment movements in southern Taiwan. *Marine Geology*, 181, pp. 357-386.

Magalhães, F. (1993). A cobertura sedimentar da plataforma e vertente continental superior a norte de Espinho. *MsC Thesis*, Lisbon University, 191p.

Magalhães, F.M.Q. (1999). Os Sedimentos da Plataforma Continental Portuguesa: contrastes espaciais, perspectiva temporal e potencialidades económicas. *PhD. Thesis*. Lisbon University, 289p.

Martins, F. (2000). Modelação Matemática Tridimensional de Escoamentos Costeiros e Estuarinos usando uma Abordagem de Coordenada Vertical Genérica. *PhD Thesis*, Lisbon Technical University, 263p.

Martins, F., Leitão, P.C., Silva, A. & Neves, R. (2001). 3D modelling of the Sado Estuary using a new generic vertical discretization approach. *Oceanologica Acta*, 24 (1), pp. 51-62.

Martinsen, E.A. & Engedahl, H. (1987). Implementation and testing of a lateral boundary scheme as an open boundary condition in a barotropic ocean model. *Coastal Engineering*, 11, pp. 603-627.

Mazé, J.P., Ahran, M. & Mercier, H. (1997). Volume budget of the eastern boundary layer off the Iberian Peninsula. *Deep-Sea Res.,* 44, pp.1543– 1574.

McCave, I.N. (2002). Sedimentary settings on continental margins – an overview. *From* Wefer, G., Billett, D., Hebbeln, D., Jorgensen, B.B., Schlüter, M. & van Weering, T. (Eds), *Ocean Margin Systems*, Springer-Verlag Berlin Heidelberg, pp 1-14.

McPhee-Shaw, E. & Kunze, E. (2002). Boundary layer intrusions from a sloping bottom: A mechanism for generating intermediate nepheloid layers. *Jour. Geophy. Res*., 107 (C6), pp. 3-1 -3-16.

McPhee-Shaw, E.E., Sternberg, R.W., Mullenbach, B. & Ogston, A.S. (2004). Observations of intermediate nepheloid layers on the northern California continental margin. *Cont. Shelf Res*., 24, pp. 693-720.

McPhee-Shaw, E. (2006). Boundary-interior exchange: Reviewing the idea that internal wave mixing enhances lateral dispersal near continental margins. *Deep-Sea Research II*, 53, pp. 42–59.

Miranda, R. (1999). Nitrogen Biogeochemical Cycle Modelling in the North Atlantic Ocean, *MsC Thesis*, Lisbon Technical University.

Miranda, R., Braunschweig, F., Leitão, P., Neves, R., Martins, F. & Santos, A. (2000). Mohid 2000, A Costal integrated object oriented model. *Hydraulic Engineering Software VIII*, WIT Press.

Monteiro, A.J. (1995). Dispersão de efluentes através de exutores submarinos. Uma contribuição para a modelação matemática. *PhD Thesis*, Lisbon Technical University.

Mulder, T. & Syvitski, J.P.M. (1995). Turbidity currents generated at river mouths during exceptional discharges to the world oceans. *Journal of Geology*, 103, pp. 285–299.

Neves, R.J.J. (1985). Étude Experimentale et Modélisation des Circulations Trasitoire et Résiduelle dans l'Estuaire du Sado. *PhD Thesis*, Liège University., 371p.

Neves, R., Coelho, H., Leitão, P., Martins, H. & Santos, A. (1998). A numerical investigation of the slope current along the western European margin. *Computational Methods in Water Resources* XII, 2, pp.369-376.

Ogston, A.S., Drexler, T.M. & Puig, P. (2008). Sediment delivery, resuspension, and transport in two contrasting canyon environments in the southwest Gulf of Lions. *Continental Shelf Research*, 28 (15), pp. 2000-2016.

Okey, T.A. (1997). Sediment flushing observations, earthquake slumping, and benthic community changes in Monterrey Canyon head. *Continental Shelf Research,* 17, pp. 877–897.

Oliveira, A. (1994). Plumas túrbidas associadas com os rios a norte de Espinho. *MsC Thesis*, Aveiro University, 182p.

Oliveira, A., Rocha, F., Rodrigues, A., Jouanneau, J.M., Dias, J.A., Weber O., & Gomes, C. (2002). Clay minerals from the sedimentary cover from the Northwest Iberian shelf, *Progr. Oceanogr.*, 52, pp. 233-247.

Oliveira, A., Santos, A.I., Rodrigues, A. & Vitorino, J. (2007). Sedimentary particle distribution and dynamics on the Nazaré canyon system and adjacent shelf (Portugal), *Marine Geology*, 246, pp. 105–122.

Oliveira, I., Valle, A. & Miranda, F. (1982). Littoral problems in the portuguese West coast. *Proc Coastal Engr. Conf.* , pp. 1950-1969.

Palanques, A., Durrieu de Madron, X., Puig, P., Fabrés, J., Guillén, J., Calafat, A., Canals, M., Heussner, S. & Bonnin, J. (2006). Suspended sediment fluxes and transport processes in the Gulf of Lions submarine canyons. The role of storms and dense water cascading. *Marine Geology,* 234, pp. 43–61.

Palanques, A., Masqué, P., Puig, P., Sanchez-Cabeza, J.A., Frignani, M. & Alvisi, F. (2008). Anthropogenic trace metals in the sedimentary record of the Llobregat continental shelf and adjacent Foix Submarine Canyon (northwestern Mediterranean). *Marine Geology*, 248 (3-4), pp. 213-227.

Partheniades, E. (1965). Erosion and deposition of cohesive soils, *J. Hydr. Div.*, ASCE, 91 (1), pp. 105-139.

Peliz, A., Dubert, J., Santos, A.M.P., Oliveira, P.B. & Le Cann, B. (2005). Winter upper ocean circulation in the Western Iberian Basin—Fronts, Eddies and Poleward Flows: an overview. *Deep Sea Res. Part I: Oceanog. Res. Papers*, 52 (4), pp. 621-646.

Pereira, J. (1937). O temporal de Janeiro de 1937 na costa de Portugal. *A Terra.,* 31, pp. 18-27.

Petruncio, E.T., Paduan, J.D. & Rosenfeld, L.K. (2002). Numerical simulations of the internal tide in a submarine canyon. *Ocean Modelling*, 4 (3-4), pp. 221-248.

Pires, O. & Pessanha, L. (1986). Wave power climate of Portugal. *In* Evans D. & Falcão A. (Eds.), *Hydrodynamics of ocean wave energy utilization*. IUTAM symposium, Lisboa, 1985, Springer, pp. 157-167.

Puig, P. & Palanques, A. (1998). Temporal variability and composition of settling particle fluxes on the Barcelona continental margin (northwestern Mediterranean). *J. Mar. Res.*, 56, pp. 639–654.

Puig, P., Palanques, A., Guillén, J. & García-Ladona, E. (2000). Deep slope currents and suspended particle fluxes in and around the Foix Submarine Canyon (northwestern Mediterranean). *Deep-Sea Res.*, I 47, pp. 343–366.

Puig, P., Ogston, A.S., Mullenbach, B.L., Nittrouer, C.A., & Sternberg R.W. (2003). Shelf-to-canyon sediment-transport processes on the Eel continental margin (northern California). *Marine Geology*, 193 (1-2), pp. 129-149.

Puig, P., Ogston, A.S., Mullenbach, B.L., Nittrouer, C.A., Parsons, J.D. & Sternberg, R.W. (2004). Storm-induced sediment gravity flows at the head of the Eel submarine canyon, northern California margin, *J. Geophys. Res.*, 109, C03019, doi:10.1029/2003JC001918.

Quaresma, L., Vitorino, J. & Oliveira, A. (2007). Evidences of sediment resuspension by nonlinear internal waves on the western portuguese mid shelf. *Mar. Geol.*, 246, pp. 123–143.

Ramos, C. & Reis, E. (2001). As cheias no sul de Portugal em diferentes tipos de bacias hidrográficas. *Finisterra*, XXXVI, 71, pp. 61-82.

Rey, J. & Diaz del Rio, V. (1987). Estructuras de unidades sedimentares recientes en la plataforma continental de Galicia (NW de España). *Cuad.Lab.Xeol.Laxe.,* 12, pp. 35-45.

Rey, J.J. & Medialdea, T. (1989). Los sedimentos cuaternarios superficiales del margen continental español. *Public. Espec. Inst. Esp. Ocean.*, 3, 29p.

Ribbe, J. & Holloway, P.E. (2001). A model of suspended sediment transport by internal tides. *Cont. Shelf Res.*, 21 (4), pp. 395-422.

Rosenfeld, L.K., Paduan, J.D., Petruncio, E.T., & Goncalves, J.E. (1999). Numerical Simulations and Observations of the Internal Tide in a Submarine Canyon. *Proceedings, 'Aha Huliko'a Hawaiian Winter Workshop*, University of Hawaii at Manoa, January 19-22, pp. 63-71.

Santos, A.J. (1995). Modelo Hidrodinâmico Tridimensional de Circulação Oceânica e Estuarina, *PhD Thesis*, Lisbon Technical University, 272p.

Schmidt, S., de Stigter, H.C. & van Weering, T.C.E. (2001). Enhanced short-term sediment deposition within the Nazaré Canyon, North-East Atlantic. *Marine Geology*, 173 (1-4), pp. 55-67.
Santos, A., Martins, H., Coelho, H., Leitão, P. & Neves, R. (2002). A circulation model for the European ocean margin. *Applied Mathematical Modelling*, 26 (5), pp. 563-582.

Santos, M., Leitão, P.C., Silva, A. & Neves, R. (2008). Effect of coastal waves over the water levels in Óbidos lagoon. *Continental Shelf Research*. In progress.

Saraiva, S., Pina, P., Martins, F., Santos, M. & Neves, R. (2007). Modelling the influence of nutrient loads on Portuguese estuaries. *Hydrobiologia*, 587, pp. 5–18.

Taborda, R. (1993). Modelação da dinâmica sedimentar induzida pela ondulação na plataforma continental portuguesa. *MsC Thesis*, Lisbon University, 126p.

Taborda, R. (1999). Modelação da dinâmica sedimentar na plataforma continental portuguesa. *PhD Thesis*, Lisbon University, 366 p.

Trancoso, A.R., Saraiva, S., Fernandes, L., Pina, P., Leitão, P. & Neves, R. (2005). Modelling macroalgae using a 3D hydrodynamic-ecological model in a shallow, temperate estuary. *Ecological Modelling*, 187, pp. 232-246.

Trincardi, F., Foglini, F., Verdicchio, G., Asioli, A., Correggiari, A., Minisini, D., Piva, A., Remia, A., Ridente, D. & Taviani M. (2007). The impact of cascading currents on the Bari Canyon System, SW-Adriatic Margin (Central Mediterranean). *Marine Geology*, 246 (2-4), pp. 193-207.

Turchetto, M., Boldrin, A., Langone, L., Miserocchi, S., Tesi, T. & Foglini, F. (2007). Particle transport in the Bari Canyon (southern Adriatic Sea). *Marine Geology*, 246, pp. 231-247.

UNESCO, (1981). Tenth Report on the joint panel on oceanographic tables and standards, Technical papers in marine science, 36, 24 p.

Van Aken, H.M. (2000a). The hydrography of the mid-latitude northeast Atlantic Ocean. I, The deep water masses. *Deep-Sea Research I*, 47 (5), pp. 757-788.

Van Aken, H.M. (2000b). The hydrography of the mid-latitude northeast Atlantic Ocean. II, The intermediate water masses. *Deep-Sea Research I*, 47 (5), pp. 789-824.

Van Aken, H.M. (2001). The hydrography of the mid-latitude northeast Atlantic Ocean. III, The thermocline water mass. *Deep-Sea Research I*, 48 (1), pp. 237-267.

Vanney, J.-R. & Mougenot, D. (1990). Un canyon sous-marin du type "gouf": le Canhão da Nazaré (Portugal). *Oceanologica Acta,* 13 (1), pp. 1-14.

Van Weering, T.C.E., de Stigter, H.C., Boer, W. & de Haas, H. (2002). Recent sediment transport and accumulation on the NW Iberian margin. *Prog. Oceanogr.,* 52, pp. 349–371.

Vaz N., Dias J.M., Leitão P.C. & Nolasco R. (2007). Application of the Mohid-2D model to a mesotidal temperate coastal lagoon. *Computers & Geosciences*, 33, pp. 1204-1209.

Villarreal, M.R., Montero, P., Tabuada, J.J., Prego, R., Leitão, P.C. & Pérez-Villar, V. (2002). Hydrodynamic model study of the Ria de Pontevedra under estuarine conditions. *Estuarine, Coastal and Shelf Science*, 54, pp. 101-113.

Vitorino, J.P.N., Oliveira, A.T.C., Jouanneau, J.M. & Drago, T.P. (2000). Winter dynamics and the transport of fine sediments on the northern Portuguese shelf. *3º Simpósio sobre a Margem Ibérica Atlântica*, Faro, pp. 279-280.

Vitorino, J., Oliveira, A., Jouanneau, J.M. & Drago, T. (2002a). Winter dynamics on the northern Portuguese shelf: Part1: Physical processes. *Progr. Oceanogr.,* 52 (2–4), pp. 129–153.

Vitorino, J., Oliveira, A., Jouanneau, J.M. & Drago T. (2002b). Winter dynamics on the northern Portuguese shelf. Part2: Bottom boundary layer and sediment dispersal. *Progress in Oceanography*, 52 (2-4), pp. 155–170.

Wollast, R. (2002). Continental Margins- review of geochemical settings. *From* Wefer, G., Billett, D., Hebbeln, D., Jorgensen, B.B., Schlüter, M. & van Weering, T. (Eds), *Ocean Margin Systems*, Springer-Verlag Berlin Heidelberg, pp 15-31.

Xing, J. & Davies, A.M. (2003). A model study of tidally induced suspended sediment transport in the Iberian shelf edge region. *Estuarine, Coastal and Shelf Science*, 58 (2), pp. 321-333.

Xu, J.P., Noble, M., Eittreim, S.L., Rosenfeld, L.K. & Schwing, F.B. (2002). Distribution and transport of suspended particulate matter in Monterey Canyon, California. *Mar. Geol*., 181, pp. 215–234.